Development of a Novel Flow Channel Apparatus and its Use in Testing the Adhesion Strength of Two Common New Zealand Algae

November 6, 2015

A thesis submitted in partial fulfilment of the
requirements for the Degree of
Master of Science in Biochemistry
at the
University of Canterbury, New Zealand

Anton V. Mather

Abstract

Adhesives produced by marine organisms are fascinating in that they often possess an ability to adsorb rapidly and robustly to a range of substrates, in a range of environmental conditions and in the presence of significant surface contamination. On top of this, they undergo curing while in contact with water. Many of the properties that make marine bioadhesives so effective remain elusive to engineers designing synthetic adhesives. An increased understanding of marine bioadhesives would allow for the design of effective, biologically-inspired adhesives with applications in the engineering, maritime and health sectors. Conversely, better understanding of the adhesives produced by fouling organisms could help with the design of new fouling-resistant surfaces. One essential element for characterising a bioadhesive is to assess its adhesion strength to the substrate. In this thesis, I present a novel flow channel apparatus for testing the adhesion strength of marine organisms to help characterise their associated adhesives. The flow channel was used with *Hormosira banksii* and *Durvillaea antarctica*, two marine macroalgae endemic to New Zealand, and assessments of adhesion strength are made with substrates of varied chemistry and topography. *H. banksii* zygotes were found to exhibit a settlement-time dependent increase in adhesion strength across all of the biomedical substrates, which included poly(methyl methacrylate) (PMMA) and three hydrogels, two of which were gelatin-based approximations of human skin. *H. banksii* did not exhibit any substrate-dependent variation in adhesive strength, suggesting an adhesive that is able to interact with a range of substrate types. *D. antarctica* exhibited more rapid adhesion to glass, PMMA, PTFE and stainless steel than did *H. banksii*, forming a particularly strong bond with stainless steel. On substrates with simple, defined topographies, *H. banksii* zygotes were found to adhere most effectively to a surface with a feature size slightly larger than the size of the zygote. A feature size smaller than the zygote resulted in a minor disruption of adhesion strength that diminished with settlement time.

Acknowledgements

Firstly, I would like to thank my supervisor Dr. Simone Dimartino for his advice, support and unending patience with me during my time as a research student. Dr. Dimartino always made himself available to me whenever I sought guidance, an offer I should have taken more often.
My thanks also to Dr. Tommaso Alestra for his help and advice on the subjects of seaweed and statistics, without which I would have spent significantly more time sitting around feeling confused.
I would also like to thank the support staff in the School of Biological Sciences and the Department of Chemical and Process Engineering at the University of Canterbury. In particular, Rayleen Fredericks for her supportive attitude and practical advice in the laboratory, and Jan McKenzie for her help with logistics and securing culturing environments. Also, my thanks to Rennie Bishop for the boat trips to collect seaweed, which were both fun and educational.
My sincere thanks to my workmates, Maria, Anna, Stacy and Lucy, for their constant support, their flexibility around my research schedule, and for providing more ears to which I could address my lamentations.
And finally, my greatest thanks to my family, my parents and step-parents: Dad, Karen, Mum and Geoff; my siblings: Zane, Abby, Kariba and Jesse; and my best friend, Gina. I don't deny that there were times during this master's when I was probably quite difficult to love, or at least listen to, but they always did both.

Contents

1 Introduction **1**

1.1 Impacts of biofouling 1

1.2 Approaches to biofouling control 3

1.3 The challenge of wet-adhesion 4

1.4 Bioadhesives as inspiration 5

1.5 Research species 5

1.5.1 *Hormosira banksii* 6

1.5.2 *Durvillaea antarctica* 7

1.6 Research aims 9

1.7 Thesis structure 9

2 Flow Channel Design **14**

2.1 Hydrodynamic testing methods 14

2.2 Selection of microfluidic laminar flow channel 17

2.3 Requirements of the flow channel 18

2.4 Final flow channel design 18

2.4.1 Channel dimensions and materials 18

2.4.2 Flow properties 19

2.4.3 Channel inaccuracies and impact on flow properties 21

2.4.4 Channel viewable area 21

2.5 Flow channel supporting infrastructure 22

2.5.1 Crossflow pumping system 22

2.5.2 Seawater treatment 22

2.5.3 Microscope and camera setup 24

2.6 Conclusions 24

3 Adhesion to Skin Models **28**

3.1 Introduction . . . 28

3.1.1 Surface selection and justification . . . 29

3.2 Materials and methods . . . 29

3.2.1 Surface preparation . . . 29

3.2.2 Surface characterisation . . . 30

3.2.3 Seaweed collection and gamete release . . . 30

3.2.4 Zygote settlement and culturing . . . 33

3.2.4.1 Culturing trays . . . 33

3.2.4.2 Substrate inoculation and culturing conditions . . . 33

3.2.5 Adhesion assessment in flow channel . . . 35

3.3 Results and discussion . . . 35

3.3.1 Contact angle measurements . . . 35

3.3.2 Germling health and development . . . 36

3.3.3 Starting densities and recruitment rate . . . 37

3.3.4 Flow channel adhesion experiments . . . 40

3.3.4.1 Influence of post-settlement time on survival . . . 40

3.3.4.2 Influence of substrate type on survival . . . 41

3.3.4.3 Location of adhesive attachment and mode of detachment . . . 42

3.4 Conclusions . . . 46

4 Adhesion to Common Materials **50**

4.1 Introduction . . . 50

4.2 Materials and methods . . . 51

4.2.1 Substrate selection and justification . . . 51

4.2.2 Surface characterisation . . . 52

4.2.2.1 Atomic force microscopy . . . 52

4.2.2.2 Contact angle measurement . . . 52

4.2.3 Substrate preparation . . . 53

4.2.3.1 Cleaning the substrates . . . 53

4.2.3.2 Soaking the substrates . . . 53

4.2.4 Seaweed collection, gamete release and settlement . . . 53

4.2.4.1 *Durvillaea antarctica* . . . 53

4.2.4.2 *Hormosira banksii* . . . 54

4.2.5 Flow channel adhesion testing . . . 56

4.3 Results and discussion . . . 56
4.3.1 Roughness measurements . . . 56
4.3.2 Contact angle measurements . . . 57
4.3.3 Settlement density and recruitment . . . 60
4.3.3.1 *Durvillaea antarctica* . . . 60
4.3.3.2 *Hormosira banksii* . . . 60
4.3.3.3 Comparing starting densities . . . 61
4.3.4 Flow channel survival experiments . . . 62
4.3.4.1 *Durvillaea antarctica* . . . 63
4.3.4.2 *Hormosira banksii* . . . 65
4.3.4.3 Comparing survival rates . . . 65
4.4 Conclusions . . . 68

5 Adhesion to Topographical Substrates 72
5.1 Introduction . . . 72
5.2 Materials and methods . . . 74
5.2.1 Topography design and justification . . . 74
5.2.2 Topographical substrate preparation . . . 74
5.2.2.1 Creating the mould . . . 74
5.2.2.2 Casting the PDMS . . . 76
5.2.3 Topographical substrate characterisation . . . 76
5.2.3.1 Contact angle measurement . . . 76
5.2.4 Seaweed collection, settlement and culturing . . . 77
5.2.5 Adhesion assessment in flow channel . . . 77
5.3 Results and discussion . . . 77
5.3.1 Contact angle measurement . . . 77
5.3.2 Starting densities and recruitment . . . 79
5.3.3 Flow channel adhesion experiments . . . 82
5.3.3.1 Germling settlement position and survival . . . 84
5.3.4 Implications for aquaculture . . . 85
5.4 Conclusions . . . 86

6 Conclusions and Future Directions 89
6.1 The flow channel . . . 89
6.2 Adhesion experiments . . . 90
6.2.1 Skin model experiment . . . 90

6.2.2 Common materials experiment 90
6.2.3 Topographical substrate experiment 90
6.2.4 Challenges encountered in experiments 91
6.3 Recommendations for future work 92
6.4 Closing remarks 92

A Re-plumbing the Crossflow **94**

B Operating the flow channel **96**
B.1 Preparing crossflow and flow channel for experiment 96
B.2 Running experiments 97
B.2.1 Loading slide into flow channel 97
B.2.2 Priming flow channel 97
B.2.3 Adhesion testing 98
B.3 Storing crossflow and flow channel when finished 98

List of Figures

1.1 (a) biofouling on the hull of a boat. This kind of fouling increases drag forces and results in higher fuel consumption and maintenance costs (image credit: MPI). (b) biofouling on aquaculture equipment in the Marlborough Sounds, New Zealand. Biofouling on equipment leads to longer processing times and can result in damage or loss of equipment form excessive loading (image credit: NIWA). 2

1.2 The two species of brown algae assessed in this thesis; (a) *Hormosira banksii* (Turner) Decaisne, and (b) *Durvillaea antarctica* (Chamisso) Hariot (Image credit: Wikipedia). 8

2.1 Fluid velocity profiles of fully developed flow for a) Laminar flow regime and b) Turbulent flow regime with the same mean fluid velocity/flow rate ($\bar{V}$). The parabolic shape of the laminar profile shows lower flow velocities near the wall and an increased central flow velocity, while lateral mixing in the turbulent flow regime decreases the distance to which the wall slows fluid velocity. 17

2.2 Cross-sectional diagram of the flow channel apparatus with dimensions from front (a) and side (b). Channel height is 0.5 mm. Hatching denotes the material being tested and the gasket is shown in black. 19

2.3 Exploded view of the flow channel apparatus showing how the Perspex top stacks with the silicone gasket (shown in red), testing surface (slide) and stainless steel base. Bolts passing through the holes in the corners hold the assembly together. . 20

2.4 Cross section of the flow channel depicting the distortion of the gasket into the flow channel space. Measurement of 3.60 mm represents the worst case scenario for gasket bowing. Image not to scale. 21

2.5 Diagram showing the area available for observation with consistent flow properties. The circles at the ends indicate the entrance and exit ports. The entrance length is for the highest velocity flow and is equal to 23 mm, while the exit length is 4 mm. Wall buffer regions around are 0.5 mm wide to take into account 0.2 mm for gasket deformation and 0.3 mm for the wall effects. 22

2.6 Crossflow flow diagram with additional plumbing leading to the flow channel. The only parts of the crossflow used are the Feed Pump and the Retentate Valve Block (R-VB-Out1) to supply seawater to the flow channel. 23

2.7 Photographs showing the flow channel sitting under the dissecting microscope from the front (A) and the right side (B). The USB camera can be seen sitting in the right ocular tube of the microscope. The flow channel easily fits under the objective lens of the microscope thanks to the microscope's long focal length. 24

3.1 *H. banksii* plants placed under halogen lights (2 × 500 W) to trigger gamete release. Light and heat exposure following a night in the fridge at 6°C "shock" the plants into releasing gametes. 31

3.2 Exudates containing gametes appearing on the surface of *H. banksii* receptacles. (a) shows male gametes (orange), while (b) shows female gametes (olive green). 32

3.3 Separate gamete suspensions achieved by washing reproductive plants in filtered seawater. The smaller beaker on the left contains an orange sperm suspension. The larger beaker on the right contains a green egg suspension. 32

3.4 Healthy, recently fertilised egg surrounded by healthy, motile sperm. 33

3.5 Diagram of a culturing tray with four separate compartments. Each compartment holds a single slide-sized substrate (25 mm × 75 mm). Separate compartments allow for the removal of a single slide without affecting adjacent slides. The sloped end on the tray permits easy access for removing slides. 34

3.6 Chart of germling growth with time. Note good agreement across all materials at each settlement time. (± S.E., $n = 10$) 37

3.7 Germling development over time on PMMA. (a) After 6 hours settlement, germlings remain spherical and are surrounded by dead sperm cells. (b) After 12 hours settlement germlings are still spherical. (c) Some cell division visible (arrows) and polarisation visible in germlings after 24 hours. There is notable formation of a proto-rhizhoid. (d) Significant cell division apparent in germling body. Rhizoid now easily visible and adhesive-containing physodes can be seen in the rhizoid tipes (arrows). 38

3.8 Germling settlement density prior to exposure to flow in the flow channel (D_0). Settlement density is low and inconsistent after only 6 hours settlement but stabilises at 12 hours settlement and above. (+ S.E., $n = 4$). 39

3.9 Germling survival with increasing flow rate for (a) PMMA, (b) Agar, (c) XL-Gel and (d) XL-Gel-Lip. (± S.E., $n = 4$). 43

3.10 Graph showing survival (S_v) on all materials for all settlement times (including 6 hours). Note the similar survival rates between the different materials at each settlement time. (± S.E., $n = 4$). 44

3.11 Series of frames showing the removal of a *Hormosira banksii* germling. Flow velocities are as follows: (a) = 0.83 m/s, (b) = 1.25 m/s, (c) = 1.67 m/s, (d) = 2.08 m/s. Note rotation of germling around fixed point at end of the rhizoid before complete removal in (d). 45

3.12 Ratio of type 1 to type 2 germling removal on substrates after 96 hours settlement. (± S.E., n = 4). 45

4.1 Beakers containing *D. antarctica* gamete suspensions. The larger beaker on the left contains eggs in suspension, the beaker on the right contains sperm in suspension. 54

4.2 (a) Diagram of a settlement guide including dimensions. The small protrusions on the sides and at the end ensure that the guide sits at the centre of the culturing tray. (b) Photograph showing four settlement guides in place in a culturing tray. Zygotes have already been added in this picture, hence the brown-green colour within the guides. Settlement guides effectively limit the area in which the zygotes can settle on the substrate. 55

4.3 R_a and R_{max} values for each of the four substrates. R_{max} generally appears to be an order of magnitude greater than R_a, except on glass, where it is two orders of magnitude greater. R_a values are plotted against the left axis, R_{max} against the right. (± S.E., n = 3) 57

4.4 3D presentations of substrates derived from AFM scans: (a) glass, (b) PMMA, (c) PTFE, (d) stainless steel (polished). Note the vertical axis is not in proportion to the horizontal axes in order to emphasise surface roughness for visual comparison. 58

4.5 Photos of water droplets on each of the four substrates: (a) glass, (b) PMMA, (c) PTFE, (d) stainless steel. Note similarity in droplet shape between glass and stainless steel indicating similar wettability by water. PTFE clearly has the highest contact angle and therefore lowest wettability by water. 59

4.6 Settlement density (D_0) for *D. antarctica* on each substrate and each settlement time. No significant difference in D_0 due to settlement time or substrate. (± S.E., n = 4) 61

4.7 Settlement density (D_0) for *H. banksii* on each substrate and each settlement time. Significant variation in D_0 as a result of both settlement time and substrate. (± S.E., n = 3) 62

4.8 *D. antarctica* germling survival with increasing fluid velocity/shear pressure for different substrates at settlement times of (a) 6 hours, (b) 12 hours, (c) 24 hours and (d) 48 hours. (± S.E., n = 4). 64

4.9 *H. banksii* germling survival with increasing fluid velocity/shear pressure for different settlement times on (a) glass, (b) PMMA, (c) PTFE and (d) stainless steel. (± S.E., n = 3). 66

4.10 Comparing $S_{2.5}$ for both *D. antarctica* and *H. banksii* germlings at all settlement times. Note there is no data for *H. banksii* at 6 hours and no data for *D. antarctica* at 96 hours. At 12 hours *H. banksii* has an $S_{2.5}$ of 0% on all surfaces. $S_{2.5}$ is similar between species for settlement times of 24 and 48 hours with the exception of on stainless steel, where *D. antarctica* appears to adhere much more strongly than *H. banksii*. (± S.E., n = 4 (*D. antarctica*), n = 3 (*H. banksii*)) 67

5.1 3D representations of topographical sections (a, c, e) and photographs of SU-8 negatives used for PDMS casting (b, d, f). (a, b) 40 µm grooved topography, (c, d) 80 µm grooved topography, (e, f) 160 µm grooved topography. Groove depth is 27 µm and grooves are separated by 40 µm wide ridges. 75

5.2 Example images of water droplets on PDMS surfaces. (a) Control - no plasma treatment, no seawater soaking, (b) No plasma treatment, 48 hour seawater soaking, (c) Plasma treatment and 48 hours seawater soaking. 78

5.3 Settlement patterning of *H. banksii* germlings 24 hours post-settlement as seen under a dissecting microscope at 3× zoom. (a) Control (flat) surface, (b) 40 µm grooved surface, (c) 80 µm grooved surface, (d) 160 µm grooved surface. Circles indicate examples where clustering of germlings has resulted in individual germlings settling on the ridge between two grooves. 80

5.4 Settlement density (D_0) with increasing settlement time (± S.E., n = 3). 81

5.5 Survival rate vs fluid velocity after (a) 12 hours settlement time; (b) 24 hours settlement time; (c) 48 hours settlement time. (± S.E., n = 3). 83

5.6 Representations of spherical germlings 80 µm in diameter on (a) 40 µm groove, (b) 80 µm groove, (c) 160 µm groove and (d) flat surface. 84

5.7 Chart showing percent of total germlings ridge-settled vs percent of removed germlings ridge-settled. Note the consistent overrepresentation of ridge-settled germlings in removal data (± S.E., n = 3). 85

A.1 Flow diagram of ÄKTAcrossflow (a) before re-plumbing, and (b) after re-plumbing. 95

List of Tables

2.1 Calculated average velocity (V), wall shear stress (τ_w) and Reynolds number for each of the flow rates (Q) used with the flow channel apparatus. Maximum flow rate selection is discussed in section 2.5.1 20

3.1 Contact angles recorded for each surface (± S.E., $n = 4$). 35

3.2 Zygote/germling diameters with increasing settlement time. (± S.E., $n = 10$) . . . 36

3.3 Two way ANOVA with replication showing significant variation in settlement density as a result of settlement time. 40

3.4 Two way ANOVA with replication showing significant variation in survival at conclusion of experiment as a result of settlement time but no significant variation as a result of substrate. This analysis only took into account survival data for settlement times of 12 hours and above. 41

4.1 R_a and R_{max} measurements for the four substrates (± S.E., n = 3). 56

4.2 Advancing contact angles as measured on all four substrates (± S.E., n = 4). . . . 57

5.1 Recorded advancing contact angles (θ_{AW}) for PDMS surfaces (± S.E., n = 3, *n = 12) 77

A.1 Plumbing changes made to ÄKTAcrossflow. Reference letters indicate position of change in the flow scheme in Figure A.1a. 94

B.1 Flow steps in pumping regime with start time. 98

Chapter 1

Introduction

For countless aquatic organisms, adhesion to a substrate is fundamental to their way of life. The ability to remain attached to a substrate in the face of significant hydrodynamic mechanical challenge allows these organisms to exploit their environment and thrive in what might otherwise be described as inhospitable locations. For sessile marine organisms in the intertidal zone, the production of an effective wet-resistant adhesive allows them to benefit from environmental features such as increased dissolved gases, nutrient content and increased waste product removal.

There is plenty to be learned from investigating the biological adhesives (bioadhesives) produced by marine organisms and their mechanisms of interaction with the substrate. On one hand, research into these bioadhesives could inform the development of superior fouling resistant surfaces. On the other hand, better understanding of the structure and adhesion and curing mechanisms of these glues could lead to the engineering of effective synthetic adhesives for a range of applications in wet environments.

1.1 Impacts of biofouling

Biofouling, or biological fouling, specifically the unwanted colonisation of surfaces by biological organisms and organic compounds, is a problem faced by a range of industries with significant health and economic impacts. Biofouling impacts various industries including naval and shipping (Figure 1.1a), aquaculture (Figure 1.1b), and the food processing and medical industries.

In the naval and shipping sector, the build up of fouling organisms on ship hulls increases drag. This drag can result in an increase in fuel consumption of up to 40% (Yebra et al., 2004). Further costs arise from efforts to control biofouling; hull cleaning and application of anti-fouling coatings not only cost money to carry out but also contribute to ship downtime and lost earnings. Total costs due to biofouling can be in the region of US$56 million (NZ$80 million) per year per vessel (for a US Navy destroyer) (Schultz et al., 2011). Other impacts from ship biofouling include the spread of invasive species, where fouled vessels act as vectors between ecosystems. Common fouling organisms on boats with significant impacts on drag include barnacles (hard foulers) and

(a) (b)

Figure 1.1: (a) biofouling on the hull of a boat. This kind of fouling increases drag forces and results in higher fuel consumption and maintenance costs (image credit: MPI). (b) biofouling on aquaculture equipment in the Marlborough Sounds, New Zealand. Biofouling on equipment leads to longer processing times and can result in damage or loss of equipment form excessive loading (image credit: NIWA).

macroalgal species (soft foulers).

Biofouling in aquaculture has negative consequences for both shellfish and finfish production. For shellfish, biofouling can cause damage to shells, interfere with normal bivalve functioning (e.g. block valves and lips), increase biological competition for resources and cause damage to production infrastructure. Negative impacts of biofouling on farmed fish stock include restriction of water exchange through net occlusion, increased disease risk due to foulers harbouring pathogenic microorganisms, and infrastructure damage and deformation from increased loading (Fitridge et al., 2012). Aquacultural biofouling in Europe alone is estimated to account for $5 - 10\%$ of production costs, equating to approximately €260 million (NZ$430 million) (Lane and Willemsen, 2004). Organisms implicated in biofouling in aquaculture include barnacles, bivalves, bryozoans, polychaetes, ascidians, hydroid sponges and algae (Fitridge et al., 2012).

Biofouling in food processing and medicine often involves the formation of bacterial biofilms on and the adsorption of organic molecules to food-processing or medical and dental equipment. Metals such as stainless steel and titanium are commonly used in food processing and the construction of medical implants and often become substrates to fouling molecules and organisms. In food processing equipment, such as equipment used in milk processing, biofouling includes the deposition of proteins and minerals on the surfaces of heat exchangers, evaporators and membrane filters. This results in decreased heat transfer coefficients, increased pressure drops, product losses, cleaning costs and environmental load (de Jong, 1997). The formation of microbial biofilms on medical devices and implants can increase the risk of infection (Veerachamy et al., 2014; Eiff et al., 2012), while biofilm formation on dental implants can result in bad odours (Verran, 2005) and potential loss of the implant.

1.2 Approaches to biofouling control

Anti-fouling approaches can be broken down into two broad categories: biocidal strategies, which use toxic compounds to kill or weaken fouling organisms, and fouling-release strategies which operate by undermining the strength of a fouling organism's adhesive connection to a substrate, either preventing attachment or resulting in easy removal of the organism.

Anti-fouling strategies traditionally used in shipping have usually revolved around biocidal approaches, with the frequent use of heavy metals as toxicants. Roman and Greek ship builders reportedly used lead sheathing on their vessels, the Romans using copper nails to hold them in place, and copper has been used by the British Navy since 1780 (Callow and Callow, 2002). One of the most successful biocidal anti-fouling coatings, introduced in the 1970s, was a self-polishing-copolymer (SPC) paint containing tributyltin (TBT). SPC paints work through the slow dissolution of the polymer and release of the biocide, simultaneously killing fouling organisms and making the treated surface smoother. However, TBT has since been found to impact non-target organisms, including shellfish, at concentrations lower than anticipated. A full prohibition on the use of TBT was introduced by the International Maritime Organisation in 2008 (IMO, 2002), and newer biocidal coatings using isothiazolinones are becoming common. Fouling control using non-biocidal

strategies, as put by Callow and Callow (2002), is essentially a problem of managing adhesion. Fouling-release type approaches to biofouling control tend to focus more on manipulation of surface chemistry, topography, and the involvement of covalently attached enzymes to digest adhesive constituents to prevent biofouling (Olsen et al., 2007; Gittens et al., 2013). Ideally, the combination of a weakened adhesive bond with the hydrodynamic drag forces generated when a vessel moves would be sufficient to control biofouling on boats.

Historically, biofouling control strategies used in aquaculture borrowed largely from those developed for use in shipping, including the use of biocide containing paints. The use of biocides in such close proximity to organisms being cultured for food does raise questions about the impact on the health of those organisms and potential bioaccumulation of biocides. In industries attempting to present a clean and green image, like many food production companies in New Zealand, the use of biocides could be counter-productive. Current biofouling control strategies in aquaculture rely on the physical removal of fouling organisms, which can be a labour intensive process (Fitridge et al., 2012). Other methods include the avoidance of natural recruitment of foulers, which can be achieved, for example, through manipulating the exposure of aquaculture stock to foulers based on seasonal variation in settlement behaviour in the fouling organisms (Fitridge et al., 2012). Non biocide-containing, fouling-release type approaches would be more environmentally friendly. However, equipment used in aquaculture may not encounter sufficient hydrodynamic forces to remove foulers since they are usually stationary structures.

Biofouling on food processing, dental and medical equipment is typically controlled by vigorous cleaning procedures and working under aseptic conditions. On food processing equipment, biofilm control and disinfection is often performed with strong oxidizing agents such as chlorine (Jang et al., 2006). Recently, fouling control strategies have focused on the use of materials or coatings with antifouling properties. Some recent antifouling coatings have used adhesion strategies inspired by mussel adhesive peptides to anchor molecules designed to prevent fouling, such as polyethylene glycol (PEG) (Dalsin et al., 2005).

In consideration of new anti-fouling strategies, Lewis (1994) proposed six criteria that should be satisfied. Considerations 1, 2, 5 and 6 apply to shipping, while all are relevant in aquaculture. Anti-fouling strategies should: (1) Work against a broad range of taxa; (2) be environmentally benign; (3) have no negative impacts on cultured species; (4) leave no residues in the cultured species; (5) withstand handling and cleaning processes and (6) be economically viable.

1.3 The challenge of wet-adhesion

While biofouling organisms have seemingly no problem achieving successful adhesion in wet environments, the challenge of achieving long-lasting, robust adhesion in a wet environment remains elusive to engineers. Potential applications for successful wet-resistant adhesives are many, from uses in medicine for repair of skin, blood vessels and bone, to aquaculture and underwater construction and repair.

Shortly after immersing a clean surface in water, it becomes host to a plethora of contaminants

including dissolved organic material and ions which readily adsorb on the surface. Bacteria colonise the surface within minutes (Callow and Callow, 2002), resulting in the production of extracellular polymeric substances (EPSs) (Dürr and Thomason, 2009). Marine organisms like mussels, barnacles and algae manage to achieve lasting adhesion to the substrate despite the presence of these EPSs, ions, organic compounds and other fouling substances. The presence of bacterial biofilms and microalgae on a surface have been found to increase the adhesion strength of at least one type of macroalgae (Norton, 1983), but generally these contaminants contribute to forming a low-energy surface while blocking direct adhesive access to the substrate. If we look at industrial bonding processes, professional bonders often rely on high energy cleaning processes, such as plasma etching, to generate high energy surfaces for use in bonding. Surfaces usually have to be dry, and immersion in water only takes place after the adhesive has cured. In contrast, bioadhesives produced by marine organisms have demonstrated an ability to adhere to surfaces that have multiple layers of contaminants (low-energy surfaces), and cure while in contact with water. Additionally, marine bioadhesives can adhere to a wide range of surface types, in a range of salinities at a range of temperatures and under turbulent conditions. Comparing the effectiveness of bioadhesives with the difficulties faced when using synthetic adhesives illustrates that there is plenty that we can learn from studying the structure and characteristics of marine bioadhesives.

1.4 Bioadhesives as inspiration

Understanding the interactions between bioadhesive compounds and their substrates would allow the design of synthetic adhesives that operate on the same adhesive mechanisms. However, the study of bioadhesives produced by marine organisms, such as macroalgae, is not entirely straightforward; these bioadhesives are often complicated, containing many constituent molecule classes including post-translationally modified proteins, glycoproteins, polyphenols and polysaccharides (Stewart et al., 2011; Bitton et al., 2006; Tarakhovskaya, 2014). They are also, by necessity, largely insoluble, undergo rapid curing processes, and are often produced in very small quantities (Petrone et al., 2011). For these reasons, extraction and purification of marine bioadhesives for chemical analysis is difficult, and study of marine bioadhesives often involves the assessment of adhesion strength of whole organisms as a proxy method to determine the strength of the bioadhesive. There are a range of methods for testing adhesion strength using hydrodynamically generated forces, and I review these in Chapter 2. Many of the designs used for hydrodynamic testing involve large or complicated equipment, and a simple, low cost method for performing assays on adhesion strength would see benefit for both anti-fouling and wet-adhesive research.

1.5 Research species

Two species of macroalgae endemic to New Zealand were selected for adhesion testing in this thesis: *Hormosira banksii* (Turner) Decaisne and *Durvillaea antarctica* (Chamisso) Hariot. *H. banksii* and *D. antarctica* are closely related; both are brown algae (Phaeophyceae) belonging

to the order Fucales. Selection of these species was motivated by several considerations: Their dioecious nature permitted me to control the timing of fertilisation and subsequent settlement; complementary reproductive seasons allowed year round reproduction and study; their contrasting habitats (exposure) allowed comparison of relative adhesion strength with respect to natural wave and tidal exposure, and their taxonomic closeness is advantageous in making these comparisons.

1.5.1 *Hormosira banksii*

H. banksii (Figure 1.2a), also known as Neptune's Necklace, is a common fucalean alga endemic to New Zealand where it occupies sheltered locations in the intertidal zone. *H. banksii* plants consist of a holdfast, attached to which are branching chains of receptacles ranging between approximately 0.5 and 2 cm in diameter. The fluid-filled receptacles are buoyant and allow the branches of the plant to float toward the surface when immersed in water. Fluid stored in the receptacles prevents desiccation during low tide, when the plant can be fully exposed for hours at a time. As water evaporates from the surface of the plant, fluid in the cells is replaced with seawater from inside the receptacle (Osborn, 1948). Given the sheltered locations that *H. banksii* inhabits, the forces exerted on germlings during settlement are lower than in the intertidal zone in exposed locations. As a result, the need for a fast-acting adhesive to facilitate strong adhesion may not be as great as in species that settle in exposed locations. Fully grown plants of *H. banksii* are very easy to remove from the substrate simply by pulling with one's hands, the holdfast failing as readily as the connecting tissue between receptacles. In the case of *H. banksii*, there may be some advantage in its relative ease of detachment in that plant detachment and drift are likely fundamental to long distance dispersal of *H. banksii* populations (McKenzie and Bellgrove, 2009).

H. banksii has a simple life story, with no alternation of generations, and is fertile year round with periods of increased reproductive activity during warmer summer months. The surfaces of the receptacles are covered in small, gamete-filled conceptacles. During the reproductive season, the conceptacles produce and release the gametes for external sexual reproduction. Gametes are haploid, and consist of a non-motile egg and motile sperm (Osborn, 1948). Gamete release is stimulated by exposure of the plant to sunlight and warmth following a cold night. Female plants release eggs in fours, while male plants release sperm in quantities of 64. Both types of gametes are enclosed in an endochite which ruptures on contact with seawater, releasing the gametes into the surrounding water column. Immediately after release, the egg adopts a spherical shape approximately $64 - 74$ µm in diameter (Osborn, 1948). Sperm cells are biflagellated, having both a posterior and anterior flagellum (Forbes and Hallam, 1978).

Fertilisation occurs when the sperm and egg cells come into contact to form a diploid zygote. Sperm maneuver toward and cluster in great numbers around the unfertilised eggs, possibly the result of chemotaxis, and fertilisation by a single sperm precedes the withdrawal and decreasing activity of the remaining sperm cells (Forbes and Hallam, 1979). Within hours of fertilisation, zygotes begin to produce a sticky mucilaginous envelope which facilitates initial adhesion to the substrate. This successful initial adhesion can occur in as little as 8 hours (Forbes and Hallam, 1979), and is crucial for the subsequent germination and establishment of the sessile part of *H. banksii*'s life

story. Within days, the germling[1] begins to develop a rhizoid (germinates). As the rhizoid grows, the mucilage-based adhesion is supplanted by adhesive deposition and adhesive connection formed at the rhizoid tip. Later, hypha-like filaments grow downward from the medulla to complement or replace the rhizoids in forming a holdfast. From here on, *H. banksii* develops further into a complete adult plant; however, this thesis is most concerned with the settlement behaviour of very young germlings (up to 4 days old).

Studies on young *H. banksii* have found compounds produced by young zygotes that are exocytosed and/or involved in cell wall formation include polyphenols such as phlorotannins, alginic acid, fucans, cellulose (Schoenwaelder and Clayton, 1998) and sulphated polysaccharides (Forbes and Hallam, 1979). Additionally, as is common in fucalean alga, it has been speculated that peroxidases are involved in cross-linking, wall-strengthening reactions involving polyphenols and alginic acid (Schoenwaelder and Clayton, 1998). Experiments in this thesis will primarily involve looking at the interaction of young zygotes/germlings with different types of surfaces. Confining research to earlier stages in *H. banksii*'s germination process means two things: (1) research is carried out on germlings that have yet to undergo significant morphology change and are still largely spherical and (2) the bulk of the adhesive strength being tested concerns interactions between the early mucilage-based adhesive and the substrate.

1.5.2 *Durvillaea antarctica*

Durvillaea antarctica (Figure 1.2b), also known as the Bull Kelp, is a common, fucalean alga endemic to New Zealand where it persists in exposed locations in the intertidal zone. *D. antarctica* plants consist of a robustly attached holdfast connected to a single stipe that branches into several flat blades (laminae) which can grow up to 10 m in length. The blades of *D. antarctica* are usually submerged, even during low tide, as they drape into the water. A honeycomb type structure within the blades gives them a spongy quality and allows them to float near the surface, providing some dampening of the hydrodynamic forces exerted on the plant due to tidal and wave action. Drag forces experienced by individual *D. antarctica* plants can be as great as 300 N (Stevens et al., 2002). The morphology of individual *D. antarctica* plants is influenced considerably by the intensity of wave action that they are exposed to; specimens with long thin laminae ("thonged" type) are more commonly found in high wave action areas, whereas plants with broader, flatter laminae ("cape" type) are common in sites with moderate wave action (South and Hay, 1979).

Reproduction by *D. antarctica* occurs in this hydrodynamically intense environment, and in order to establish the sessile stage in its life story, *D. antarctica* zygotes need to produce an adhesive that facilitates adhesion to the substrate in spite of the water motion. The contrast between the habitats of *D. antarctica* and *H. banksii* suggests a necessity for *D. antarctica* to achieve more substantial adhesion strength than *H. banksii*. Indeed, research by Taylor and Schiel (2003) demonstrated that propagules of *D. antarctica* achieved more rapid adhesion to the substrate than *H. banksii*, suggesting that *D. antarctica* has a more effective adhesion strategy than *H. banksii*. With grown

[1] For consistency in this thesis, unsettled zygotes are referred to simply as zygotes, while zygotes that have adhered to a substrate are referred to as germlings, whether or not they have germinated.

(a)

(b)

Figure 1.2: The two species of brown algae assessed in this thesis; (a) *Hormosira banksii* (Turner) Decaisne, and (b) *Durvillaea antarctica* (Chamisso) Hariot (Image credit: Wikipedia).

plants of *D. antarctica*, the holdfast is significantly larger and stronger than that of *H. banksii*. Composite holdfasts, that is interwoven holdfasts from multiple individual plants, is common in *D. antarctica* (Hay, 1977). Unlike *H. banksii*, removal of adult plants from the substratum by hand is extremely difficult, if not impossible. It is not uncommon to see, in instances where *D. antarctica* has been dislodged by natural forces such as storm action, a holdfast is still connected to a piece of rock that used to be part of the substratum. Like *H. banksii*, the buoyancy of *D. antarctica* means that individual plants and laminae can stay afloat once detached from the substrate, and rafts of floating *D. antarctica* can be involved in long distance dispersal (Smith, 2002b; Garden et al., 2014).

D. antarctica is fertile in cooler months, generally being reproductive from April through to September (Hay, 1977). *D. antarctica* produces and releases gametes from conceptacles that are present all over the surface of the blade. Like *H. banksii*, gamete release is stimulated when *D. antarctica* is exposed to sunlight following a cold night. When released, eggs appear dark brown, and are non-motile, negatively buoyant and approximately 35 µm in diameter, while sperm cells are flagellated and motile. Fertilisation in *D. antarctica* occurs externally in the water column; a single sperm cell fertilises an egg, which initiates the production of an adhesive mucilage and begins the sessile stage of its life story. The composition of the compounds involved in early *D. antarctica* adhesion are not well documented, though the homologous presence of certain molecules across different species of brown algae (such as phlorotannins) does mean that some of the adhesion mechanisms may be similar to those of *H. banksii*, albeit more rapidly acting (Taylor and Schiel, 2003).

1.6 Research aims

The aim of this thesis was to develop a low-cost apparatus for testing the adhesion strength of small marine organisms and use this apparatus in to assess the relative adhesion strength of two common New Zealand macroalgae to a range of surface types.

1.7 Thesis structure

In this thesis I introduce a novel flow channel for use in adhesion testing of small aquatic organisms and use it to assess the adhesion strength of two common New Zealand macroalgae. In Chapter 2, I review other hydrodynamic testing methods before introducing the design of my own flow channel, describing its features, mode of operation and limitations. The subsequent three chapters are experimental, and involve using the flow channel in a series of experiments designed to demonstrate the flow channel's performance as an adhesion testing apparatus, further understand its limitations to guide future refinement, and generally add to the body of knowledge for describing bioadhesives. In Chapter 3, I use the flow channel to test the adhesion strength of *H. banksii* germlings to surfaces of biomedical relevance, namely poly(methyl methacrylate) and three hydrogels. Two of the hydrogels are protein based and are intended to be an approximation of human skin. The purpose of Chapter 3 is to establish *H. banksii*'s suitability as inspiration for the design of glues

for medical applications. In Chapter 4, I use the flow channel with *H. banksii* and *D. antarctica* to compare the relative stickability of the two species to a range of surfaces commonly used in engineering and manufacturing. In Chapter 5, I use the flow channel to test the adhesion of *H. banksii* zygotes to surfaces with defined microtopographies (topographies between 1 and 1000 µm). In each of the experimental chapters I have combined the results and discussion section as I find this leads to better comprehension of results by the reader.

Bibliography

Bitton, R., M. Ben-Yehuda, M. Davidovich, Y. Balazs, P. Potin, L. Delage, C. Colin, and H. Bianco-Peled (2006, September). Structure of Algal-Born Phenolic Polymeric Adhesives. *Macromolecular Bioscience 6*(9), 737–746.

Callow, M. E. and J. A. Callow (2002, February). Marine biofouling: a sticky problem. *Biologist 49*(1), 10.

Dalsin, J. L., L. Lin, S. Tosatti, J. Vörös, M. Textor, and P. B. Messersmith (2005, January). Protein Resistance of Titanium Oxide Surfaces Modified by Biologically Inspired mPEG-DOPA. *Langmuir 21*(2), 640–646.

Dürr, S. and J. Thomason (2009). *Biofouling* (1 ed.). Hoboken: Wiley.

Eiff, P. D. C. v., B. Jansen, W. Kohnen, and K. Becker (2012, September). Infections Associated with Medical Devices. *Drugs 65*(2), 179–214.

Fitridge, I., T. Dempster, J. Guenther, and R. de Nys (2012, August). The impact and control of biofouling in marine aquaculture: a review. *Biofouling 28*(7), 649–669.

Forbes, M. and N. Hallam (1978). Gamete structure and fertilization in the brown alga Hormosira banksii (Turner) Decaisne. *British Phycological Journal 13*(4), 299–310.

Forbes, M. and N. Hallam (1979). Embryogenesis and substratum adhesion in the brown alga Hormosira banksii (Turner) Decaisne. *British Phycological Journal 14*(1), 69–81.

Garden, C., K. Currie, C. Fraser, and J. Waters (2014). Rafting dispersal constrained by an oceanographic boundary. *Marine Ecology Progress Series 501*, 297–302. cited By 1.

Gittens, J. E., T. J. Smith, R. Suleiman, and R. Akid (2013, December). Current and emerging environmentally-friendly systems for fouling control in the marine environment. *Biotechnology Advances 31*(8), 1738–1753.

Hay, C. H. (1977). A biological study of Durvillaea antarctica (Chamisso) Hariot and D. Willana Lindauer in New Zealand.

International Maritime Organisation (2002). Anti-fouling systems.

Jang, A., J. Szabo, A. A. Hosni, M. Coughlin, and P. L. Bishop (2006, January). Measurement of chlorine dioxide penetration in dairy process pipe biofilms during disinfection. *Applied Microbiology and Biotechnology 72*(2), 368–376.

Lane, A. and P. Willemsen (2004). *Collaborative effort looks into biofouling. Fish Farming Int September 2004*, 34–35. cited By 1.

Lewis, J. A. (1994). Biofouling and fouling protection: A defense perspective. In *Biofouling: Problems and Solutions, Proceedings of an International Workshop*, pp. 39–43.

McKenzie, P. F. and A. Bellgrove (2009, September). Dislodgment and attachment strength of the intertidal macroalga Hormosira banksii (Fucales, Phaeophyceae). *Phycologia 48*(5), 335–343.

Norton, T. A. (1983, February). The resistance to dislodgement of Sargassum muticum germlings under defined hydrodynamic conditions. *Journal of the Marine Biological Association of the United Kingdom 63*(01), 181–193.

Olsen, S. M., L. T. Pedersen, M. H. Laursen, S. Kiil, and K. Dam-Johansen (2007). Enzyme-based antifouling coatings: a review. *Biofouling 23*(5), 369–383.

Osborn, J. E. (1948). The structure and life history of Hormosira banksii (Turner) Decaisne. In *Transactions of the Royal Society of New Zealand*, Volume 77, pp. 47–71. J. Hughes, Printer.

Petrone, L., R. Easingwood, M. F. Barker, and A. J. McQuillan (2011, March). In situ ATR-IR spectroscopic and electron microscopic analyses of settlement secretions of Undaria pinnatifida kelp spores. *Journal of the Royal Society, Interface / the Royal Society 8*(56), 410–422.

Schoenwaelder, M. E. A. and M. N. Clayton (1998, December). Secretion of Phenolic Substances into the Zygote Wall and Cell Plate in Embryos of Hormosira and Acrocarpia (fucales, Phaeophyceae). *Journal of Phycology 34*(6), 969–980.

Schultz, M. P., J. A. Bendick, E. R. Holm, and W. M. Hertel (2011, January). Economic impact of biofouling on a naval surface ship. *Biofouling 27*(1), 87–98.

Smith, S. D. A. (2002b, January). Kelp rafts in the Southern Ocean. *Global Ecology and Biogeography 11*(1), 67–69.

South, G. R. and C. H. Hay (1979, September). Influence of wave action and latitute on morphology and standing crop of New Zealand Durvillaea antarctica (Chamisso) Hariot (Phaeophyta, Durvilleales). *Journal of the Royal Society of New Zealand 9*(3), 289–296.

Stevens, C. L., C. L. Hurd, and M. J. Smith (2002, March). Field measurement of the dynamics of the bull kelp Durvillaea antarctica (Chamisso) Heriot. *Journal of Experimental Marine Biology and Ecology 269*(2), 147–171.

Stewart, R. J., T. C. Ransom, and V. Hlady (2011, June). Natural underwater adhesives. *Journal of Polymer Science Part B: Polymer Physics 49*(11), 757–771.

Tarakhovskaya, E. R. (2014, January). Mechanisms of bioadhesion of macrophytic algae. *Russian Journal of Plant Physiology 61*(1), 19–25.

Taylor, D. I. and D. R. Schiel (2003, June). Wave-related mortality in zygotes of habitat-forming algae from different exposures in southern New Zealand: the importance of 'stickability'. *Journal of Experimental Marine Biology and Ecology 290*(2), 229–245.

Veerachamy, S., T. Yarlagadda, G. Manivasagam, and P. K. Yarlagadda (2014, October). Bacterial adherence and biofilm formation on medical implants: A review. *Proceedings of the Institution of Mechanical Engineers, Part H: Journal of Engineering in Medicine 228*(10), 1083–1099.

Verran, J. (2005, March). Malodour in denture wearers: an ill-defined problem. *Oral Diseases 11*, 24–28.

Yebra, D. M., S. Kiil, and K. Dam-Johansen (2004, July). Antifouling technology—past, present and future steps towards efficient and environmentally friendly antifouling coatings. *Progress in Organic Coatings 50*(2), 75–104.

Chapter 2

Flow Channel Design

2.1 Hydrodynamic testing methods

To characterise the interaction between adhesives produced by marine organisms and their substrate, one critical parameter to observe is mechanical adhesive strength. Adhesives can fail in one of two ways: adhesive failure occurs when the adhesive-substrate connection is disrupted while cohesive failure is when the internal adhesive structure is compromised. Information on both aspects is important for characterising a bioadhesive, however it is observation of the former that is most useful in the analysis of adhesive-substrate interaction and, consequently, the impact of the substrate's properties on adhesive success. Methods commonly used in the assessment of adhesives include tensile, shear and peel tests, and often require a ready supply of pure adhesive. Application of these methods in testing the adhesives produced by marine organisms is somewhat challenging, as the low volumes of adhesive produced, rapid cross linking, and unknown chemical structure make it difficult to effectively extract and purify the adhesive compounds (Petrone et al., 2011). Rather than testing the strength of an adhesive compound in isolation, adhesion testing can be performed on whole organisms as attached to a surface. This approach represents a method for characterising the bioadhesive involved without the need to isolate the adhesive.

Applying a force directly to an attached organism has been used with success in the assessment of adhesion strength for barnacles (Conlan et al., 2008), where a computer controlled actuator applied a shear stress to dislodge individual barnacles and subsequently calculate critical removal stress. However, applying force directly to smaller, soft-bodied organisms such as the zygotes and spores of marine macro-algae is not feasible with this type of equipment. Pull out forces have been measured for fully grown marine macro-algae, where a pulling force applied at various angles to the substrate have been used to test the adhesive strength of *Hormosira banksii* (McKenzie and Bellgrove, 2009). Meanwhile, for smaller organisms, atomic force microscopy (AFM) can be used to test the adhesive strength between organism and substrate: Arce et al. (2004) presented a technique where a tipless AFM probe was functionalised with a live diatom cell to form a bio-probe. The bio-probe was then used to investigate the strength of adhesive interaction between

the extra-cellular polymeric substances produced by the diatom and different material surfaces.

However, adhesion testing using hydrodynamic forces remains the most attractive approach when considering the marine macroalgal species assessed in this thesis. The use of hydrodynamic forces for adhesion testing for marine organisms is already well established, and has two major advantages: (i) the organism is tested under physiological conditions common for these species such as appropriate temperature and salinity, and (ii) the flow conditions used to test the organism are similar to the flow conditions present in the organism's natural environment.

Of the hydrodynamic testing methods employed in the assessment of marine organisms, the simplest would be exposure to artificially- and naturally-generated waves. Taylor and Schiel (2003) used waves generated both in the lab and in the field to challenge the adhesion of three types of marine algae after different settlement times. While this ensures that the magnitude of the forces experienced by the settled cells is ecologically relevant, it relies on qualitative descriptions of the wave intensity and does not allow for the calculation and measurement of accurate, controlled hydrodynamic forces such as shear stress or drag force.

Water-jet type apparatuses use a jet of pressurised water directed at a surface to test the adhesion strength of attached organisms. These can generate very high surface pressures, in the region of 250 kPa (Finlay et al., 2002; Swain and Schultz, 1996). Charters et al. (1973) designed a "water-broom" consisting of two rectangular nozzles attached to a common distributor and used it for testing algal spore adhesion, while a water jet placed eccentrically on a rotating shaft (spinjet) was designed and implemented by Cassé et al. (2007) for use in conjunction with 24 well plates for semi-high throughput adhesion assays. The surface pressures generated by the water jets can be related to a shear pressure which is usually several orders of magnitude lower than the surface pressures generated. For example, shear pressures up to 325 Pa are generated when the surface pressure reaches the maximum value of 250 kPa in Finlay et al.'s apparatus, while the spinjet apparatus generated between 5 and 44 Pa shear stress when generating 18 kPa and 152 kPa surface pressures, respectively (Cassé et al., 2007; Finlay et al., 2002).

Radial flow channels (RFCs) have been used in the assessment of shear stress on the development and attachment strength of bacterial bio-films (Duddridge et al., 1982) and starch particle aggregates (Detry et al., 2009). Radial flow channels consist of a circular chamber made up of two parallel discs separated by a small gap. Water enters the chamber at the centre of one of the plates and flows from the centre of the chamber to the outside where it is collected by a manifold. The motion of the water from the centre to the outside generates a shear stress on the testing surface, the magnitude of which decreases with increasing distance from the flow inlet, i.e. with increasing radius. The RFC used by Duddridge et al. (1982) achieved shear pressures between 6 and 130 Pa. Radial flow channels are unique in that they allow the testing of a range of shear stresses simultaneously on a single surface, which can then be used to identify a critical shear stress for detachment by observing the radius to which the surface is de-fouled. Problems with RFCs can arise when the inlet geometry causes variation in the flow downstream. This can be particularly significant at low radii for high inlet velocities where the flow through the rest of the channel becomes affected by areas of re-circulation. Shear stress values obtained by calculation

should therefore be used with caution, particularly at flows where the Reynolds number for the inlet pipe is > 1500 (Detry et al., 2009). The behavior of fluid flow affected by entrance effects also challenges the assumption that the flow through the channel is axisymmetrical, with different wedges of the substrate disc experiencing different flow conditions.

Annular flow chambers are made from a pair of concentric cylinders, the space between which is filled with water. The internal cylinder rotates, driven by a motor, while the outer cylinder remains stationary. The rotation of the inner cylinder causes the water between the two cylinders to move, generating a shear stress across the inner surface of the outer cylinder. Testable materials can be placed on the inner walls of the outer cylinder, and the shear stress can then be used to test the adhesion ability of fouling organisms. While the simple and well defined flow patterns generated in an annular flow chamber make them attractive, for shear stress determination to remain accurate, the testing materials must be curved and sit flush with inner wall of the outer cylinder, making it difficult to find compatible, low cost substrates (Zhou et al., 2011).

Finally, laminar and turbulent parallel plate flow channels are frequently used in the adhesion testing of fouling organisms. Laminar systems have been used in the study of bacterial, biofilm and terrestrial microalgal adhesion (Arpa-Sancet et al., 2012; Barberousse et al., 2007; Pedersen, 1982), and turbulent systems have been used in the assessment of diatom adhesion (Schultz et al., 2000; Hodson et al., 2012). Turbulent flow channels are typically capable of generating higher shear stresses than laminar flow channels and generally have higher flow rates and fluid velocities to achieve Reynolds numbers greater than 2800. For accurate shear stress approximation, flow in a turbulent channel must be fully developed before it reaches the test section. Durst et al. (1998) suggested that an entrance length of at least 60 channel heights is sufficient to achieve fully developed flow. Schultz et al. (2000) used a 750 mm entrance length for a 7.19 mm high channel, equivalent to 104 channel heights, while for their flow channel measuring 6mm high, Hodson et al. (2012) employed an entrance length of 960 mm, equivalent to 160 channel heights. Calculation of shear stress in a turbulent flow channel relies on measuring the pressure drop across the region of interest and using the following formula:

$$\tau_w = -\frac{h}{2}\frac{dP}{dx}$$

where h is the channel height, P is the static pressure and dx the stream-wise distance across which the pressure drop is measured. For fully developed turbulent flow, the relationship between pressure drop and stream wise distance is linear. Calculating the shear stress generated in a turbulent channel therefore necessitates the inclusion of pressure taps to take pressure readings. Treatment of the fluid entering a turbulent channel is also fairly complicated, with settlement chambers, diffusers, meshes and flow straighteners commonly used to make the flow uniform before it is made turbulent (Schultz et al., 2000; Hodson et al., 2012). Although the Reynolds numbers in the channel indicate natively turbulent flow, a tripping wire is often used at the entrance of the flow channel to trigger turbulent mixing as soon as fluid enters the channel, which also helps to ensure turbulent flow at lower Reynolds numbers.

Laminar flow channels usually have less treatment of the fluid entering the channel than turbulent

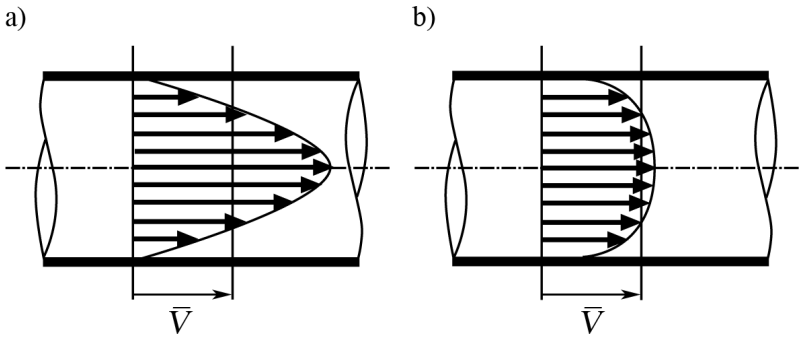

Figure 2.1: Fluid velocity profiles of fully developed flow for a) Laminar flow regime and b) Turbulent flow regime with the same mean fluid velocity/flow rate ($\bar{V}$). The parabolic shape of the laminar profile shows lower flow velocities near the wall and an increased central flow velocity, while lateral mixing in the turbulent flow regime decreases the distance to which the wall slows fluid velocity.

flow channels, with the flow natively taking on a laminar profile for Reynolds numbers less than 2300. While a high aspect ratio helps reduce the Reynolds number for laminar flow channels, they also usually have lower volumetric flow rates and lower mean fluid velocities than turbulent flow channels. The development length (L_e) for laminar flows in a rectangular duct can be calculated using the following equation from (Han, 1960):

$$L_e = 0.01(D_H Re)$$

where D_H is the hydraulic diameter of the rectangular profile of the flow channel:

$$D_H = \frac{4hw}{2(h+w)}$$

where h and w are the channel's height and width, respectively.

Fully developed laminar and turbulent flows have different flow profiles. Turbulent flows have more of a square shaped velocity profile, while the laminar velocity profile is parabolic (Figure 2.1). This indicates that, under the same average velocity and flow rate, turbulent flow regimes achieve a higher velocity flow at a lower distance from the channel wall than do laminar flow regimes. Depending on the size of the organism attached to the channel wall, the fluid velocity gradient around the organism could be significantly different between turbulent and laminar flow conditions.

2.2 Selection of microfluidic laminar flow channel

A laminar type parallel plate flow channel was chosen as the basis for the flow channel designed in this thesis. Considering the zygote size for *Hormosira banksii* (approximately 70 µm) and

Durvillaea antarctica (35 µm), I reasoned that a small form, microfluidic channel would be large enough to accommodate a high enough number of zygotes to perform adhesion experiments on. Since the laminar flow channel does not require the flow straightening and tripping used in turbulent flow channels such as in the designs by Schultz et al. (2000) and Hodson et al. (2012), the design of the channel could be simplified significantly. Integration with a separate pumping system was therefore also simplified by use of simple plumbing connections between the channel and the supporting infrastructure.

2.3 Requirements of the flow channel

The flow channel had to be able to test a range of different surface materials and treatments, and allow rapid exchange of these surfaces. A simple way to do this was to use microscope slides and/or microscope slide sized pieces of material (25 mm x 75 mm) as this would allow easy manipulation, observation by microscope and sufficient testable surface area for the species being tested. The flow channel should allow observation of settled zygotes during operation; this would allow testing multiple flow rates on single replicate as settlement data could be collected without removing the slide and interrupting the experiment. The flow channel also needed to integrate easily with a pumping system with temperature controlled seawater supply and an accurate, programmable flow control to deliver accurate and repeatable shear stress. Other considerations for the flow channel related to production cost, speed and ease of manufacture, so simplicity in design and the use of common materials was a high priority.

2.4 Final flow channel design

2.4.1 Channel dimensions and materials

The final flow channel internal dimensions measure 4 mm wide, 0.5 mm high and 65 mm long (Figure 2.2), giving the flow channel a cross sectional area of 2 mm^2 with an aspect ratio of 1:8 height:width. The footprint of the channel, i.e. 4 mm by 65 mm, fits comfortably along the centre of a microscope slide or similarly sized piece of material. The flow channel is made by sandwiching a slide of interest between two pieces of material (Figure 2.3): the Perspex top measuring 100 mm wide, 75 mm deep and 22 mm thick, and the stainless steel base measuring 100 mm wide, 75 mm deep and 10 mm thick. On the underside of the Perspex top piece, a 5 mm wide groove surrounds a polished rectangle measuring 4 mm x 65 mm that runs along the centre of the Perspex. The polished rectangle is recessed by 0.5 mm from the bottom surface of the Perspex to form the height of the channel. The groove accommodates a silicone gasket, approximately 1 mm wide and 0.7 mm thick, which is held in place with room temperature vulcanising (RTV) sealant. The Perspex top and silicone gasket assembly is bolted to the stainless steel base by four bolts on the corners which feed into threaded holes on the stainless steel base and are tightened using a socket wrench. The significant thickness of the Perspex top helps prevent flexing when tension is applied using

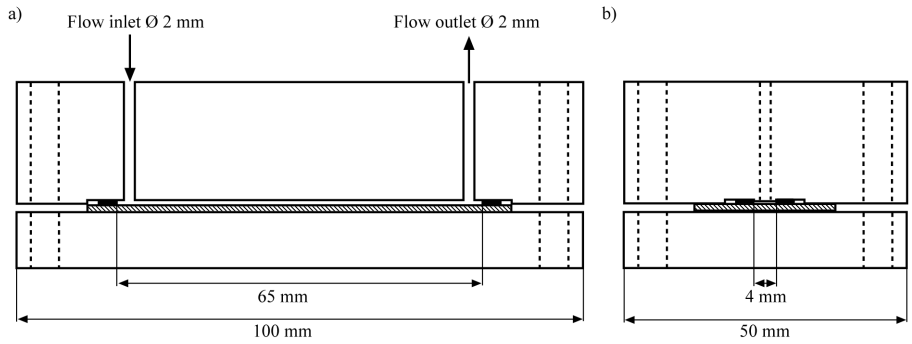

Figure 2.2: Cross-sectional diagram of the flow channel apparatus with dimensions from front (a) and side (b). Channel height is 0.5 mm. Hatching denotes the material being tested and the gasket is shown in black.

the corner bolts. Tightening of the bolts compresses the silicon gasket until the bottom surface of the Perspex top touches the top surface of the material to be tested. The stainless steel base was spray-painted white to give a solid background for clear slides to help distinguish zygotes while also protecting the metal from prolonged exposure to salt water. The underside of the Perspex top creates the top surface of the flow channel and the testing surface creates the lower surface of the flow channel. The remaining four walls are formed by the silicone gasket. Compression of the gasket as the flow channel is tightened ensures a watertight seal.

2.4.2 Flow properties

Reynolds numbers (Re) in the flow channel are calculated using the following equation:

$$Re = \frac{\rho v D_H}{\mu}$$

where ρ and μ are the density and viscosity of seawater at 15 °C, namely 1026 kg/m^3 and 1.08 × 10^{-3} Pa s respectively (Cox et al., 1970). Flow is described as laminar in the flow channel for flow regimes where the calculated Reynolds number is below 2300.

Wall shear stress, or wall shear rate, is the most commonly used parameter when testing and comparing the adhesion strength of adhesive organisms with hydrodynamic systems (Arpa-Sancet et al., 2012; Barberousse et al., 2007; Charters et al., 1973; Detry et al., 2009; Duddridge et al., 1982; Schultz et al., 2000). The magnitude of the shear stress generated depends on the channel dimensions, fluid flow rate and fluid viscosity. The shear stress generated at the wall of the flow channel was estimated using the following:

$$\tau_w = \frac{6Q\mu}{h^2 w}$$

where Q is the flow rate in m^3/s. Shear stress in the flow channel was calculated to be between 5.4 to 32.4 Pa for 50 ml/min and 300 ml/min, respectively. This is comparable to the shear stress

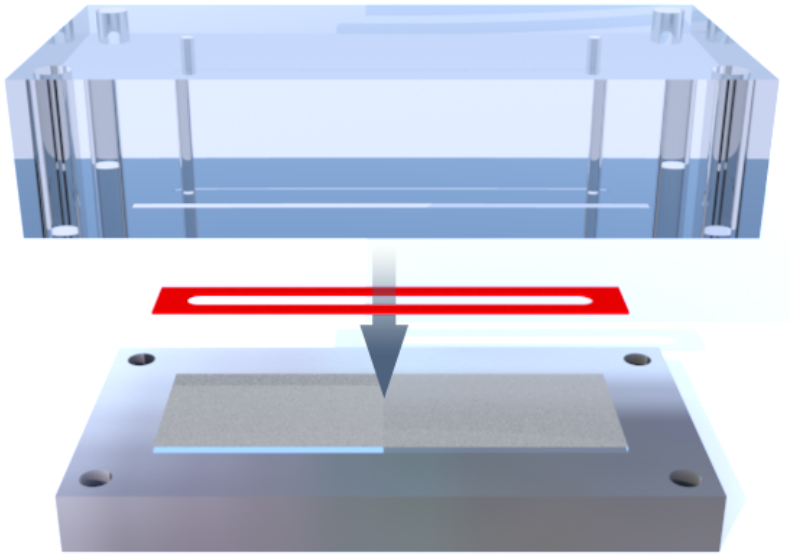

Figure 2.3: Exploded view of the flow channel apparatus showing how the Perspex top stacks with the silicone gasket (shown in red), testing surface (slide) and stainless steel base. Bolts passing through the holes in the corners hold the assembly together.

generated in the flow channels used by Schultz et al., (2000) and Hodson et al. (2012), despite having a laminar rather than turbulent flow regime. It is important to note that the calculation of wall shear stress in this way assumes a channel with smooth walls, so flow disturbances generated by the settled organisms are ignored. Table 2.1 shows the calculated values for the fluid velocity, shear stress and Reynolds number generated for each of the flow steps in the pumping regime. The high aspect ratio of the flow channel allows for laminar flow profiles for flow rates up to 300 ml/min, or flow velocities up to 2.50 m/s.

Table 2.1: Calculated average velocity (V), wall shear stress (τ_w) and Reynolds number for each of the flow rates (Q) used with the flow channel apparatus. Maximum flow rate selection is discussed in section 2.5.1

Q (ml/min)	V (m/s)	τ_w(Pa)	Re
50	0.42	5.40	352
100	0.83	10.8	704
150	1.25	16.2	1056
200	1.67	21.6	1407
250	2.08	27.0	1759
300	2.50	32.4	2111

The entrance length required to achieve fully developed flow in the described system can be calculated using the formula proposed by Han (1960). Entrance length increases with increasing Reynolds number, which in turn increases with flow rate. The required entrance length for fully developed flow was calculated for the highest experimental flow velocity (2.5 m/s) and found to

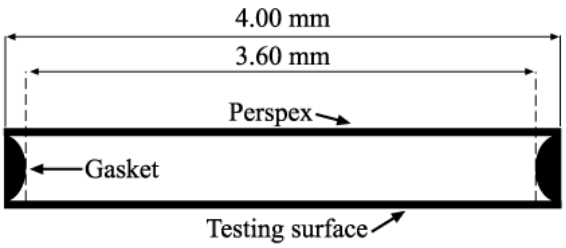

Figure 2.4: Cross section of the flow channel depicting the distortion of the gasket into the flow channel space. Measurement of 3.60 mm represents the worst case scenario for gasket bowing. Image not to scale.

be 19 mm. However, this estimation doesn't take into account the effects of the inlet port on the flow dynamics. The inlet port is perpendicular to the direction of the main flow channel and is associated with a change in duct shape from round to rectangular, so there are likely downstream effects from this configuration. Computational fluid dynamic (CFD) modeling of this flow channel from Dimartino et al. (2015) indicated that, when taking into consideration the flow variation introduced by the inlet port, fluid flow was fully developed after an entrance length of 23 mm at the highest flow rate. Similarly, CFD results also indicated that flow effects from the exit port were confined to within 4 mm of the exit. CFD modeling revealed wall effects from the sides of the flow channel were limited to within 0.3 mm of the walls as a result of the flow channel's high aspect ratio.

2.4.3 Channel inaccuracies and impact on flow properties

Some deformation of the gasket can be witnessed when it is fully compressed; the gasket can be seen to bow into the flow channel, reducing the flow cross section and potentially affecting the flow profile close to the walls. Measuring this deformation showed an apparent reduction in total channel width of a maximum of 0.4 mm (0.2 mm per channel side) when viewed from above, giving a worst case scenario reduction of channel width to 3.6 mm. A change in channel width of this magnitude corresponds to a maximum error of an 11% increase in generated shear stress. Given that the silicone intrusion into the channel due to compression is rounded, the real reduction in channel area, and consequently the actual error, should be less than 11% (see Figure 2.4). Variations in channel height have a much more significant impact on the fluid dynamics, where a deviation of 0.1 mm from the design height of 0.5 mm yields an error in the order of 30%. It is therefore important when using the channel to ensure that the underside of the Perspex top comes into contact with the top surface of the testing material to ensure accurate channel height.

2.4.4 Channel viewable area

As a result of the flow development length, exit effects, gasket deformation and wall effects outlined above, the area in the flow channel within which consistent flow is available is restricted to a strip

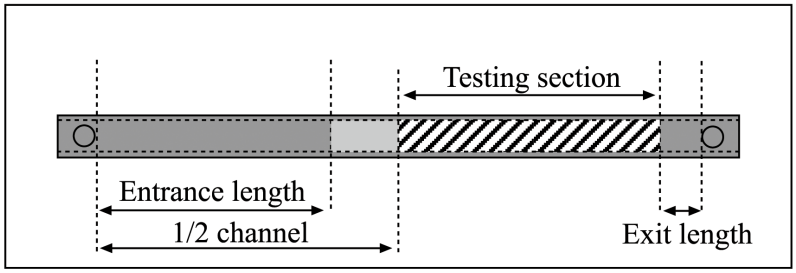

Figure 2.5: Diagram showing the area available for observation with consistent flow properties. The circles at the ends indicate the entrance and exit ports. The entrance length is for the highest velocity flow and is equal to 23 mm, while the exit length is 4 mm. Wall buffer regions around are 0.5 mm wide to take into account 0.2 mm for gasket deformation and 0.3 mm for the wall effects.

in the latter part of the flow channel that is bound by the entrance length, the exit length and a buffer region next to the walls. A diagram of the channel footprint is shown in Figure 2.5, and depicts the eligible area for testing as hatched, while areas with developing or wall-affected flow are indicated in dark grey. Observation of settled zygotes during flow channel operation was restricted to this area of consistent flow.

2.5 Flow channel supporting infrastructure

2.5.1 Crossflow pumping system

Seawater is fed through the flow channel by the feed pump (P-984, 4 pump heads) of an ÄKTAcrossflow (GE Healthcare, Uppsala, Sweden), capable of a maximum flow rate of 600 ml/min. The ÄKTAcrossflow was re-plumbed to bypass the normal reservoir and the rest of the diagnostic equipment. A flow diagram of the modified flow scheme through the ÄKTAcrossflow and flow channel is shown in Figure 2.6. Chilled seawater (see Section 2.5.2) is drawn through the feed pump and retentate valve block (RVB) of the crossflow and passed through the flow channel before returning to the seawater reservoir. 3 mm internal diameter clear PVC tubing was used for all additional plumbing, allowing observation of fluid flow and identification of any bubbles in the flow scheme. The ÄKTAcrossflow is controlled by Unicorn software which allows for accurate control of the feed pump system as well as the operation of automated flow programs. The feed pump system is capable of providing smooth fluid flow up to approximately 350 ml/min, above which some pulsing becomes apparent. 300 ml/min was therefore selected as the maximum flow rate for use with the flow channel.

2.5.2 Seawater treatment

All seawater used in the operation of the flow channel was collected from Sumner, Christchurch, New Zealand (43°57'15.31" S, 172°76'56.70" E). Before use, seawater was filtered at 0.22 µm to remove contaminants and sonicated for 10 minutes per litre bottle to degas the seawater and

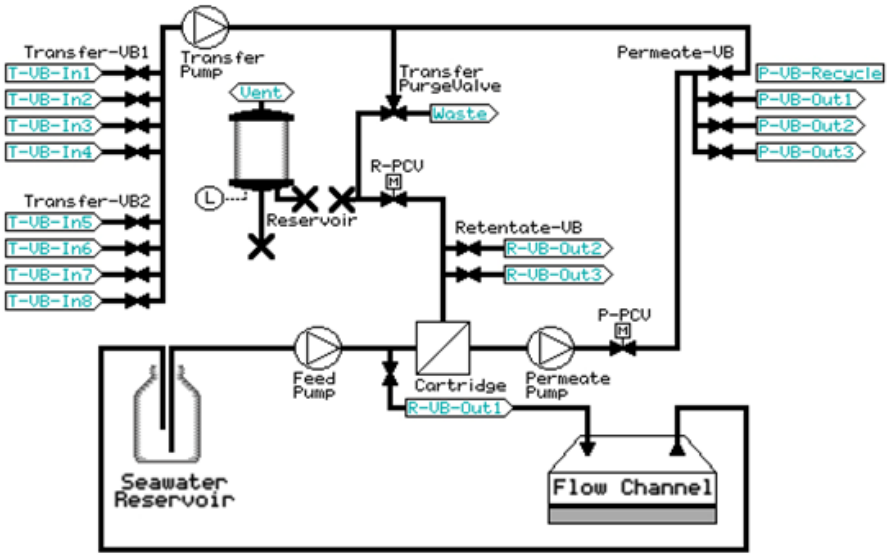

Figure 2.6: Crossflow flow diagram with additional plumbing leading to the flow channel. The only parts of the crossflow used are the Feed Pump and the Retentate Valve Block (R-VB-Out1) to supply seawater to the flow channel.

minimise air bubble formation in the crossflow/flow channel plumbing. Air bubbles in the flow channel are undesirable as an air bubble passing through the flow channel creates a wave front, the shear stress of which is not easily estimated, making the adhesion data inaccurate. The temperature of the seawater increases significantly when passing through the feed pump block and tubing. To ensure minimal stress to the zygotes from increased fluid temperature, seawater was cooled to temperatures several degrees lower than what was desired in the flow channel. This was done by storing several 1 litre bottles of seawater in a small bar fridge set to approximately 3°C. During an experiment, a single bottle of chilled seawater would be used per four replicates. Once four replicates had been tested, the bottle would be replaced with a fresh bottle of chilled seawater. Seawater inlet and outlet tubes were also covered in thick lagging to further minimise the increase in seawater temperature as a result of heat exchange with the environment. The temperature of the seawater entering the flow channel was monitored by measuring the temperature between the tubing and the lagging using a thermometer with a wired probe attachment. The temperature difference between the inside of the tubing (i.e. water entering the flow channel) and the area between the PVC piping and lagging was calibrated to allow accurate approximation of the temperature of seawater entering the flow channel during operation without having to interrupt the flow or insert the thermometer probe into the line of flow. The temperature of the water entering the flow channel was also dependent on the flow rate, with faster flow rates causing less warming of the seawater than slower flow rates. Due to this flow-dependent variation in temperature, totally stable temperature in the channel was not achieved. Temperature in the channel therefore fell within a range of 15°C $\pm$ 5°C. This level of variation was deemed acceptable, and does not exceed the range of temperatures that the testing species would be exposed to in their natural environment.

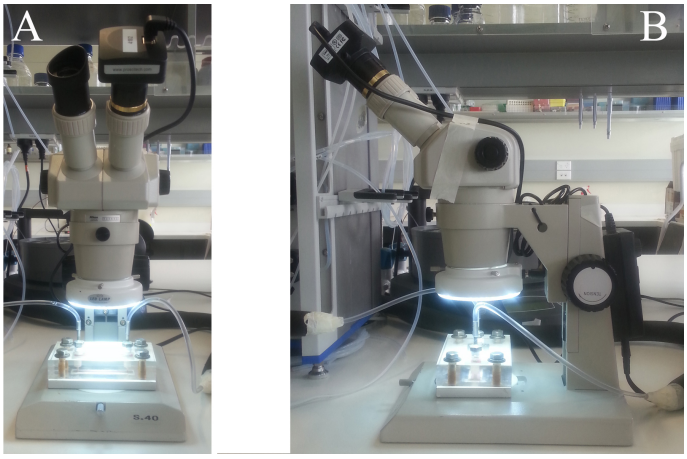

Figure 2.7: Photographs showing the flow channel sitting under the dissecting microscope from the front (A) and the right side (B). The USB camera can be seen sitting in the right ocular tube of the microscope. The flow channel easily fits under the objective lens of the microscope thanks to the microscope's long focal length.

2.5.3 Microscope and camera setup

A Nikon SMZ-1B binocular dissecting microscope (Nikon Corporation, Tokyo, Japan) was used in conjunction with a 1.3 megapixel USB CMOS camera (UCMOS1300KPA, ToupTek Photonics, Hangzhou, China) to observe and record the flow channel during operation. The microscope with camera attachment are shown in Figure 2.7. The CMOS camera has a tubular lens attachment that fits into one of the ocular tubes of the dissecting microscope. The microscope is capable of a maximum zoom of 3.5×, and its long focal length easily accommodates the flow channel between the objective lens and the microscope stage. The flow channel is illuminated by a ring light fitted to the objective lens. Observation of the flow channel at 3× zoom allows for easy differentiation between settled zygotes. At 3× zoom, the observable area measures 3.3 mm horizontally (stream wise axis in channel) by 2.6 mm vertically (across channel), yielding a viewable area of 8.58 mm^2. ToupView software (x64 v3.7.1691, ToupTek Photonics, Hangzhou, China) was used to record images and video footage of the cells during channel operation. Video footage was recorded over a two minute interval, corresponding to the length of the pumping program executed by Unicorn.

2.6 Conclusions

The flow channel apparatus presented in this chapter satisfied the requirements outlined in Section 2.3, including the simple design and easy integration with existing pumping equipment. There is no reason that the flow channel cannot be integrated into other pumping systems, whether they be other automated, high accuracy systems like the crossflow, peristaltic pumping systems, or a simple pump and rotameter system for a low-cost set up. Wall shear stresses achievable by the flow channel with the crossflow are not dissimilar to those achieved by Schultz (2000) and Hodson (2012) in their testing of diatoms using a turbulent system, but using a plumbing set up that is

considerably less complicated. Observation of the testing surfaces during flow channel operation is easily achieved using a dissecting microscope and low cost USB camera, allowing the collection of video footage that can be processed into meaningful data at a later date. While gasket deformation presents some error in the flow properties, this is not deemed unacceptable in magnitude. In the following chapters, the flow channel is used to test the adhesion strength of zygotes of *Hormosira banksii* and *Durvillaea antarctica* to a variety of surface types.

Bibliography

Arce, F. T., R. Avci, I. B. Beech, K. E. Cooksey, and B. Wigglesworth-Cooksey (2004, December). A Live Bioprobe for Studying Diatom-Surface Interactions. *Biophysical Journal 87*(6), 4284–4297.

Arpa-Sancet, M. P., C. Christophis, and A. Rosenhahn (2012). Microfluidic assay to quantify the adhesion of marine bacteria. *7*(1), 26.

Barberousse, H., R. Brayner, A. M. B. Do Rego, J.-C. Castaing, P. Beurdeley-Saudou, and J.-F. Colombet (2007). Adhesion of façade coating colonisers, as mediated by physico-chemical properties. *23*(1), 15–24.

Cassé, F., S. J. Stafslien, J. A. Bahr, J. Daniels, J. A. Finlay, J. A. Callow, and M. E. Callow (2007). Combinatorial materials research applied to the development of new surface coatings v. application of a spinning water-jet for the semi-high throughput assessment of the attachment strength of marine fouling algae. *23*(2), 121–130.

Charters, A. C., M. Neushul, and D. Coon (1973). The effect of water motion on algal spore adhesion. *Limnology and Oceanography - LIMNOL OCEANOGR 18*(6), 884–896.

Conlan, S. L., R. J. Mutton, N. Aldred, and A. S. Clare (2008). Evaluation of a fully automated method to measure the critical removal stress of adult barnacles. *24*(6), 471–481.

Cox, R. A., M. J. McCartney, and F. Culkin (1970). The specific gravity/salinity/temperature relationship in natural sea water. *17*(4), 679–689.

Detry, J. G., C. Deroanne, M. Sindic, and B. B. B. Jensen (2009). Laminar flow in radial flow cell with small aspect ratios: Numerical and experimental study. *64*(1), 31–42.

Detry, J. G., B. B. B. Jensen, M. Sindic, and C. Deroanne (2009). Flow rate dependency of critical wall shear stress in a radial-flow cell. *92*(1), 86–99.

Dimartino, S., A. V. Mather, T. Alestra, S. Nawada, and M. Haber (2015). Experimental and computational analysis of a novel flow channel to assess the adhesion strength of sessile marine organisms. *5*(1), 20140059.

Duddridge, J. E., C. A. Kent, and J. F. Laws (1982). Effect of surface shear stress on the attachment of pseudomonas fluorescens to stainless steel under defined flow conditions. *24*(1), 153–164.

Durst, F., M. Fischer, J. Jovanović, and H. Kikura (1998). Methods to Set Up and Investigate Low Reynolds Number, Fully Developed Turbulent Plane Channel Flows. *Journal of Fluids Engineering 120*(3), 496.

Finlay, J. A., M. E. Callow, M. P. Schultz, G. W. Swain, and J. A. Callow (2002). Adhesion strength of settled spores of the green alga enteromorpha. *18*(4), 251–256.

Han, L. S. (1960). Hydrodynamic entrance lengths for incompressible laminar flow in rectangular ducts. *27*(3), 403–409.

Hodson, O. M., J. P. Monty, P. J. Molino, and R. Wetherbee (2012). Novel whole cell adhesion assays of three isolates of the fouling diatom *Amphora coffeaeformis* reveal diverse responses to surfaces of different wettability. *28*(4), 381–393.

McKenzie, P. F. and A. Bellgrove (2009). Dislodgment and attachment strength of the intertidal macroalga hormosira banksii (fucales, phaeophyceae). *48*(5), 335–343.

Pedersen, K. (1982). Factors regulating microbial biofilm development in a system with slowly flowing seawater. *44*(5), 1196.

Petrone, L., R. Easingwood, M. F. Barker, and A. J. McQuillan (2011). In situ ATR-IR spectroscopic and electron microscopic analyses of settlement secretions of undaria pinnatifida kelp spores. *8*(56), 410–422.

Schultz, M. P., J. A. Finlay, M. E. Callow, and J. A. Callow (2000). A turbulent channel flow apparatus for the determination of the adhesion strength of microfouling organisms. *15*(4), 243–251.

Swain, G. W. and M. P. Schultz (1996). The testing and evaluation of non-toxic antifouling coatings. *10*(1), 187–197.

Taylor, D. I. and D. R. Schiel (2003). Wave-related mortality in zygotes of habitat-forming algae from different exposures in southern new zealand: the importance of 'stickability'. *290*(2), 229–245.

Zhou, J., C. G. Lin, and D. X. Duan (2011). Progress on measurement of adhesion strength of marine microfouling organisms. *299-300*, 883–886.

Chapter 3

Adhesion to Skin Models

3.1 Introduction

One of the most exciting applications of novel, wet-resistant adhesives is in the field of medicine, where the human body could reasonably be considered a wet environment. Synthetic adhesives have already been used as a substitute for conventional sutures (Applebaum et al., 1993), while other possible applications of adhesives lie in the repair of blood vessels, bones, and the reattachment of disconnected muscles and tendons to bone. Research on adhesive-skin interaction often uses porcine skin samples (Ninan et al., 2003; Cohen et al., 2013) or human volunteers (Charkoudian et al., 1988). However, while experiments with human volunteers yield relevant data for human medicine, they can be costly and time consuming to run while also suffering from high variability in the volunteers' skin (Charkoudian et al., 1988). Synthetic skin models based on cross-linked gelatin have been designed to provide a consistent substrate for skin-based adhesion testing and have demonstrated properties similar to human skin (Charkoudian et al., 1988; Lir et al., 2007).

Adhesive proteins extracted from mussels have previously been assessed as potential medical adhesives and they performed comparably to fibrin adhesives (Ninan et al., 2003). Meanwhile the biocompatibility of seaweed and seaweed extracts (Bitton et al., 2009) make them an attractive candidate for research aimed at designing medical adhesives and drug delivery systems (Qurrat-ul-Ain et al., 2003; Jayant et al., 2009). Finding a suitable candidate species for biomimetic inspiration requires characterisation of the adhesive-substrate interaction. One important component of this interaction is the mechanical strength of the adhesive bond, or the force required to break the adhesive's bond to the substrate. This presented an opportunity to use the flow channel to test the adhesion strength of a candidate species, *Hormosira banksii*, to substrates of biomedical relevance.

The assessment of *H. banksii*'s adhesion strength to the various substrates was intended to identify any relative adhesion-strength differences between *H. banksii* germlings and the substrates with increasing settlement time. Additionally, I wanted to determine if the adhesive produced by *H. banksii* warranted further investigation as a model for bioinspired, synthetic adhesives for medical applications.

3.1.1 Surface selection and justification

Four surfaces were used for adhesion testing with *H. banksii* in the flow channel. The four surfaces were selected based on three considerations: (i) the composition of biofilms covering the substrate in the natural environment; (ii) relevance in biomedical applications, and (iii) diversity of chemical compositions.

The first of the four surfaces was PMMA. PMMA is a common material in the biomedical arena and exhibits good biocompatibility in humans. Its applications range from use in intraocular lenses to inclusion as a component in cement for bones (Frazer et al., 2005) as well as being widely used in dentistry (Leigh, 1975). The remaining three surfaces were PMMA slides coated with a layer of hydrogel. The first hydrogel surface was carbohydrate based and made from agarose. The agar surface was chosen as it approximates the polysaccharide component of extracellular polymeric substances (EPSs) produced by bacterial biofilms (Dürr and Thomason, 2009), and is a common polysaccharide present on substrates typically colonised by marine macroalgae (Fletcher and Callow, 1992a). The other two hydrogel surfaces were protein based and made using cross-linked gelatin (collagen), one of which containing an additional lipid component. The gelatin based surfaces, and particularly the lipid containing surface, were simplified versions of human skin models as described by Lir et al. (2007). Cross-linked gelatin is frequently used in medicine as absorbable haemostats, tissue adhesives and sealants, and scaffolds for tissue engineering (Lir et al., 2007; Yoshizawa and Taguchi, 2014; Bertoni et al., 2006).

3.2 Materials and methods

3.2.1 Surface preparation

Seawater used in the preparation of surfaces was collected from Sumner, Christchurch, New Zealand (43°57'15.31" S, 172°76'56.70" E), and filtered through a 0.22 µm filter (Whatman, GE Healthcare and Lifesciences, Fairfield, CT, USA). Agar (bacteriological agar; Oxoid Ltd, Basingstoke, UK) was purchased from Thermo-Fisher Scientific. Absolute ethanol was obtained from Nuplex Specialties (Auckland, New Zealand). The ingredients used to prepare the skin model substrates were used as received without further purification: gelatin (type A, 275 bloom porcine skin; Gelita, Sergeant Bluff, IA, USA), lipid (Prolipid 141; International Specialty Products, Wayne, NJ, USA) and a cross-linker, microbial transglutamase (Activa TG; Ajunomoto, Tokyo, Japan). (PMMA) flat sheet with a thickness of 2 mm was purchased from Dotmar Engineering Plastics (Christchurch, New Zealand).

Carbohydrate-based substrates (agar) were prepared from a 1.5% w/v solution of agar dissolved in purified water (Milli-Q, Millipore) at 70°C. 100 µl aliquots of agar solution were transferred to clean PMMA slides (25 × 75 mm) and spread uniformly across the slide surface by dragging across the slide with the straight edge of another slide, ensuring coverage of the hydrogel solution right to the edges of the PMMA base slide. The gelatin hydrogels (XL-Gel) were prepared using a 5% w/v gelatin solution in filtered seawater at a temperature of 50°C. Cross linking of the protein

fraction was induced by adding a 5% w/v stock solution of the cross-linker in purified water to give a final concentration of 0.2% of the cross-linker in the gelatin solution. 100 µl aliquots of the cross-linker and gelatin solution were transferred to clean PMMA slides before the cross-linking reaction completed. The gelatin hydrogels with added lipid (XL-Gel-Lip) were prepared following the same protocol, with the addition of a 20% w/v lipid solution in ethanol to give a final concentration of 0.8% lipid in the gelatin solution prior to the addition of the cross-linker. All slides were left to dry overnight under ambient conditions. The thickness of the hydrogel layers was 50 ± 3 µm.

16 slides of each substrate were prepared (64 slides in total) for adhesion testing. Two additional slides of each substrate type were also prepared, one to be seeded with *H. banksii* zygotes to be used for monitoring germling development and the other to be used for contact angle measurement. All substrate slides were placed in trays and soaked in 30 ml of filtered seawater for 24 hours prior to inoculation with zygotes (see section 3.2.4).

Atomic force microscopy (AFM) was performed on the PMMA surface only (see Chapter 4). The arithmetic average of roughness (R_a) for PMMA was found to be 63 nm ± 17nm, while the maximum distance between the highest peak and the lowest valley (R_{max}) was 857 nm ± 245 nm. Since R_{max} is approximately two orders of magnitude lower than the size of the *H. banksii* zygotes, the degree of roughness was deemed negligible.

Substrates will be referred to as PMMA, Agar (agarose hydrogel), XL-Gel (cross-linked gelatin) and XL-Gel-Lip (cross-linked gelatin with lipid component) for the remainder of this chapter.

3.2.2 Surface characterisation

Contact angle measurements were performed using a goniometer equipped with high speed camera (CAM200; KSV Instruments Ltd, Helsinki, Finland). Advancing contact angles (θ_{AW}) were taken following deposition of a 2 µl droplet of deionized water on each of the four surfaces. 10 images of the water droplet, spaced 6 s apart, were taken following a 30 s delay after initial deposition of the water droplet. The ten images were analysed using the associated goniometer software (KSV CAM Software v 4.01), which fit the droplet shape to the Young-Laplace equation. The average contact angle was then calculated across the ten images and this average represented the contact angle measurement for a single replicate. Contact angle measurements were performed four times on each substrate and a final average was obtained from these four measurements.

3.2.3 Seaweed collection and gamete release

The protocol used to obtain zygote suspensions is similar to that previously described by Taylor et al. (2003; 2010). *H. banksii* samples were collected at low tide from Shag Point, near Moeraki, on the west coast of the South Island of New Zealand (45°27'35.50" S, 170°48'47.26" E), in April of 2014. Collected plants were washed in filtered seawater to remove larger contaminants before being stored in the dark overnight in a temperature controlled room at approximately 6°C. The following day, the *H. banksii* plants were placed under halogen lights (two lights, 500 W each) for 30 – 60 minutes at a temperature of 25°C (Figure 3.1). Egg and sperm releases on reproductively

Figure 3.1: *H. banksii* plants placed under halogen lights (2 × 500 W) to trigger gamete release. Light and heat exposure following a night in the fridge at 6°C "shock" the plants into releasing gametes.

mature plants could be easily identified by the appearance of gamete-containing exudates on the surface of the plant. The sex of the plants was determined by the colour of the exudates, with bright orange sperm indicating a male plant (Figure 3.2a) and pale olive-green eggs indicating a female plant (Figure 3.2b). Not all of the plants collected were reproductively viable; a significant proportion of the plants (30%) did not exhibit any gamete release and were discarded.

Male and female reproducing plants were washed separately into two beakers of 0.22 µm filtered seawater to create separate egg and sperm suspensions (Figure 3.3). The egg and sperm solutions were then filtered through a 105 µm and 25 µm filter, respectively, to remove some of the larger particulate matter. The egg suspension was further clarified by allowing the eggs to settle to the bottom of the beaker, a process that took between five and 10 minutes, followed by removal of the supernatant, the addition of fresh seawater and mixing of the new suspension. This process was repeated three times to obtain a clean egg suspension. The sperm suspension was not clarified in any way beyond the initial 25 µm filtering. Egg and sperm solutions were then mixed to initiate fertilisation. Egg and sperm viability were confirmed by observation under a compound microscope (Nikon model SE, Tokyo, Japan) equipped with a USB CMOS camera and viewed using ToupView microscopy software. Eggs were deemed healthy if they had a largely uniform, round shape and a consistent colouring. Sperm health was confirmed by the observation of movement in the sperm cells and clustering of sperm cells around healthy egg cells, as can be seen in Figure 3.4. Following fertilisation, the egg cell changes in appearance slightly, where the formerly uniform green pigmentation appears to cluster to the centre of the zygote and a more noticeable cell wall begins to form. The volume of the zygote suspension was adjusted with fresh, filtered seawater to achieve a concentration of approximately 20,000 zygotes per ml.

(a) (b)

Figure 3.2: Exudates containing gametes appearing on the surface of *H. banksii* receptacles. (a) shows male gametes (orange), while (b) shows female gametes (olive green).

Figure 3.3: Separate gamete suspensions achieved by washing reproductive plants in filtered seawater. The smaller beaker on the left contains an orange sperm suspension. The larger beaker on the right contains a green egg suspension.

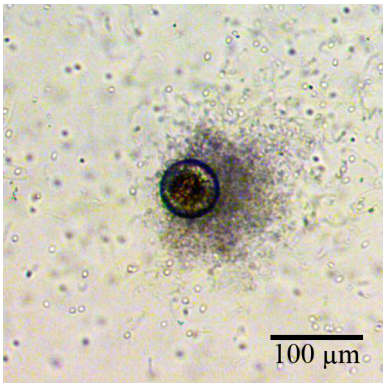

Figure 3.4: Healthy, recently fertilised egg surrounded by healthy, motile sperm.

3.2.4 Zygote settlement and culturing

3.2.4.1 Culturing trays

Zygotes had to be cultured in separate trays of seawater so that the removal of one slide for testing did not cause any disruption to the remaining slides. Custom culture trays were designed using Google Sketchup (version 8.0.16846) and printed in acrylonitrile butadiene styrene (ABS) using an UP Mini 3D printer (Beijing Tiertime Technology Co., Ltd., Beijing, China). The trays were designed to hold four slides, each slide in its own compartment measuring 27 mm wide, 80 mm long and 20 mm high (Figure 3.5). One side with a 45° slope for easy access was also designed. Early testing of the trays revealed that a few of them suffered from slow leaks due to inconsistent fusion between ABS layers during manufacture. Culture trays were treated with acetone, a solvent for ABS, to seal possible leaks. Culture trays measured approximately 115 mm wide and 103 mm long. Their small footprint allowed several trays to be placed side by side in a relatively small area, minimising differences in exposure to light in the culturing environment. Prior to zygote inoculation, substrates were placed in their trays and soaked in filtered seawater for 24 hours.

3.2.4.2 Substrate inoculation and culturing conditions

Each replicate of the four substrate types were seeded with 2 ml (approximately 40,000 cells) of zygote suspension using a pipette. An additional slide of each substrate (four total) were seeded in the same way to be used to monitor germling development over the course of the experiment. From here on, eggs that have been fertilised will be termed zygotes, while zygotes that have attached to a substrate will be referred to as germlings.

The germlings were cultured in a temperature-controlled room set to 15°C, which corresponds roughly to sea temperatures in the South Island during April. Light was provided by a pair of fluorescent bulbs (light intensity = 40 µmol photons/m^2/s PAR) on a 12 hours:12 hours light:dark cycle. Seawater in the culture trays was replaced at a rate of 50% every 24 hours to prevent nutrient depletion. Using a syringe to replace the seawater minimised the impact on the germlings from water motion, while replacing only 50% of the seawater prevented the drying out of the sample

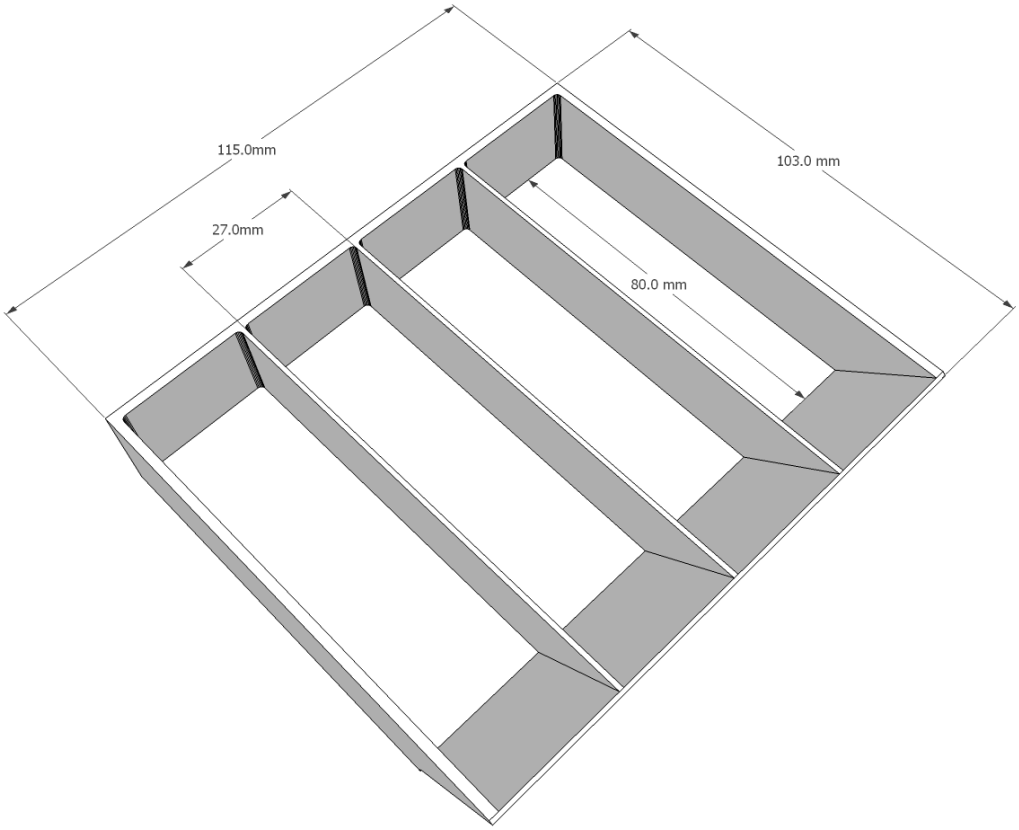

Figure 3.5: Diagram of a culturing tray with four separate compartments. Each compartment holds a single slide-sized substrate (25 mm × 75 mm). Separate compartments allow for the removal of a single slide without affecting adjacent slides. The sloped end on the tray permits easy access for removing slides.

Table 3.1: Contact angles recorded for each surface (± S.E., $n = 4$).

Substrate	Contact angle (θ_{AW})
PMMA	71.9° ± 2.8°
Agar	30.7° ± 2.6°
XL-Gel	55.7° ± 1.8°
XL-Gel-Lip	65.2° ± 1.4°

slides. Germling adhesion to the different surfaces was assessed after post-settlement times of 6, 12, 24 and 96 hours. Four replicates of each substrate were randomly selected to be assessed in the flow channel at each of the post-settlement times. Germling health and development were also checked at each of the post-settlement times by taking microscopic pictures at 10× magnification and measuring the diameters of germlings settled on the additional slides.

3.2.5 Adhesion assessment in flow channel

Germling adhesion strength to four replicates of each substrate was tested after settlement times of 6, 12, 24 and 96 hours. The flow channel was operated according to the protocol outlined in Appendix B. Briefly, fluid velocity in the channel increased from 0.42 m/s (5.4 Pa) at the lowest flow rate to 2.50 m/s (32.4 Pa) at the highest, increasing in six even steps 15 seconds in duration. Videos of germlings in the flow channel were processed in VLC to extract single frames from the beginning of the experiment and at the end of each flow step. Germling numbers were counted in each frame to establish the germling survival rate for each flow velocity and shear pressure.

3.3 Results and discussion

Initial attempts to form a model skin surface involved the casting of the cross-linked gelatin and lipid in a silicone skin-mould negative to achieve a skin model complete with human skin-like topography. However, the depth of gelatin required to fully transfer the features of the silicone skin negative was too great to be used with the flow channel as the "skin" feature height intruded into and blocked the 500 µm high channel. Instead, a thin layer of flat, cross-linked gelatin was used as a chemical approximation of skin for preliminary adhesion experiments.

3.3.1 Contact angle measurements

Contact angles were measured on the four substrates to establish their degree of surface hydrophobicity/hydrophilicity, or surface wettability. Surface wettability can be a significant factor when considering the adhesion speed and strength of marine organisms (Callow et al., 2000), where factors such as the spreading of an adhesive over a surface is a function of the nature of the adhesive compound, the substrate and the surrounding water. Table 3.1 shows the average contact angles recorded for each surface. All four of the test surfaces exhibited hydrophilic character, with θ_{AW} recorded to be less than 90° on each of the substrates. However, there was some variation

Table 3.2: Zygote/germling diameters with increasing settlement time. (± S.E., $n = 10$)

	Diameter (µm)			
Stage of Development	**PMMA**	**Agar**	**XL-Gel**	**XL-Gel-Lip**
Zygotes		65.9 ± 0.9		
6 h Germling	67.0 ± 1.3	67.1 ± 1.0	66.9 ± 0.7	65.4 ± 1.2
12 h Germling	68.5 ± 0.3	68.3 ± 0.6	70.0 ± 0.9	68.3 ± 0.6
24 h Germling	70.7 ± 0.6	71.4 ± 0.9	71.1 ± 0.9	70.8 ± 1.0
96 h Germling	75.6 ± 1.4	75.7 ± 1.3	75.6 ± 1.3	76.3 ± 1.5

in the relative degrees of hydrophilicity between the surface types; Agar demonstrated the most hydrophilic characteristics ($\theta_{AW} = 31^{\circ}$) as a result of the abundance of hydroxyl groups present in the saccharide monomers that constitute the polysaccharide chain (Finlay et al., 2010). PMMA was the least hydrophilic ($\theta_{AW} = 72^{\circ}$). PMMA is inherently hydrophobic, though modification by introduction of hydrophilic hydroxyl groups to the polymeric structure is often used to decrease hydrophobicity for biomedical applications (Kim et al., 2010). The two cross-linked gelatin surfaces fell in-between the other two surfaces, with the addition of the lipid component to the gelatin increasing the average contact angle by approximately 9° from $\theta_{AW} = 56^{\circ}$ for XL-Gel, to $\theta_{AW} = 65^{\circ}$ for XL-Gel-Lip. While one might expect the components of hydrogels to form highly hydrophilic surfaces, owing to their obvious affinity for water, relative differences in hydrophilicity between the carbohydrate based hydrogel (agar) and the two protein based hydrogels (XL-Gel and XL-Gel-Lip) can potentially be explained by the different degrees of freedom permitted by the carbohydrate and protein molecules. The rigid, linear structure of the polysaccharide chains of the agar hydrogel ensure that there is an abundance of hydroxyl groups present at the surface. Meanwhile, hydrophobic amino acids in the protein hydrogel may rotate to face the outer surface of the gelatin hydrogels, resulting in surfaces that are less hydrophilic than the carbohydrate hydrogels.

3.3.2 Germling health and development

Germling health was monitored on extra slides that were inoculated for this purpose. The four extra slides, one of each material, were cultivated under the same conditions as the slides used for adhesion testing but were not subjected to exposure to shear stress in the flow channel. Germlings appeared to develop healthily on all of the surfaces. Germlings were measured in order to compare the change in germling size across the different materials. Measurements were taken using a compound microscope and CMOS eyepiece camera described in section 2.5.3. Germling size refers to the diameter of the main body of the germling, which was measured by fitting a circle to the main body of the germling using the 3 point circle measurement mode in ToupView. An initial measurement was taken of 10 freshly fertilised eggs (zygotes), and further measurements were taken of 10 germlings after 6, 12, 24 and 96 hours development on each of the test surfaces. There was good agreement between germling sizes across the materials, with no significant differences in germling size associated with the different materials (Table 3.2 & Figure 3.6). Zygotes (0h), 6 h germlings and 12 h germlings were all approximately spherical (Figure 3.7, a and b). Morphology changes were noticeable after 24 hours post-settlement, with the beginnings of a proto-rhizoid and

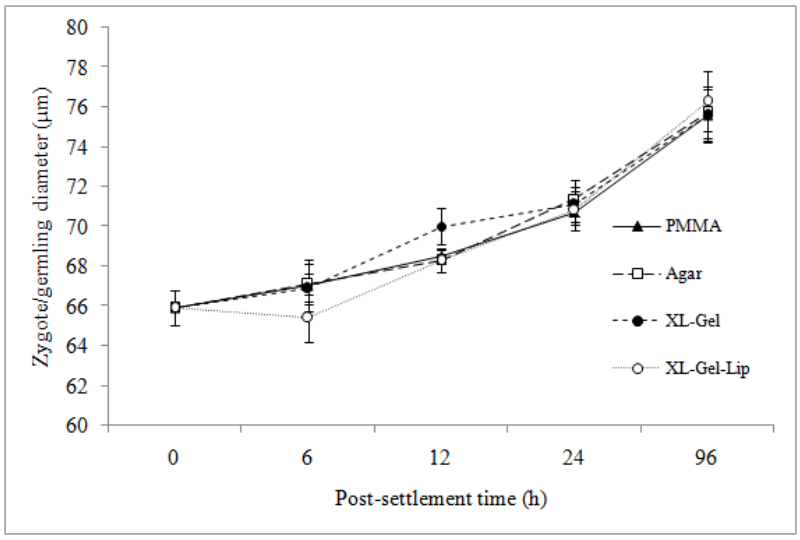

Figure 3.6: Chart of germling growth with time. Note good agreement across all materials at each settlement time. (± S.E., $n = 10$)

cell division becoming visible (Figure 3.7, c). After 96 hours settlement there is clear development of the rhizoid, with rhizoid length approximately one to two times the length of the main germling body (Figure 3.7, d). At 96 hours, the rhizoid also appears to contain vesicles of coloured material in the tip which is most likely adhesive containing physodes involved in the deposition of adhesive (arrows, Figure 3.7, d) (Schoenwaelder and Clayton, 1998).

3.3.3 Starting densities and recruitment rate

H. banksii zygotes take some time to achieve a basic degree of attachment to the substrate; as a result, there is some variation in settlement density/recruitment rate as a function of post-settlement time. As germling settlement density has a non-negligible effect on the actual drag force exerted on each germling (Dimartino et al., 2014), the initial settlement densities of settled germlings need to be comparable across the surfaces if the starting conditions are to be considered identical. Germlings were counted before exposure to any fluid flow/shear stress to obtain a measure for starting density. Images taken from the flow channel footage before exposure to any flow were analysed, and the germling numbers were divided by the area captured in the frame (8.58 mm^2) to obtain a germling density in terms of germlings per mm^2. Starting density values are presented in figure 3.8.

Starting densities were erratic and significantly lower after only 6 hours settlement time than at post-settlement times of 12 hours and above. After 6 hours settlement time *H. banksii* germlings are very weakly, if at all, adhered to the surface. The shear stress generated by removing the slide from its culture tray is therefore sufficient to dislodge a significant number of germlings. The low and variable starting density for the 6 hours settlement meant that statistical analyses of survival could not be performed on the 6 hour settlement samples. Two-factor analysis of vari-

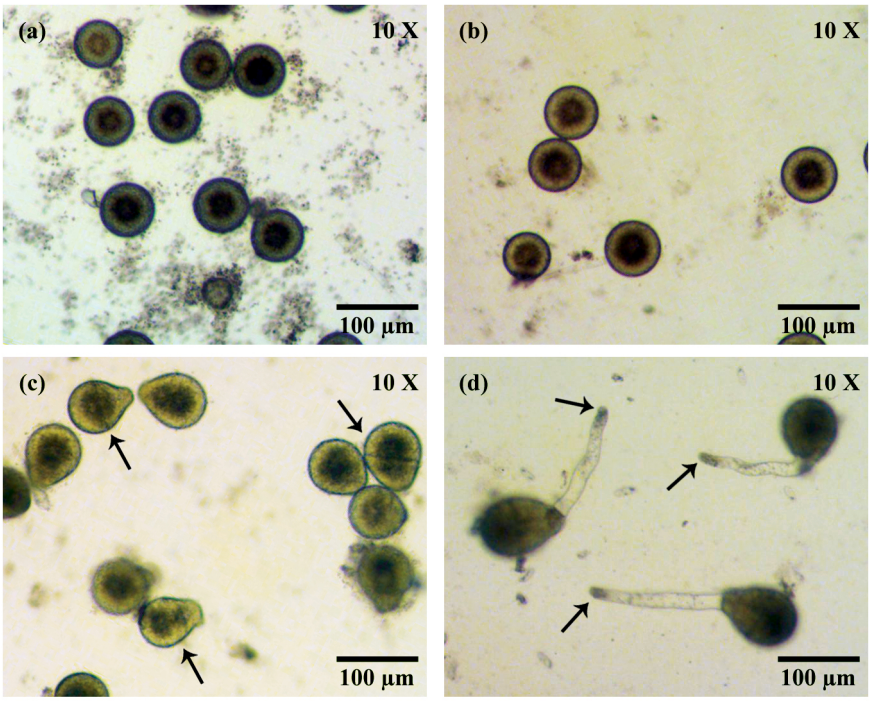

Figure 3.7: Germling development over time on PMMA. (a) After 6 hours settlement, germlings remain spherical and are surrounded by dead sperm cells. (b) After 12 hours settlement germlings are still spherical. (c) Some cell division visible (arrows) and polarisation visible in germlings after 24 hours. There is notable formation of a proto-rhizhoid. (d) Significant cell division apparent in germling body. Rhizoid now easily visible and adhesive-containing physodes can be seen in the rhizoid tipes (arrows).

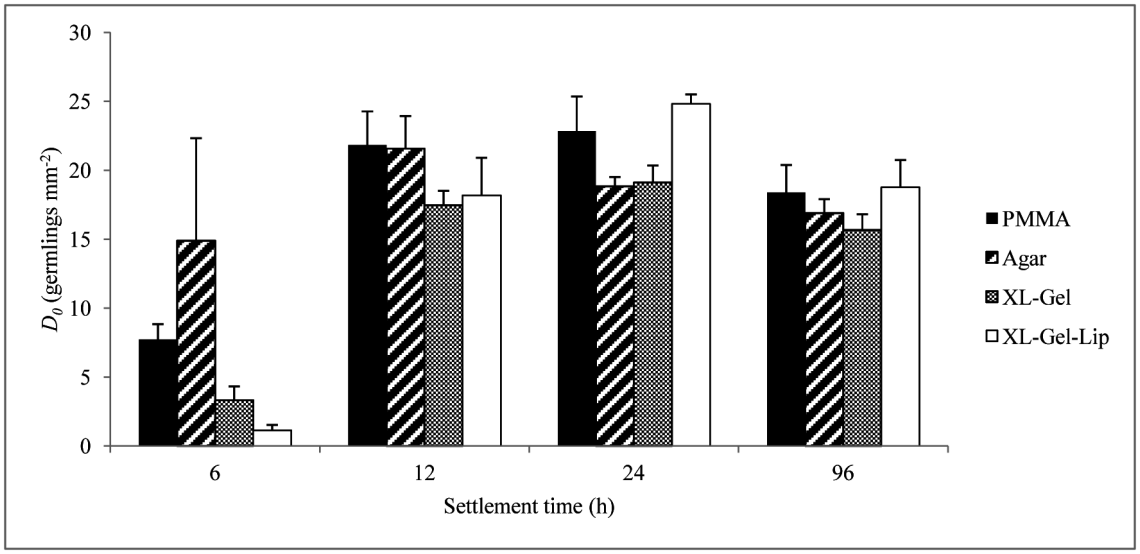

Figure 3.8: Germling settlement density prior to exposure to flow in the flow channel (D_0). Settlement density is low and inconsistent after only 6 hours settlement but stabilises at 12 hours settlement and above. (+ S.E., $n = 4$).

ance (ANOVA) performed on the settlement density values for the remaining settlement times (12, 24 and 96 hours) found no significant difference between either settlement times or material, so statistical analyses could be performed on the survival data under the assumption that starting conditions for germlings in the flow channel were equivalent. After 6 hours settlement there is a suggested, albeit non-significant, increased settlement density for the Agar surface. While this may be due to the uncontrolled variability in the stresses generated when transferring the slides to the channel, it is also possible that this is a result of rapid interactions between the polyphenolic adhesive secretion, the hydroxyl groups on the substrate and positive ions present in seawater, namely Ca^{2+} and Mg^{2+} (Stewart et al., 2011). Alternatively, an increased recruitment rate on Agar may lie in haloperoxidase-mediated cross-linking reactions between polyphenolic adhesive compounds and agarose chains in the substrate (Bitton et al., 2006; Vreeland et al., 1998; Bitton et al., 2007). Conversely, starting density appears to be lowest on the XL-Gel-Lip surface. Hydrophobic lipid chains embedded in the collagen network may negatively influence the adsorption of the adhesive to the substrate, possibly by limiting the electrostatic forces involved in adsorption and/or by sterically hindering adhesive access to receptive functional groups on the substrate. However, comparison of germling adhesion when exposed to shear stress shows that even exposure to the lowest flow rate was enough to remove the vast majority of germlings, suggesting that germling adhesion is defeated at shear stresses much lower than 5 Pa, regardless of substrate. These results are consistent with those of Taylor and Schiel (2003), who found that *H. banksii* zygotes exhibit feeble adhesion strength between 1 and 6 hours post-settlement. In their experiments, *H. banksii* zygotes were settled on fibre-based cement plates and challenged with artificially generated and natural waves. Survival rates of *H. banksii* were in the region of 50-60% after 6 hours post settlement. These are somewhat higher survival values for 6 hours post-settlement than found in my

Table 3.3: Two way ANOVA with replication showing significant variation in settlement density as a result of settlement time.

Effect	*df*	MS	F	P
Settlement time	3	694.051	28.71	0.0000
Substrate	3	59.1644	2.45	0.0751
Settlement time × substrate	9	50.275	2.08	0.0502
RES	48	24.1738		

experiment, but given the differences in substrate material and means of hydrodynamic challenge, direct comparison is difficult. Lack of variation in settlement density at 12 hours and above post-settlement times indicates that the adhesion achieved after 12 hours is strong enough to neglect the shear stresses exerted on the slides during transfer from the culture tray to the flow channel.

3.3.4 Flow channel adhesion experiments

Survival data were obtained for flow rates between 50 and 300 ml/min, corresponding to mean fluid velocities between 0.42 and 2.5 m/s. Reynolds numbers for these flow parameters were between 352 and 2111, indicating a laminar flow regime and the theoretical wall shear stress generated in the channel for this flow range was between 5 and 32 Pa. Germling survival (S_v) was calculated by comparing the surface density of attached germlings following exposure to each flow step (D_v) to the germling starting density (before exposure to any shear stress in the channel, D_0) using the following formula:

$$S_v = \frac{D_v}{D_0} \times 100$$

Percentage survival at each flow rate was calculated for each of the four replicates of each material and each settlement time. The mean survival value from the four replicates was then plotted against mean fluid velocity and shear stress to obtain a chart of survival with increasing hydrodynamic challenge.

A commonly used metric for the comparison of relative adhesion strength is to identify and compare a "critical shear stress", or a shear stress at which there is a 50% detachment of germlings. For the range of flows tested in this flow channel, with the exception of the 6 hour settlement data, germling survival did not drop below 50% so this could not be used to compare survival. Instead, survival across different treatments was compared by looking at percentage survival following exposure at a given flow rate. I used survival percentage after exposure to the maximum flow rate ($S_{2.5}$) as a parameter to compare relative adhesion strength between treatments. $S_{2.5}$ is also used in later chapters when comparing survival data.

3.3.4.1 Influence of post-settlement time on survival

While the recruitment rate of germlings to the substrate was clearly lower at 6 hours post-settlement time (see Section 3.3.3), differences in adhesion strength to the substrate as a function of settlement time had to be established by exposure to shear stress. Visually comparing survival rates between

Table 3.4: Two way ANOVA with replication showing significant variation in survival at conclusion of experiment as a result of settlement time but no significant variation as a result of substrate. This analysis only took into account survival data for settlement times of 12 hours and above.

Effect	*df*	MS	F	P
Settlement time	2	5527.888	32.23	0.0000
Substrate	3	194.701	1.14	0.3479
Settlement time × substrate	6	152.8771	0.89	0.5116
RES	36	171.5355		

12, 24 and 96 hours post-settlement data showed a significant difference in survival between 12 and 24 hours post-settlement time, where 12 hour post-settlement survival can be seen to decrease more rapidly with increasing flow, but little difference between 24 and 96 hours post-settlement time was observed (see Figures 3.9a, 3.9b, 3.9c and 3.9d). Analysis of $S_{2.5}$ was performed for 12, 24 and 96 hours post-settlement time. 6 hour post-settlement time data were ignored for this analysis as the condition of identical starting conditions was not met. ANOVA of survival data at the conclusion of the experiment indicated that there was a significant difference in survival attributable to post-settlement time ($p<0.001$). Student-Newman-Keuls (SNK) tests were performed in order to rank the means, which found that survival at the conclusion of the experiment was lower for 12 hours post-settlement time than for 24 and 96 hours post-settlement time. There was no significant difference in survival between 24 and 96 hours post settlement. There does appear to be some divergence in survival rates at the conclusion of the flow regime between 24 and 96 hours, although not significant, it might indicate that if the flow channel were capable of generating a higher shear stress we might begin to see further distinction between these two post-settlement times. The increase in survival with increasing post-settlement time was observed on all substrates.

3.3.4.2 Influence of substrate type on survival

Figure 3.10 compares the survival rate against shear stress for all of the substrates for all settlement times. While the change in survival with settlement time is clear, there is no difference in adhesion strength across the different substrates. This lack of variation in survival rate across the different surfaces suggests that the adhesive compound produced by *H. banksii* is capable of successful adhesion to a variety of surface types. While all of the substrates tested in this chapter were hydrophilic ($\theta_{AW} < 90°$), variations in the relative hydrophobicity of the substrates had no apparent impact on the adhesion strength of the *H. banksii* germlings. The consistency in adhesion strength to the various substrates could be due to the presence of a range of functional groups in the adhesive responsible for interacting with the substrate, such as glycoproteins and anionic polysaccharides (Vreeland et al., 1998; Petrone et al., 2011), allowing interaction with a range of substrates. Complementary functional groups present on the carbohydrate- and protein-based substrates, as well as the polar moieties of PMMA, provide a wealth of locations for adsorption interactions. The agar substrate is host to a high number of hydroxyl groups which could be involved in the formation of metal ion coordination complexes involving anionic components in the adhesive. The hydroxyl groups may also be used in the formation of haloperoxidase-mediated

cross-linked networks (Vreeland et al., 1998). Similarly, high proportions of glycine and argninie residues found in gelatine (Eastoe, 1955) could facilitate the formation of hydrogen bonds between a polar adhesive compound and the substrate. This observation of promiscuous adhesion success is interesting when compared to the performance of adhesives produced by other marine organisms. Substrate type had a significant effect on the adhesion strength of the diatoms *Navicula perminuta*, *Amphora coffeaformis* and *Craspedostauros australis*, where the critical shear stresses (50% removal) were found to be 25, 10 and 3 Pa, respectively, on glass, but more than 53, 24 and 17 Pa, respectively, on polydimethylsiloxane elastomer following 2 hours settlement (Holland et al., 2004). Conversely, adhesives produced by mussels also exhibit strong adhesion to a range of inorganic and organic surfaces (Lee et al., 2006). The ability to adhere to a range of surface types is essential for exploiting the variety of substrates present in the marine environment as a result of different inorganic (e.g. rock) chemistries and organic chemistries provided by the EPSs produced by bacterial biofilms that are commonly present on surfaces available for macroalgal colonisation.

3.3.4.3 Location of adhesive attachment and mode of detachment

The adhesion of the zygotes to the substrate appeared to take place in two stages. An initial adhesion stage occurs immediately after fertilisation, where an adhesive material present on the surface of the new zygote comes into contact and forms a bond with the substrate. As the germling develops and the rhizoid grows, the location of adhesion migrates to the rhizoid tip while the adhesive bond between the germling body and the substrate weakens. This transfer of adhesion locus from germling body to rhizoid tip allows the germling body to move away from the substrate and lift higher into the water body. Evidence for the transfer of attachment point to the rhizoid as germlings aged was observed as a change in the way the germlings were removed from the surface during adhesion testing. Using the video footage recorded during the experiment it was noted that younger germlings (6, 12 and 24 hours old), which did not exhibit much rhizoid development, tended to detach in a single event; one moment they were still attached to the substrate, the next they had been removed. However, for older germlings (96 hours) with a somewhat developed rhizoid, it was noted that, in some instances, adhesion between the germling body and the substrate was disrupted first and followed by the detachment of the rhizoid. On video this appeared as the free moving germling body rotating about the tip of the rhizoid which remained stationary (Figure 3.11). This observation at 96 hours post-settlement indicates that the transfer of adhesion locus occurs sometime between 24 and 96 hours, signifying the start of the next step in the germling's life story where it begins to grow out into the water body for better nutrient access and waste removal. Germling removal on the 96 hour settlement samples were classified as either a total detachment event (type 1) or a detachment where the germling body detaches first, followed by the rhizoid (type 2). A graph showing the incidence of type 1 and type 2 detachments is shown on page 45 (Figure 3.12). From the graph, it can be seen that germlings on Agar and XL-Gel were more likely to detach in a single event (type 1), while germlings on PMMA and XL-Gel-Lip were more likely to detach at the germling body first, followed by the rhizoid (type 2). Comparing these detachment modes with surface wettability in Section 3.3.1, it appears that mode 1 detachments

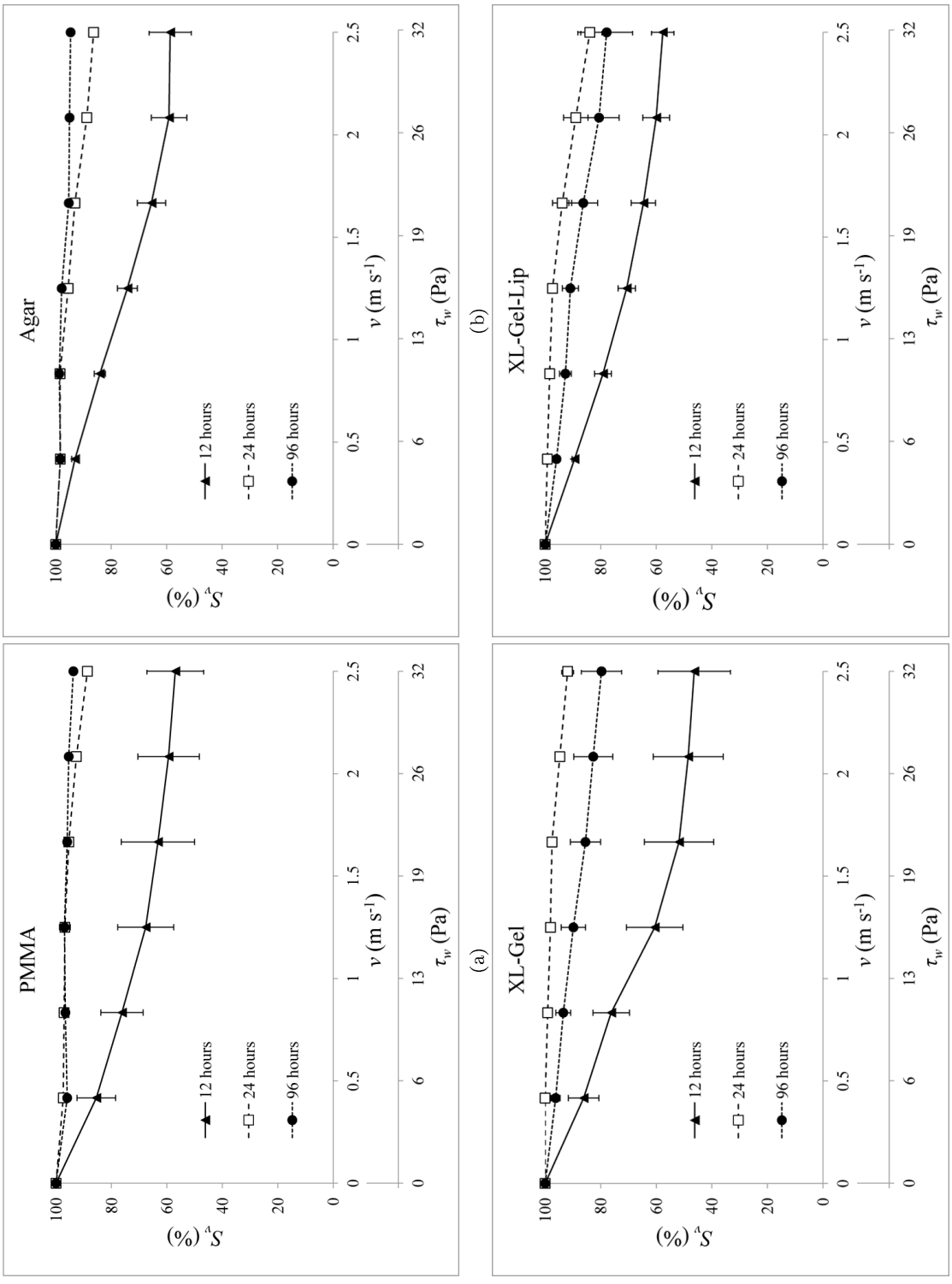

Figure 3.9: Germling survival with increasing flow rate for (a) PMMA, (b) Agar, (c) XL-Gel and (d) XL-Gel-Lip. ($\pm$ S.E., $n = 4$).

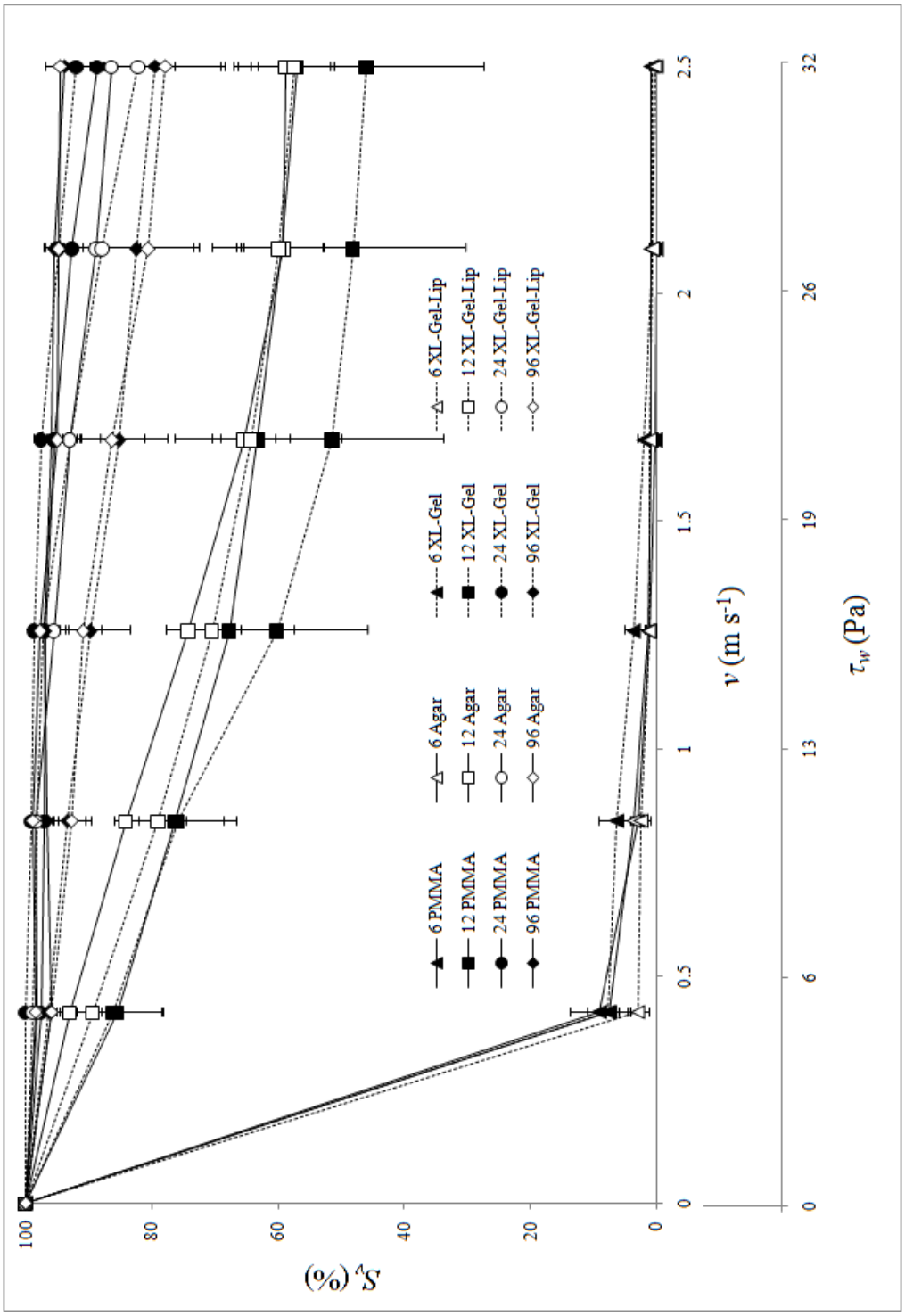

Figure 3.10: Graph showing survival (S_v) on all materials for all settlement times (including 6 hours). Note the similar survival rates between the different materials at each settlement time. ($\pm$ S.E., $n = 4$).

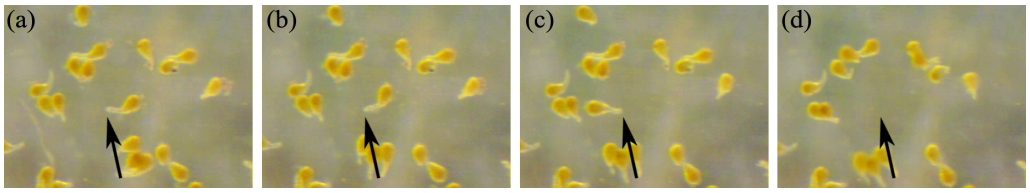

Figure 3.11: Series of frames showing the removal of a *Hormosira banksii* germling. Flow velocities are as follows: (a) = 0.83 m/s, (b) = 1.25 m/s, (c) = 1.67 m/s, (d) = 2.08 m/s. Note rotation of germling around fixed point at end of the rhizoid before complete removal in (d).

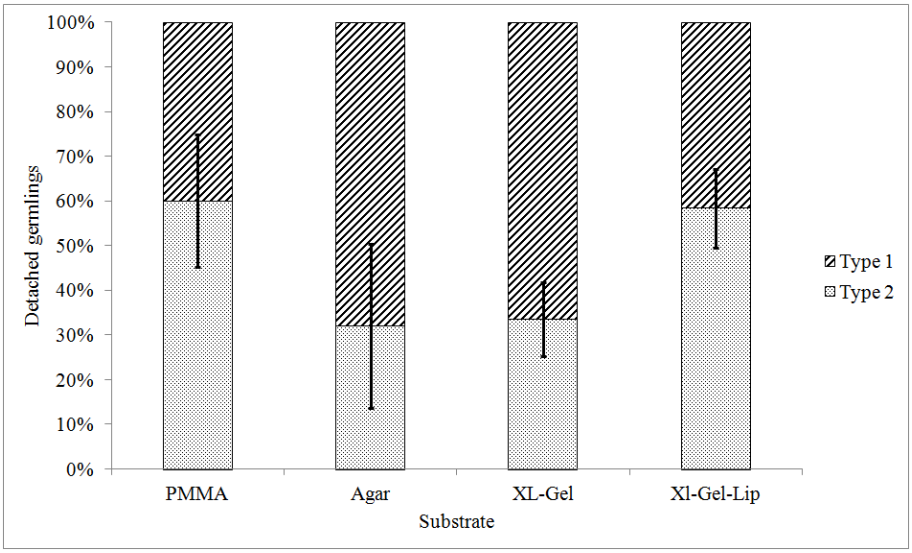

Figure 3.12: Ratio of type 1 to type 2 germling removal on substrates after 96 hours settlement. (± S.E., n = 4).

occur more on surfaces with higher wettability, while the inverse is true for mode 2 detachments. It is possible that the adhesive deposited at the rhizoid adheres more successfully to less hydrophilic substrates than the adhesive responsible for the initial connection between the germling body and the substrate. However, these results should be considered carefully because the data were derived from still images which might not accurately represent the germling detachment type. Further studies into the mechanism of detachment, including filming at high frame rates, would help to further delineate the germling adhesion and detachment processes.

3.4 Conclusions

In this chapter the flow channel was used to observe the adhesion strength of the marine macroalgae *H. banksii* to surfaces of biomedical relevance, namely PMMA and three hydrogel surfaces, two of which were intended to mimic, to some degree, human skin. The goal of the experiment was to establish whether or not *H. banksii* warranted further investigation as potential inspiration for the development of synthetic, wet-resistant adhesives for use in medical applications, such as in place of sutures. Results from the experiment indicate that, while adhesion strength clearly increases with post-settlement time, there is no difference in adhesion strength between the different substrates. There is, however, an apparent difference in detachment type across the different substrates, the mechanism of which warrants further investigation. These findings suggest that the mechanism of adhesion employed by *H. banksii* zygotes is somewhat promiscuous, and is capable of binding with a similar degree of strength to a range of surfaces. Also notable was the absence of a critical shear stress at which germling survival decreased dramatically. Rather, there appears to be a relatively even distribution of adhesion strengths in a given population. Given its ability to adhere to a range of substrates, the adhesive produced by *H. banksii* does warrant further investigation with a view to developing adhesives with medical applications.

Bibliography

Applebaum, J. S., T. Zalut, and D. Applebaum (1993, July). The use of tissue adhesion for traumatic laceration repair in the emergency department. *Annals of Emergency Medicine 22*(7), 1190–1192.

Bertoni, F., N. Barbani, P. Giusti, and G. Ciardelli (2006, May). Transglutaminase Reactivity with Gelatine: Perspective Applications in Tissue Engineering. *Biotechnology Letters 28*(10), 697–702.

Bitton, R., M. Ben-Yehuda, M. Davidovich, Y. Balazs, P. Potin, L. Delage, C. Colin, and H. Bianco-Peled (2006, September). Structure of Algal-Born Phenolic Polymeric Adhesives. *Macromolecular Bioscience 6*(9), 737–746.

Bitton, R., M. Berglin, H. Elwing, C. Colin, L. Delage, P. Potin, and H. Bianco-Peled (2007, December). The Influence of Halide-Mediated Oxidation on Algae-Born Adhesives. *Macromolecular Bioscience 7*(12), 1280–1289.

Bitton, R., E. Josef, I. Shimshelashvili, K. Shapira, D. Seliktar, and H. Bianco-Peled (2009, June). Phloroglucinol-based biomimetic adhesives for medical applications. *Acta Biomaterialia 5*(5), 1582–1587.

Bixler, G. D., A. Theiss, B. Bhushan, and S. C. Lee (2014, April). Anti-fouling properties of microstructured surfaces bio-inspired by rice leaves and butterfly wings. *Journal of Colloid and Interface Science 419*, 114–133.

Callow, M. E., J. A. Callow, L. K. Ista, S. E. Coleman, A. C. Nolasco, and G. P. López (2000, August). Use of Self-Assembled Monolayers of Different Wettabilities To Study Surface Selection and Primary Adhesion Processes of Green Algal (Enteromorpha) Zoospores. *Applied and Environmental Microbiology 66*(8), 3249–3254.

Charkoudian, J. C., P. Technologies, and D. O. The (1988). A model skin surface for testing adhesion to skin. *Journal of Cosmetic Science 39*(4), 225–234.

Cohen, B., O. Pinkas, M. Foox, and M. Zilberman (2013, November). Gelatin-alginate novel tissue adhesives and their formulation-strength effects. *Acta Biomaterialia 9*(11), 9004–9011.

Dimartino, S., A. V. Mather, T. Alestra, S. Nawada, and M. Haber (2014, February). Experimental and computational analysis of a novel flow channel to assess the adhesion strength of sessile marine organisms. *Interface Focus 5*(1), 20140059.

Dürr, S. and J. Thomason (2009). *Biofouling* (1 ed.). Hoboken: Wiley.

Eastoe, J. E. (1955, December). The amino acid composition of mammalian collagen and gelatin. *Biochemical Journal 61*(4), 589.

Finlay, J. A., S. M. Bennett, L. H. Brewer, A. Sokolova, G. Clay, N. Gunari, A. E. Meyer, G. C. Walker, D. E. Wendt, M. E. Callow, J. A. Callow, and M. R. Detty (2010). Barnacle settlement and the adhesion of protein and diatom microfouling to xerogel films with varying surface energy and water wettability. *Biofouling 26*(6), 657–666.

Fletcher, M. and J. H. Pringle (1985, March). The effect of surface free energy and medium surface tension on bacterial attachment to solid surfaces. *Journal of Colloid and Interface Science 104*(1), 5–14.

Fletcher, R. L. and M. E. Callow (1992a). The settlement, attachment and establishment of marine algal spores. *British Phycological Journal 27*(3), 303–329.

Frazer, R. Q., R. T. Byron, P. B. Osborne, and K. P. West (2005). PMMA: An Essential Material in Medicine and Dentistry. *Journal of Long-Term Effects of Medical Implants 15*(6), 629–639.

Holland, R., T. M. Dugdale, R. Wetherbee, A. B. Brennan, J. A. Finlay, J. A. Callow, and M. E. Callow (2004). Adhesion and motility of fouling diatoms on a silicone elastomer. *Biofouling 20*(6), 323–329.

Jayant, R. D., M. J. McShane, and R. Srivastava (2009). Polyelectrolyte-coated alginate microspheres as drug delivery carriers for dexamethasone release. *Drug delivery 16*(6), 331–340.

Kim, K., S. W. Park, and S. S. Yang (2010, June). The optimization of PDMS-PMMA bonding process using silane primer. *BioChip Journal 4*(2), 148–154.

Lee, H., N. F. Scherer, and P. B. Messersmith (2006, August). Single-molecule mechanics of mussel adhesion. *Proceedings of the National Academy of Sciences 103*(35), 12999–13003.

Leigh, J. A. (1975, July). Use of PMMA in expansion dental implants. *Journal of Biomedical Materials Research 9*(4), 233–242.

Lir, I., M. Haber, and H. Dodiuk-Kenig (2007). Skin surface model material as a substrate for adhesion-to-skin testing. *Journal of Adhesion Science and Technology 21*(15), 1497–1512.

Ninan, L., J. Monahan, R. L. Stroshine, J. Wilker, and R. Shi (2003, October). Adhesive strength of marine mussel extracts on porcine skin. *Biomaterials 24*(22), 4091–4099.

Petrone, L., R. Easingwood, M. F. Barker, and A. J. McQuillan (2011, March). In situ ATR-IR spectroscopic and electron microscopic analyses of settlement secretions of Undaria pinnatifida kelp spores. *Journal of the Royal Society, Interface / the Royal Society 8*(56), 410–422.

Qurrat-ul-Ain, S. Sharma, G. K. Khuller, and S. K. Garg (2003, April). Alginate-based oral drug delivery system for tuberculosis: pharmacokinetics and therapeutic effects. *Journal of Antimicrobial Chemotherapy 51*(4), 931–938.

Schoenwaelder, M. E. A. and M. N. Clayton (1998, December). Secretion of Phenolic Substances into the Zygote Wall and Cell Plate in Embryos of Hormosira and Acrocarpia (fucales, Phaeophyceae). *Journal of Phycology 34*(6), 969–980.

Stewart, R. J., T. C. Ransom, and V. Hlady (2011, June). Natural underwater adhesives. *Journal of Polymer Science Part B: Polymer Physics 49*(11), 757–771.

Sullivan, T. and F. Regan (2011, December). The characterization, replication and testing of dermal denticles of Scyliorhinus canicula for physical mechanisms of biofouling prevention. *Bioinspiration & Biomimetics 6*(4), 046001.

Taylor, D., S. Delaux, C. Stevens, R. Nokes, and D. Schiel (2010). Settlement rates of macroalgal propagules: Cross-species comparisons in a turbulent environment. *Limnology and Oceanography 55*(1), 66.

Taylor, D. I. and D. R. Schiel (2003, June). Wave-related mortality in zygotes of habitat-forming algae from different exposures in southern New Zealand: the importance of 'stickability'. *Journal of Experimental Marine Biology and Ecology 290*(2), 229–245.

van Wachem, P. B., T. Beugeling, J. Feijen, A. Bantjes, J. P. Detmers, and W. G. van Aken (1985, November). Interaction of cultured human endothelial cells with polymeric surfaces of different wettabilities. *Biomaterials 6*(6), 403–408.

Vreeland, V., J. H. Waite, and L. Epstein (1998). Minireview: Polyphenols and Oxidases in Substratum Adhesion by Marine Algae and Mussels. *Journal of Phycology 34*(1), 1–8.

Yoshizawa, K. and T. Taguchi (2014, January). Enhanced Bonding Strength of Hydrophobically Modified Gelatin Films on Wet Blood Vessels. *International Journal of Molecular Sciences 15*(2), 2142–2156.

Chapter 4

Adhesion to Common Materials

4.1 Introduction

The pursuit of novel, biomimetic adhesives and the design of fouling-resistant surfaces would both benefit from the characterisation of the interaction between bio-foulers and their substrates. In Chapter 3, I looked at the adhesion strength of *Hormosira banksii* to surfaces of biomedical relevance, namely two protein based hydrogels, a carbohydrate based hydrogel and poly(methyl methacrylate) (PMMA). The aim of Chapter 3 was to establish *H. banksii*'s suitability as a candidate species as inspiration for biomimetic adhesives with applications in biomedicine. Naturally, an extension of this research is to study additional bio-adhesive-producing aquatic species, as well as expand the range of substrates under investigation.

The ability of *H. banksii* to adhere with equal strength to PMMA and a range of hydrogels suggests the production of a promiscuous adhesive capable of interacting with a range of surface chemistries (see Chapter 3). *H. banksii* typically occupies sheltered regions in the intertidal zone, and is naturally exposed to lower hydrodynamic forces than, for example, *Durvillaea antarctica*, which occupies exposed areas in the intertidal zone. Specific habitat aside, *H. banksii* and *D. antarctica* are similar species with similar life stories; both species reproduce sexually without alternation of generations. The male and female gametes of both species combine to form a diploid zygote which measures tens of microns in diameter (*H. banksii* ≈ 70 µm, *D. antarctica* $= 35$ µm). Zygotes of both species are non-motile, so the distribution and settlement location of zygotes is governed by the motion of surrounding water. Zygote settlement for these species is therefore relatively passive, and one might speculate that being unable to actively select a substrate, these species would benefit from being able to readily adhere to whatever substrate is available. Research by Taylor and Schiel (2003) shows that *D. antarctica* achieves more rapid adhesion to the substrate than *H. banksii*, but this research only looked at one surface type and germlings were challenged by natural and artificially generated waves, the hydrodynamics of which are difficult to quantify.

In this chapter, I aim to compare the adhesion strength of zygotes of the two fucoid algae, *D. antarctica* and *H. banksii*, to four commonly used materials: glass, poly(methyl methacrylate),

polytetrafluoroethylene and polished stainless steel. These materials were chosen to represent materials commonly used in fields such as medicine, food processing, aquaculture and engineering, and commonly involved in adhesion and fouling processes. I was also interested in the impact of settlement time on the adhesion strength of the different species. The novel flow channel described in Chapter 2 was used to test germling adhesion/survival rates against increasing shear pressures. Relevant settlement times were selected for each species, ranging from 6 to 48 hours for *D. antarctica* and 12 to 96 hours for *H. banksii*. I hypothesised that, given its persistence in exposed locations and consequent persistence in the face of substantial hydrodynamic challenge, *D. antarctica* will exhibit both more rapid and more robust adhesion to the various substrates than *H. banksii*.

4.2 Materials and methods

4.2.1 Substrate selection and justification

Four materials were chosen for testing the adhesion strength between *H. banksii* and *D. antarctica* and the substrate. These were glass, poly(methyl methacrylate) (PMMA), virgin polytetrafluorethylene (PTFE) and polished stainless steel.

Glass was chosen because it is commonly used for microscope slides, which the flow channel was specifically designed to accommodate. Glass is a basic silicate material made primarily of networked silica dioxide (SiO_2) molecules. The surface of glass is covered in hydroxyl groups bound to silicon atoms, allowing polar interactions with water molecules and making the surface hydrophilic. The SiO_2 composition of glass is not dissimilar to the structure of silicate rocks, so the glass slides could potentially be considered a chemical approximation of the inorganic rock substrates present in various marine environments, albeit significantly smoother. The glass slides used in these experiments were standard microscope slides measuring approximately 25mm × 75 mm × 1 mm.

PMMA slides (25 mm × 75 mm) were cut from a 2 mm thick sheet of bulk PMMA (Dotmar Engineering Plastics). PMMA is a transparent thermoplastic polymer made of repeating methyl methacrylate monomers, and is commonly sold under the names Perspex, Acrylite, Lucite and Plexiglass. PMMA is not as strong as polycarbonate, but is cheaper to produce and is often used as a lightweight alternative to soda-lime and borosilicate glasses. The surface of PMMA is hydrophobic, although chemical modification can be used to create a hydrophilic surface. PMMA is largely biocompatible, so it is widely used in medicinal applications such as in intraocular lenses, bone cements and dentures (Frazer et al., 2005; Leigh, 1975). PMMA is also widely used in scientific and industrial applications, from microfluidic channel formation for lab-on-a-chip applications (Mathur et al., 2009; Hong et al., 2010), to windows of high-speed aircraft (Weaver et al., 1993).

Polytetrafluoroethylene (PTFE), sold under the brand name Teflon, is a hydrophobic, non-stick substance used in a variety of applications such as the coating of cookware, piping and gaskets. PTFE is formed from monomers of tetrafluoroethylene, the strong bond between carbon and fluorine rendering it highly chemically resistant, while the high electronegativity of fluorine prevents

polar interactions at the surface, making it hydrophobic. PTFE's low reactivity makes it suitable for the transport of reactive and corrosive chemicals, while its non-stick properties also allow it to be an effective lubricant for moving parts in machinery and as an antifouling coating. 75 mm × 25 mm slides were cut from a sheet of 1 mm thick virgin Teflon sheet (TETRON S, Dotmar Universal Plastics) for use as a hydrophobic non-stick substrate.

Stainless steel is used in a wide range of applications, again including biomedical, food and chemical processing, and structural engineering. Stainless steel is a metal alloy consisting of iron and carbon with additional chromium and nickel, the proportions of which depend on the specific type of stainless steel. For experiments in this chapter I used polished stainless steel type 304 cut into 75 mm × 25 mm slides at 1.6 mm thick. Type 304 stainless steel typically has a composition of 18% chromium, 8% nickel, 2% manganese, 1% silicon, 0.2% phosphorus, at least 0.15% sulphur and carbon, and 0.6% molybdenum, with the remainder made up of iron.

From here on the substrates will be referred to as glass, PMMA, PTFE and stainless steel.

4.2.2 Surface characterisation

4.2.2.1 Atomic force microscopy

Atomic force microscopy (AFM) was performed on each of the surfaces to establish the degree of roughness and to estimate if the surface roughness was of a sufficient magnitude to impact the adhesion success of the settled zygotes. Ideally, the physical (topographical) nature of the substrates would be identical, as chemical composition is the property that we were most interested in testing. AFM scans were performed using a Digital Instruments Dimension 3100 Atomic Force Microscope on tapping mode. The scan area was 100 µm x 100 µm, the largest resolution that can be achieved by this model. The scan rate was set to 0.1 lines/s, and scans were taken in triplicate from three randomly selected spots on single slides of each material type.

4.2.2.2 Contact angle measurement

Contact angle measurements were taken using the same procedure as described in Chapter 3. Advancing contact angles (θ_{AW}) were measured following deposition of a 2 µl droplet of deionized water on each of the four surfaces. 10 images of the water droplet, spaced 6 s apart, were taken following a 30 s delay after initial deposition of the water droplet. The ten images were analysed using the associated goniometer software (KSV CAM Software v 4.01), which fit the droplet shape to the Young-Laplace equation. The average contact angle was then calculated across the ten images and this average represented the contact angle measurement for a single replicate. Contact angle measurements were performed four times on each substrate and a final average was obtained from these four measurements.

4.2.3 Substrate preparation

4.2.3.1 Cleaning the substrates

Slides were handled using rubber gloves at all times to prevent contamination with dirt and oils from skin. The slides were first soaked in hot water with dishwashing detergent for one hour before being physically cleaned using a soft sponge to avoid scratching the surfaces. The slides were then rinsed with copious amounts of distilled water to remove any detergent residue and left to dry under ambient conditions on a paper towel.

4.2.3.2 Soaking the substrates

The dried slides were transferred to the settlement trays (described in Chapter 3), 20 ml of fresh, 0.22 µm filtered seawater was then poured into each compartment of the settlement trays. Slides were left to soak in the seawater for at least 24 hours before they were inoculated with zygotes of *D. antarctica* or *H. banksii*.

4.2.4 Seaweed collection, gamete release and settlement

4.2.4.1 *Durvillaea antarctica*

D. antarctica samples were collected from a rocky platform between Breeze Bay and Livingstone Bay, Lyttelton harbour (43°35'54.71"S, 172°46'24.29"E) in September 2014. Individual blades of *D. antarctica* were cut from adult plants using a sharp knife. An effort was made to sample blades from a large number of different plants to ensure collection of both male and female reproducing plants with diverse genetics. *D. antarctica* samples were treated in the same way as *H. banksii* samples in Chapter 3 to induce gamete release. The collected blades of *D. antarctica* were washed in filtered seawater before being stored at 6°C overnight in the dark. The following day the *D. antarctica* blades were laid out on plastic trays and placed under a halogen light source (500 W x 2). The exposure to heat and light following storage at 6°C stimulated the release of gametes which appeared on the surface of the blade. Gamete sex was determined by colour; brown bubbles indicated female gametes (eggs), while a colourless/milky-white slime indicated male gametes (sperm). The male and female reproducing plants were each rinsed in separate beakers of 0.22 µm filtered seawater to prepare sperm and egg suspensions (Figure 4.1). The two gamete suspensions were mixed together in a beaker to trigger fertilisation and form what I will refer to as a zygote suspension. The zygote suspension was gently agitated periodically to keep the gametes mixed and prevent gamete settlement in the beaker. The volume of the zygote suspension was adjusted with fresh, filtered seawater to achieve a concentration of approximately 20,000 zygotes per ml. Constant, low level agitation was maintained using a magnetic stirrer while 5 ml of the zygote suspension was transferred to each of the settlement trays containing a substrate slide. Settled zygotes (here on referred to as germlings) were cultured at 15°C under a pair of fluorescent bulbs (light intensity = 40 µmol photons/m^2/s PAR) on a 12 hours:12 hours on:off cycle. Seawater in the culturing tray was replaced at a rate of 50% every 24 hours. Four replicates of each of the four substrates were

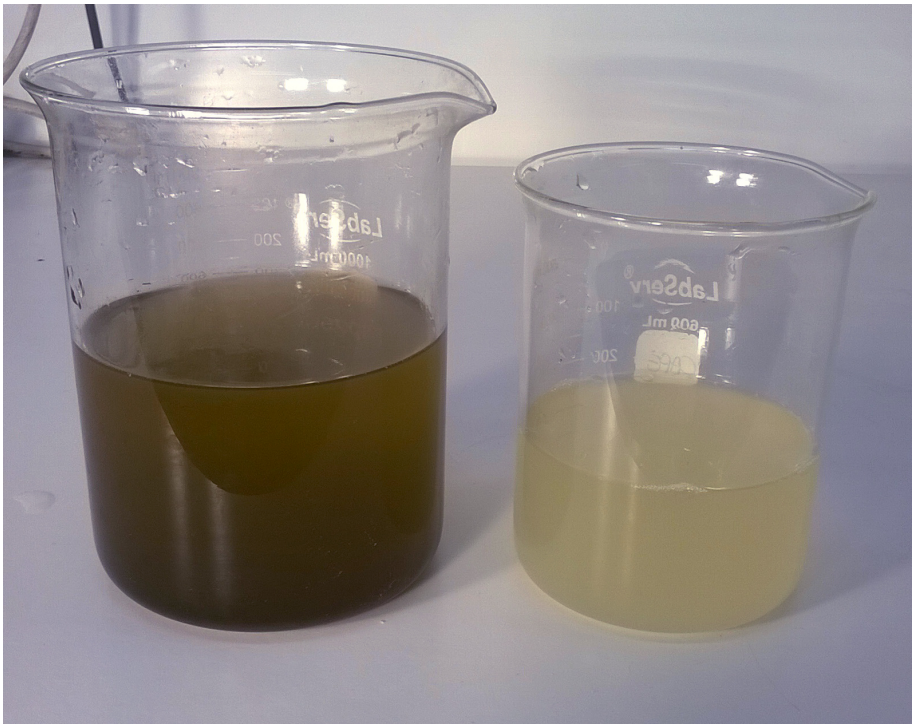

Figure 4.1: Beakers containing *D. antarctica* gamete suspensions. The larger beaker on the left contains eggs in suspension, the beaker on the right contains sperm in suspension.

selected at random following settlement times of 6, 12, 24 and 48 hours and used for adhesion testing in the flow channel.

4.2.4.2 *Hormosira banksii*

H. banksii was collected from Pile Bay, Lyttelton Harbour (43°37'13.6"S, 172°45'38.7"E) in January 2015. *H. banksii* gamete release procedure was identical to that performed in Chapter 3. The *H. banksii* settlement procedure differed slightly from that in Chapter 3; due to low gamete yield causing a low concentration zygote solution (approximately 1,000 germlings per ml), zygote settlement density was increased through the use of 3D printed settlement guides. As only the central portion of the slide would be observed or tested in the flow channel, it was not necessary to cover the entire slide in zygotes. Zygote settlement area was restricted using the settlement guide. The settlement guide has internal dimensions measuring 5 mm wide and 40 mm long, giving a vertical channel with a cross sectional area of 200 mm^2 (Figure 4.2a). One guide was placed in each compartment of a settlement tray containing a slide and filtered seawater. 5 ml zygote suspension was then pipetted into the middle of the settlement guide. Given the total area of a standard microscope slide is 1875 mm^2, use of the guide reduces available surface area for the zygotes to settle by approximately 90%. Figure 4.2b shows four settlement guides in place in a culturing tray. After giving the zygotes a few minutes to sink and come in contact with the substrate the settlement guide is removed from the culturing tray to ensure it doesn't interfere with exposure of the settled

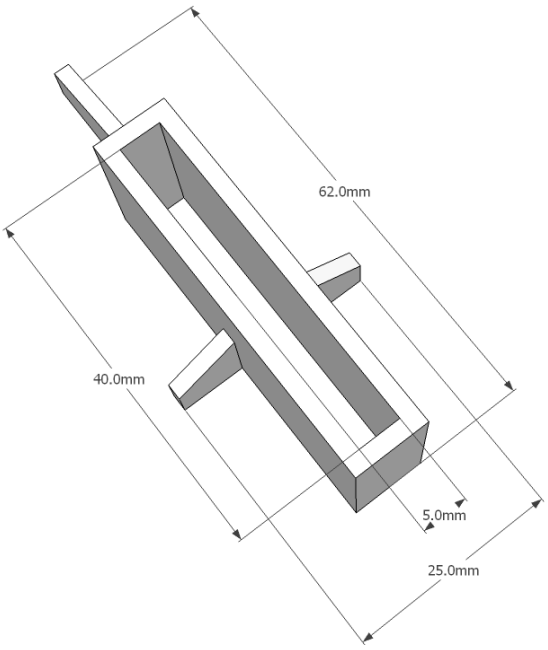

(a)

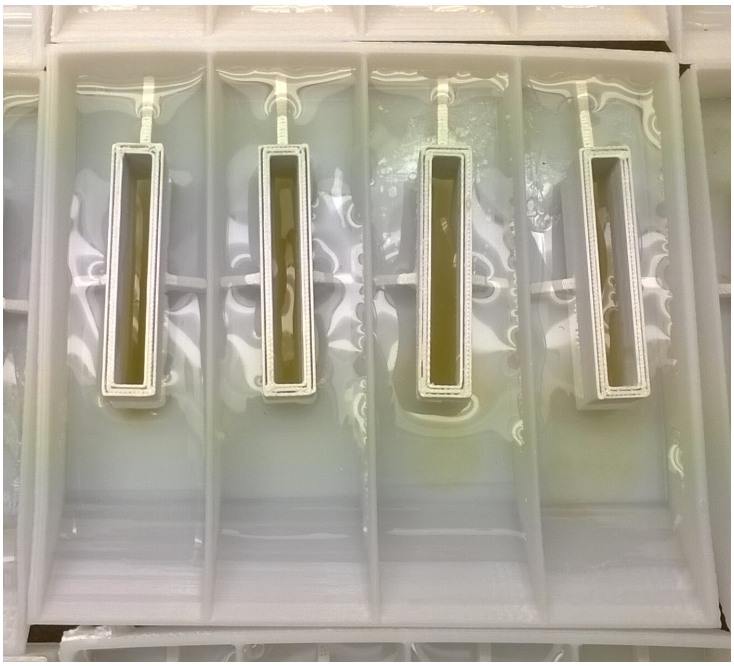

(b)

Figure 4.2: (a) Diagram of a settlement guide including dimensions. The small protrusions on the sides and at the end ensure that the guide sits at the centre of the culturing tray. (b) Photograph showing four settlement guides in place in a culturing tray. Zygotes have already been added in this picture, hence the brown-green colour within the guides. Settlement guides effectively limit the area in which the zygotes can settle on the substrate.

Table 4.1: R_a and R_{max} measurements for the four substrates (± S.E., n = 3).

Substrate	R_a (nm)	R_{max} (nm)
Glass	1.20 ± 0.01	225 ± 7.07
PMMA	63.47 ± 16.82	856.67 ± 244.68
PTFE	121.43 ± 26.28	1235.67 ±100.79
Stainless steel	15.97 ± 1.87	411.67 ± 55.84

zygotes to light. Culturing conditions (temperature and light) were the same as for *D. antarctica* gametes. Four settlement times were selected for adhesion testing with the flow channel: 12, 24, 48 and 96 hours. No adhesion testing was performed after 6 hours settlement as the results in Chapter 3 indicate severely low levels of adhesion when germlings are only given 6 hours to settle. Three replicates[1] of each of the four substrates were selected at random following settlement times of 12, 24, 48 and 96 hours and used for adhesion testing in the flow channel.

4.2.5 Flow channel adhesion testing

The flow channel was operated according to the procedure outlined in Appendix B for all substrate replicates for both species. Briefly, fluid velocity in the channel increased from 0.42 m/s (5.4 Pa) at the lowest flow rate to 2.50 m/s (32.4 Pa) at the highest, increasing in six even steps 15 seconds in duration. Videos of germlings in the flow channel were processed in VLC to extract single frames from the beginning of the experiment and at the end of each flow step. Germling numbers were counted in each frame to establish the germling survival rate for each flow velocity and shear pressure.

4.3 Results and discussion

4.3.1 Roughness measurements

AFM scans were performed on each of the four substrates to measure surface roughness. The two parameters used for comparison were R_a and R_{max}. R_a is the arithmetic average of the absolute values of the profile height deviations from the mean line and is the most widely used metric for comparing roughness. R_{max} is simply the distance between the top of the highest peak and the bottom of the lowest valley on a sample, so represents the largest possible feature depth that can be found on a surface. AFM data were analysed using NanoScope Analysis (version 1.40) and flattening and plane fitting of surfaces were performed as needed prior to roughness analysis. R_a and R_{max} values are reported in Table 4.1. A chart of R_a and R_{max} is shown in Figure 4.3, and 3 dimensional representations of each surface are shown in Figure 4.4 (a – d). Glass had the lowest roughness, with an R_a of 1.20 nm and an R_{max} of 225 nm. The seemingly high R_{max} value for glass was likely caused by the presence of dust particles on the glass surface (spikes in Figure

[1] Three replicates of each substrate were seeded with *H. banksii* while four of each substrate were prepared with *D. antarctica*. Between the two experiments I changed my protocol, deeming three replicates sufficient, which incidentally helped increase settlement numbers in the event of low gamete yield/zygote concentration.

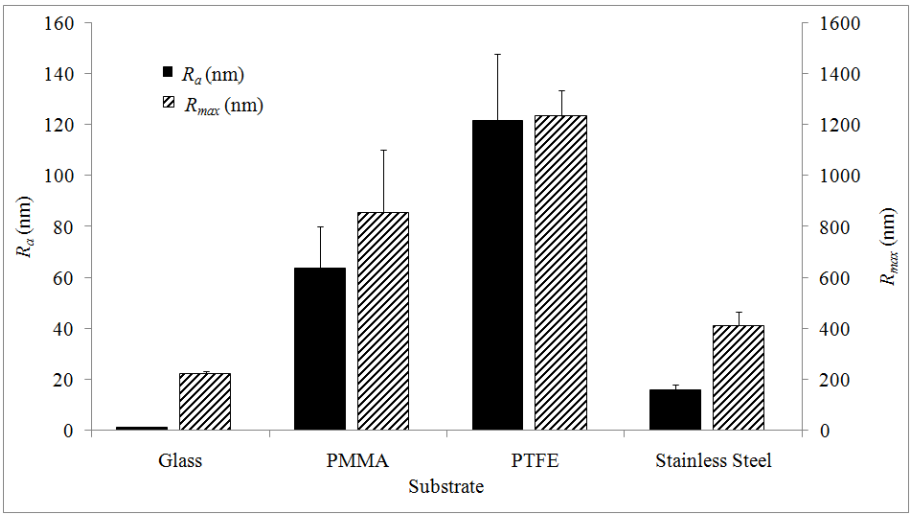

Figure 4.3: R_a and R_{max} values for each of the four substrates. R_{max} generally appears to be an order of magnitude greater than R_a, except on glass, where it is two orders of magnitude greater. R_a values are plotted against the left axis, R_{max} against the right. (± S.E., n = 3)

Table 4.2: Advancing contact angles as measured on all four substrates (± S.E., n = 4).

Substrate	Advancing contact angle (θ_{AW})
Glass	57° ± 2°
PMMA	74° ± 5°
PTFE	103° ± 1°
Stainless steel	57° ± 2°

4.4a). Stainless steel was the next smoothest substrate (R_a = 16 nm, R_{max} = 412 nm), followed by PMMA (R_a = 63 nm, R_{max} = 857 nm). PTFE had the highest roughness, having an R_a of 121 nm and with an R_{max} of 1236 nm (approximately 1.2 µm) PTFE is the only surface to exhibit a degree of roughness, or texture, at a scale greater than 1 micron. Zygotes of *D. antarctica* and *H. banksii*, at 35 µm and 70 µm in diameter, respectively, are at least one order of magnitude larger than substrate roughness. While this magnitude of roughness was deemed insignificant compared to zygote size, it is possible that some features of the adhesives might benefit form the elevated roughness of some topographies.

4.3.2 Contact angle measurements

Table 4.2 reports the average advancing contact angles for all surfaces. Photos of water droplets on each surface can be seen in Figure 4.5. Glass, PMMA and stainless steel all exhibited hydrophilic surface character while PTFE alone exhibited hydrophobic character. Glass and stainless steel were the most hydrophilic, both showing an average θ_{AW} of 57° ± 2°. PMMA was less hydrophilic with an average θ_{AW} of 74° ± 5°, similar to the value reported in Chapter 3. PTFE had an average θ_{AW} of 103° ± 1°. The surface of glass is hydrophilic due to the abundance of hydroxyl functional groups which form hydrogen bonds with water molecules. Metal ions present in the stainless steel

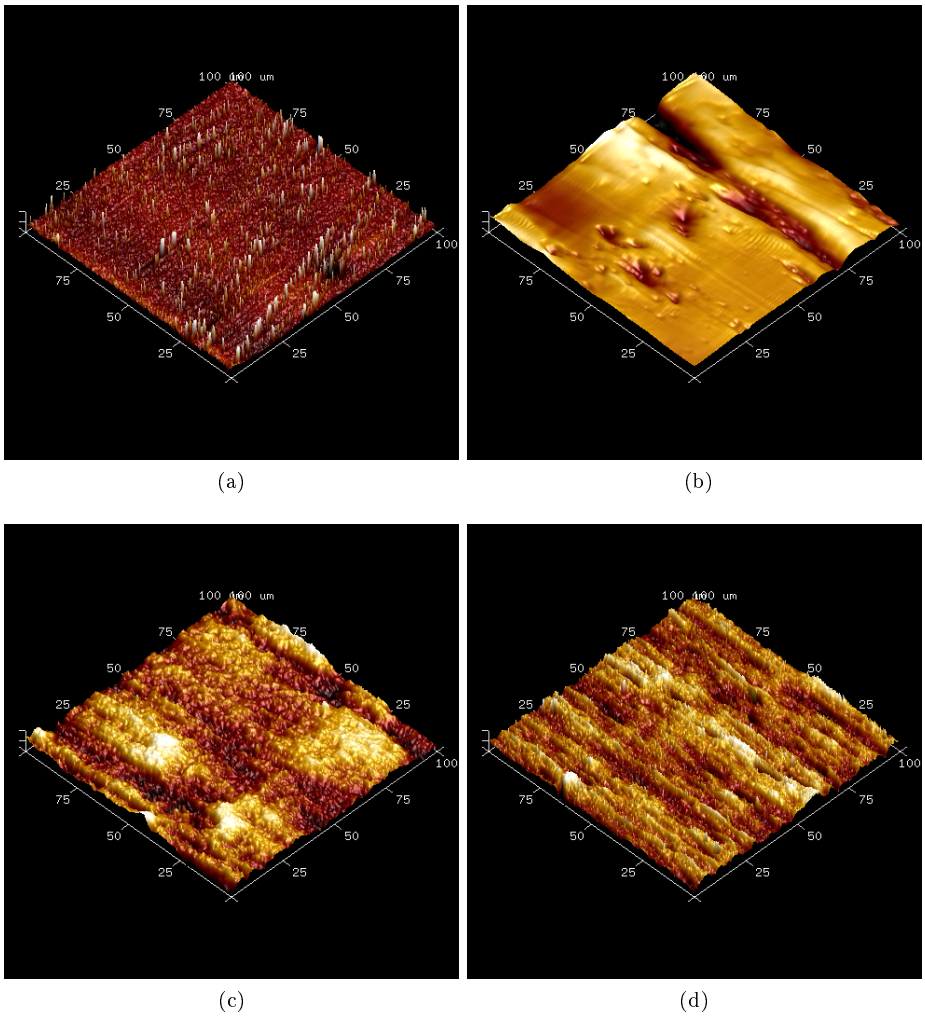

Figure 4.4: 3D presentations of substrates derived from AFM scans: (a) glass, (b) PMMA, (c) PTFE, (d) stainless steel (polished). Note the vertical axis is not in proportion to the horizontal axes in order to emphasise surface roughness for visual comparison.

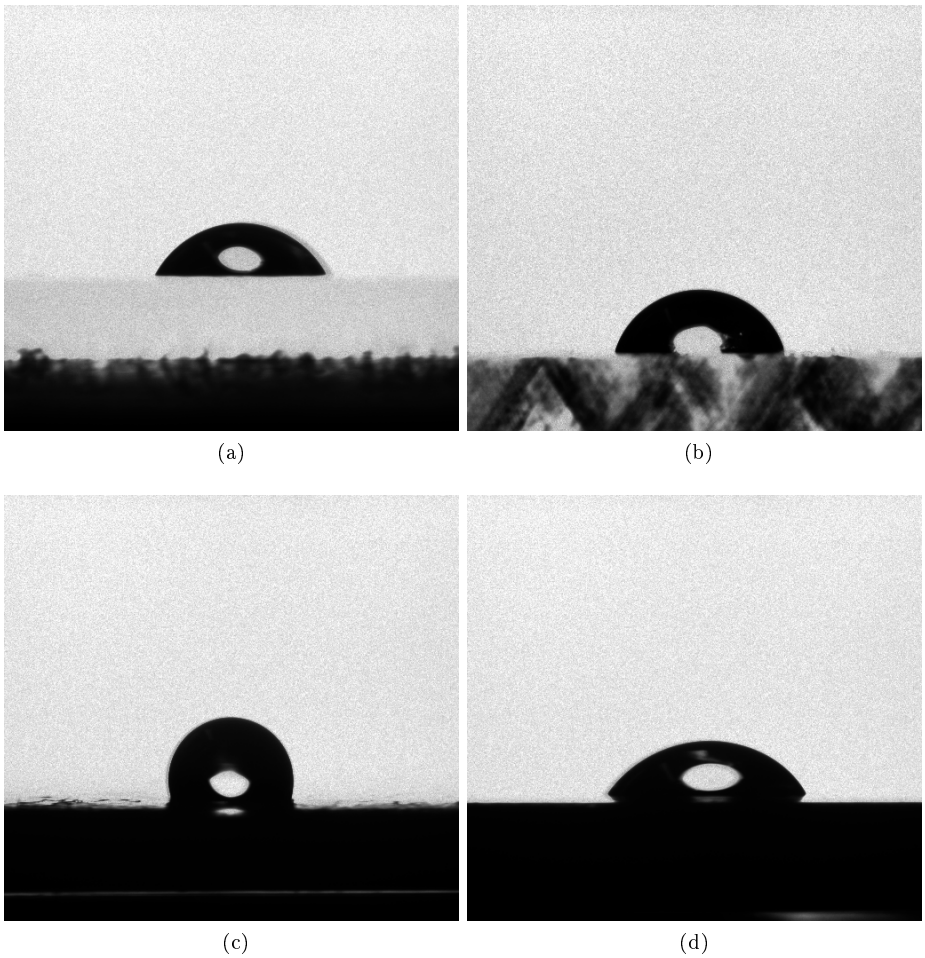

(a) (b)

(c) (d)

Figure 4.5: Photos of water droplets on each of the four substrates: (a) glass, (b) PMMA, (c) PTFE, (d) stainless steel. Note similarity in droplet shape between glass and stainless steel indicating similar wettability by water. PTFE clearly has the highest contact angle and therefore lowest wettability by water.

readily interact with polar solvents such as water, while surface bound hydroxyl groups belonging to metal-hydroxides can be involved in hydrogen bonding, also making it hydrophilic. While the hydrophilic character of the surfaces can be explained somewhat by surface chemistry, it is curious to note that the contact angles measured across the surfaces correspond to the roughness measurements in that substrates with higher roughness are less hydrophilic. While this does not necessarily imply causation, surface roughness and topography have been implicated in surface wettability (Onda et al., 1996; Sun et al., 2005; Barthlott and Neinhuis, 1997).

4.3.3 Settlement density and recruitment

Settlement density (D_0) on each substrate at each settlement time was calculated by dividing the number of germlings visible in the initial frame capture (before exposure to fluid flow in the channel) by the viewable area (8.58 mm^2). D_0 is therefore expressed as number of germlings per mm^2. Analysis of variance (ANOVA) was performed on the settlement density values for both species to determine variances in settlement due to substrate and settlement time.

4.3.3.1 *Durvillaea antarctica*

A chart showing *D. antarctica* D_0 for all substrates and settlement times is shown in Figure 4.6. D_0 is stable across all substrates and settlement times with no significant differences due to settlement time ($p = 0.15$), substrate ($p = 0.38$) or the interaction between settlement time and substrate ($p = 0.25$). This stability suggests a rapid formation of a base level of adhesion that is capable of withstanding the stress exerted on the slide as it is transferred from culture tray to the flow channel. The overall average D_0 for all settlement times and material was approximately 60 germlings per mm^2.

4.3.3.2 *Hormosira banksii*

A chart showing *H. banksii*'s D_0 for all substrates and settlement times is shown in Figure 4.7. In contrast to that of *D. antarctica*, D_0 was highly variable for *H. banksii* samples, with significant variation due to both settlement time ($p < 0.01$) and substrate ($p = 0.014$). The unstable D_0 across settlement times and substrates indicates that *H. banksii* less readily forms a base level of adhesion to the substrate so is more greatly impacted by the stress induced when transferring the slides from culture trays to flow channel. D_0 for *H. banksii* samples only seems to stabilise after 48 hours settlement time, although there is still significant variation between the different substrates at the higher settlement times. A suggested elevation in D_0 on PTFE, particularly after 48 and 96 hours settlement time, is similar to observations made by Finlay et al., (2002), where motile *Ulva* zoospores were found to settle preferentially on hydrophobic surfaces, although *H. banksii* zygotes are non-motile and thus cannot "choose" a surface.

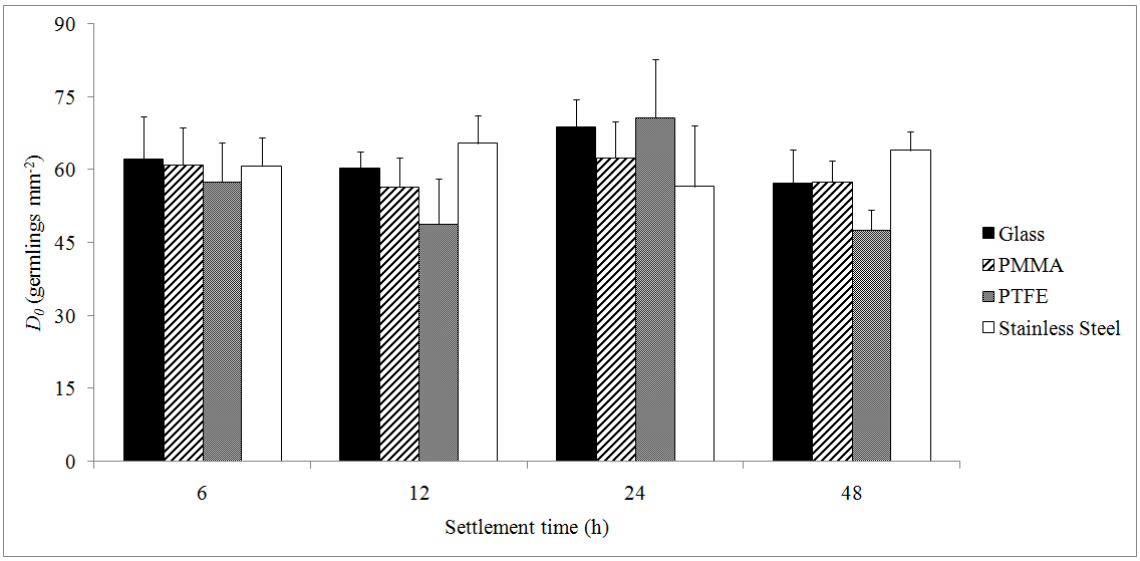

Figure 4.6: Settlement density (D_0) for *D. antarctica* on each substrate and each settlement time. No significant difference in D_0 due to settlement time or substrate. (± S.E., n = 4)

4.3.3.3 Comparing starting densities

Comparison of starting densities between the two species suggests a more rapid formation of an adhesive bond with the substrate by *D. antarctica* than by *H. banksii* ($\leq$ 6 hours compared to approximately 48 hours). There are several potential causes for the differences seen in D_0 between the two species. *D. antarctica* germlings are approximately half the size of *H. banksii* germlings (35 µm compared to 65 µm), so it is likely that the amount of drag force experienced by a *H. banksii* germling would be higher than that experienced by a *D. antarctica* germling when slides are being moved to the flow channel. *D. antarctica* may also produce a greater quantity of adhesive compound early in the settlement process, which could spread over a greater surface area relative to the germling body size. Differences in the chemistry of the adhesives produced may also mean that *D. antarctica* adsorbs more readily on available surfaces and/or undergoes curing processes more rapidly. The suggestion that *D. antarctica* obtains a base level of adhesion more rapidly than *H. banksii* echoes findings by Taylor and Schiel (2003) which illustrated more rapid adhesion to fibre plates by *D. antarctica* than *H. banksii*.

Comparison of D_0 achieved by *H. banksii* in this experiment to D_0 with PMMA and hydrogels (Chapter 3) or on topographical PDMS surfaces (Chapter 5) shows lower values at low settlement times than in Chapters 3 and 5. While the differences could be in part due to the different substrates used in the different experiments, PMMA, which was common to this experiment and the experiment in Chapter 3, still shows a significant difference in D_0. In Chapter 3, D_0 on PMMA stabilised at approximately 21 germlings/mm^2 after 12 hours. In contrast, D_0 for *H. banksii* on PMMA in this experiment only stabilised at approximately 15 germlings/mm^2 after 24 hours. Lower D_0 could be explained by inoculation with a less concentrated zygote suspension, but that does not explain the differences in time taken for D_0 to become consistent. It is possible that the

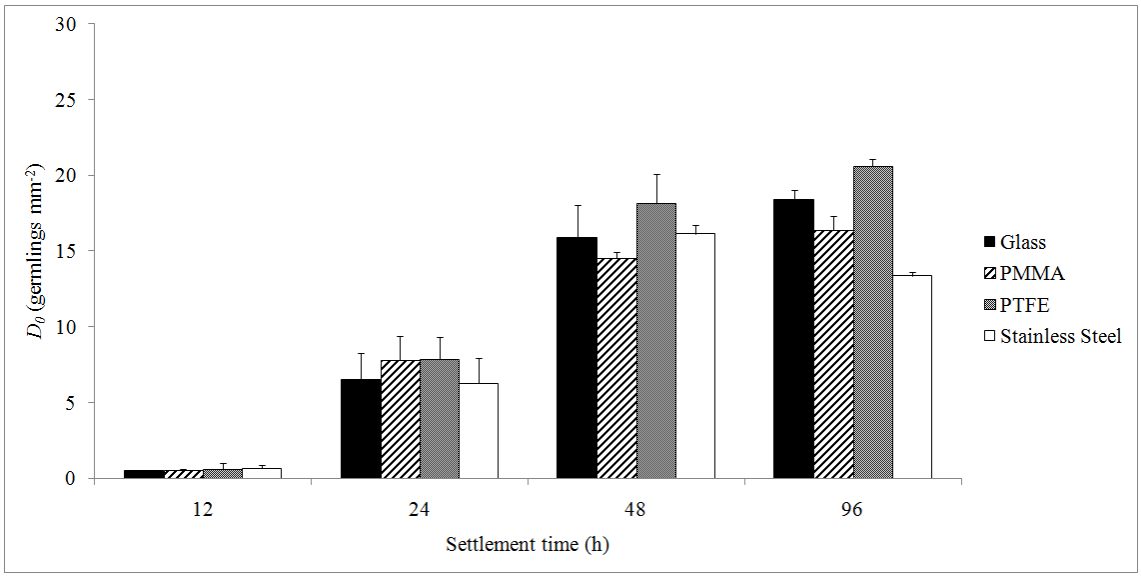

Figure 4.7: Settlement density (D_0) for *H. banksii* on each substrate and each settlement time. Significant variation in D_0 as a result of both settlement time and substrate. (± S.E., n = 3)

H. banksii used in this experiment may have been in less-than-optimal health, potentially affecting adhesion processes. The weak gamete release, which necessitated the use of settlement guides to increase germling density, may be indicative of some external factor (e.g. seasonal) governing *H. banksii*'s ability to reproduce and adhere successfully, which further supports my suspicions of poor sample health. Unfortunately, time constraints and seasonal factors meant that collecting further data was not possible.

4.3.4 Flow channel survival experiments

D. antarctica and *H. banksii* germling adhesion was assessed after different settlement time ranges for each species. Preliminary experiments and work by Taylor and Schiel (2003) showed more rapid adhesion of *D. antarctica* zygotes to the substrate than *H. banksii* zygotes, so *D. antarctica* was assessed after settlement times of 6, 12, 24 and 48 hours, while H. banksii was assessed after 12, 24, 48 and 96 hours settlement. Survival after each flow step (S_v) was calculated by comparing the density of germlings remaining after each flow step (D_v) to the starting density of germlings (D_0) using the following formula:

$$S_v = \frac{D_v}{D_0} \times 100$$

Direct comparison between settlement times and substrates was achieved by observing the percentage survival at the conclusion of the experiment, i.e. after exposure to the highest flow rate ($S_{2.5}$). $S_{2.5}$ was used to compare relative adhesion strength of the settled germlings as differences in survival are larger at higher flow rates, making a statistically significant difference more apparent.

4.3.4.1 *Durvillaea antarctica*

The consistent settlement densities seen with *D. antarctica* samples show that starting conditions for adhesion testing could be considered identical. With that requirement satisfied, ANOVA analysis on survival was performed. Analysis of survival rates at the conclusion of experiments ($S_{2.5}$) showed no significant variation in survival as a result of settlement time ($p = 0.064$), which echoes the results for settlement density. There was, however, significant variation in survival as a result of substrate ($p < 0.01$). Figures showing germling survival with increasing flow rate (v) and shear pressure (τ_w) are shown in Figures 4.8a, 4.8b, 4.8c and 4.8d. I have only included survival charts for comparing substrates since there was no variation due to settlement time. Survival was consistently highest on stainless steel for all settlement times, while survival was the lowest on PTFE for all settlement times. PTFE was the only hydrophobic substrate as well as the most rough ($\theta_{AW} = 103°$, $R_a = 121$ nm), while stainless steel had highest equal hydrophilicity (57°) and the second lowest roughness ($R_a = 16$ nm). Glass, which had the lowest roughness and equal wettability to stainless steel, generally exhibited the second highest survival rates. Differences in survival rates on glass and stainless steel indicate that smoothness and wettability aren't the only factors governing adhesion strength and chemical differences between the surfaces are likely the cause of the different survival rates. The high survival on stainless steel suggests that the mechanisms governing adhesive success of *D. antarctica* adhesives work particularly well with metal substrates and may be due to the involvement of readily available metal ions in a rapid curing process. Ferric ions have been found in high concentrations in the byssuses of the mussel *Mytilus edulis*, where they have been implicated in the formation of complexes with proteins containing the post-translationally modified amino acid DOPA (3,4-dihydroxyphenylalanine) and subsequent curing processes (Taylor et al., 1994, 1996). Calcium and magnesium ions were involved in the gelation of polysaccharides in the adhesive produced by *Undaria pinnatifida*, while phosphorylated moieties in the adhesive were witnessed in direct contact with a TiO_2 substrate (Petrone et al., 2011). Phosphate-substrate interaction could be through electrostatic interaction with positively charged substrate-based metal ions or covalent bonding through surface-bound hydroxyl groups and operate through mono- or multi-dentate interactions with one or more surface-bound atoms. It's possible that the adhesive produced by *D. antarctica* contains functional groups capable of forming non-covalent complexes with surface-coordinated metal ions or covalently bonding with metal oxides, such as chromium oxide present on stainless steel surfaces, leading to rapid adsorption. As potentially with *U. pinnatifida*, this might be through phosphorylated protein moieties. Soluble metal ions leached into the seawater could also facilitate rapid curing through formation of complexes with phosphorylated moieties in adhesive proteins or through coordination with polyphenolic compounds (Hider et al., 2001) such as phlorotannin, a common component in the formation of brown algal cell walls (Ragan and Glombitza, 1986). Close proximity to the stainless steel substrate could mean a supply of metal ions such as Fe^{3+}, Mn^{2+}, Ni^{2+} and Cr^{2+} which could be involved in the complex formation and adhesive curing. Other mechanisms of curing via cross-linking involving phlorotannins and alginate likely include the polymerising action of peroxidises (Tarakhovskaya, 2014; Bitton et al., 2007), but it is unclear if the stainless steel substrate would be involved in accelerating this process.

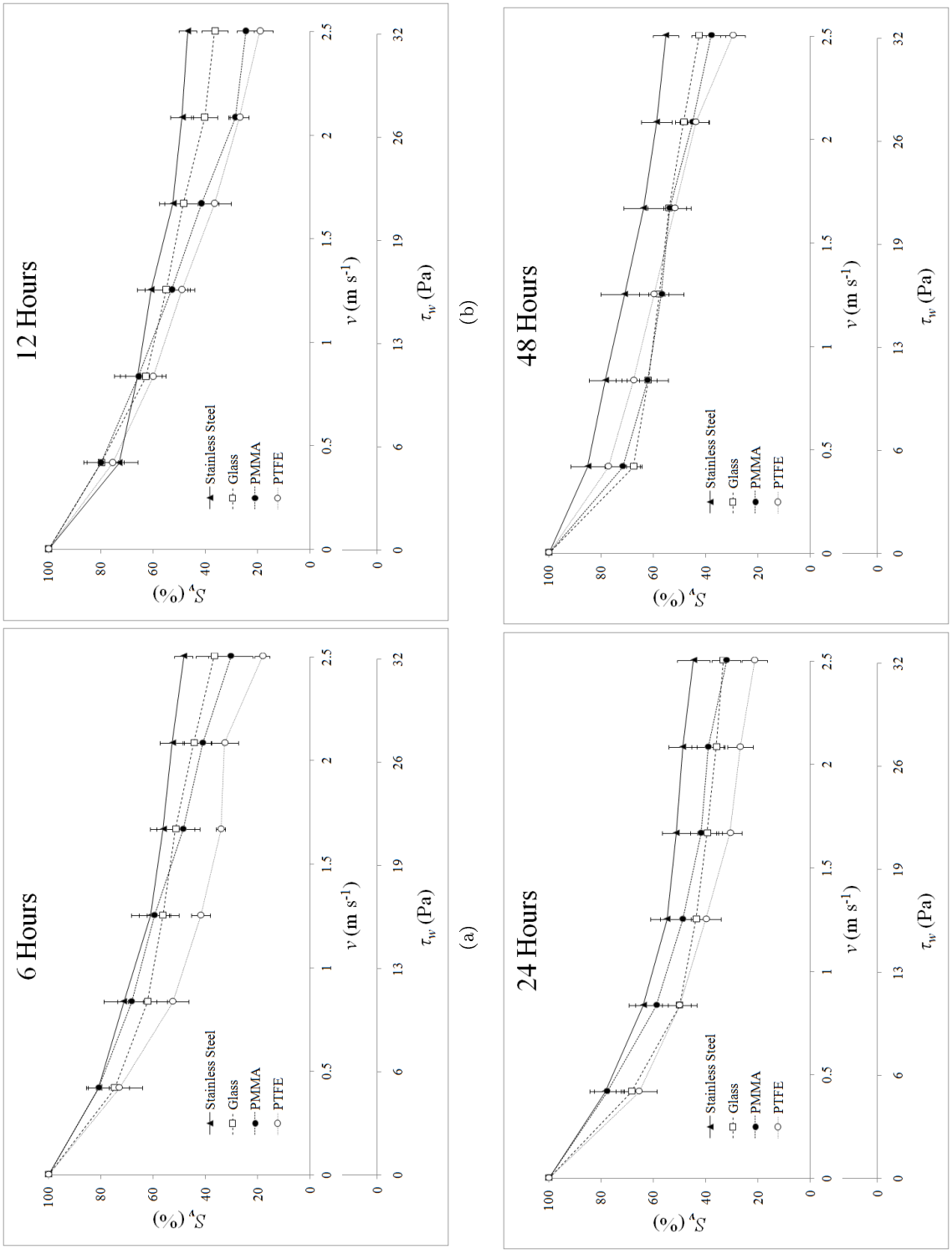

Figure 4.8: *D. antarctica* germling survival with increasing fluid velocity/shear pressure for different substrates at settlement times of (a) 6 hours, (b) 12 hours, (c) 24 hours and (d) 48 hours. (± S.E., n = 4).

The suggested interaction between an adhesive functional group, such as polyphosphoprotein, with surface-bound metal oxides may also be supported by the survival of *D. antarctica* on glass, where silicate-based oxygen atoms could be involved in covalent bonding, facilitating rapid adsorption. Differences in survival on stainless steel and glass might therefore be to do with differences in curing processes due to different availability of metal ions and/or extra adhesion strength from interactions with metal hydr(oxides) and ions.

The particular success of *D. antarctica* on stainless steel singles *D. antarctica* out for possible further research and inspiration for wet-resistant adhesives with particular applications involving metal substrates.

4.3.4.2 *Hormosira banksii*

In contrast to *D. antarctica*, the starting conditions (D_0) for *H. banksii* cannot considered identical. As a result, further statistical analyses (ANOVA) on the survival data are not strictly statistically sound. However, it is still interesting to look at the survival data for these experiments, but conclusions drawn from these data should be considered with caution. Graphs of survival with increasing v and Pa are shown in Figures 4.9a, 4.9b, 4.9c and 4.9d. Comparing $S_{2.5}$ across the different settlement times and substrates shows a clear effect due to settlement time, with $S_{2.5}$ at 0% for all substrates after 12 hours and rising somewhat by 24, 48 and 96 hours settlement time. Indeed, settlement densities for 12 hour samples were so low that it is hard to draw any real conclusion about the adhesive strength. It seems that following 12 hours settlement simply transferring the slide from its culture tray to the flow channel was sufficient to remove the vast majority of tentatively settled zygotes, often resulting in a D_0 of less than 1 germling per mm^2. This is similar to the response seen after 6 hours settlement time in Chapter 3, though clearly the germlings in this experiment took even longer to achieve a base level of adhesion. Nevertheless, ignoring data after 12 hours settlement and observing data from settlement times of 24, 48 and 96 hours settlement time still indicates that there is some variation in $S_{2.5}$ as a result of substrate type. Unlike with *D. antarctica*, there was no consistent best or worst performing substrate, although it does appear that glass and PMMA both performed better than PTFE and stainless steel. Given the different performance of glass and stainless steel, despite identical contact angles, it seems unlikely that wettability is the primary determinant for adhesion strength. Similarly, the possibility that the higher roughness of the PTFE surface is responsible for its low survival rate seems contradicted by the relatively high adhesion to PMMA (second roughest substrate) and low survival on stainless steel (second smoothest substrate).

4.3.4.3 Comparing survival rates

A chart comparing $S_{2.5}$ for all settlement times and both species is shown in Figure 4.10. Settlement times common to both species were 12, 24 and 48 hours; 6 hours was only observed for *D. antarctica* and 96 hours was only observed for *H. banksii*. The largest and most interesting discrepancy in survival data, besides the obvious differences with settlement time, was the discrepancy in the adhesion strength of the two species attached to stainless steel. Stainless steel easily exhibited the

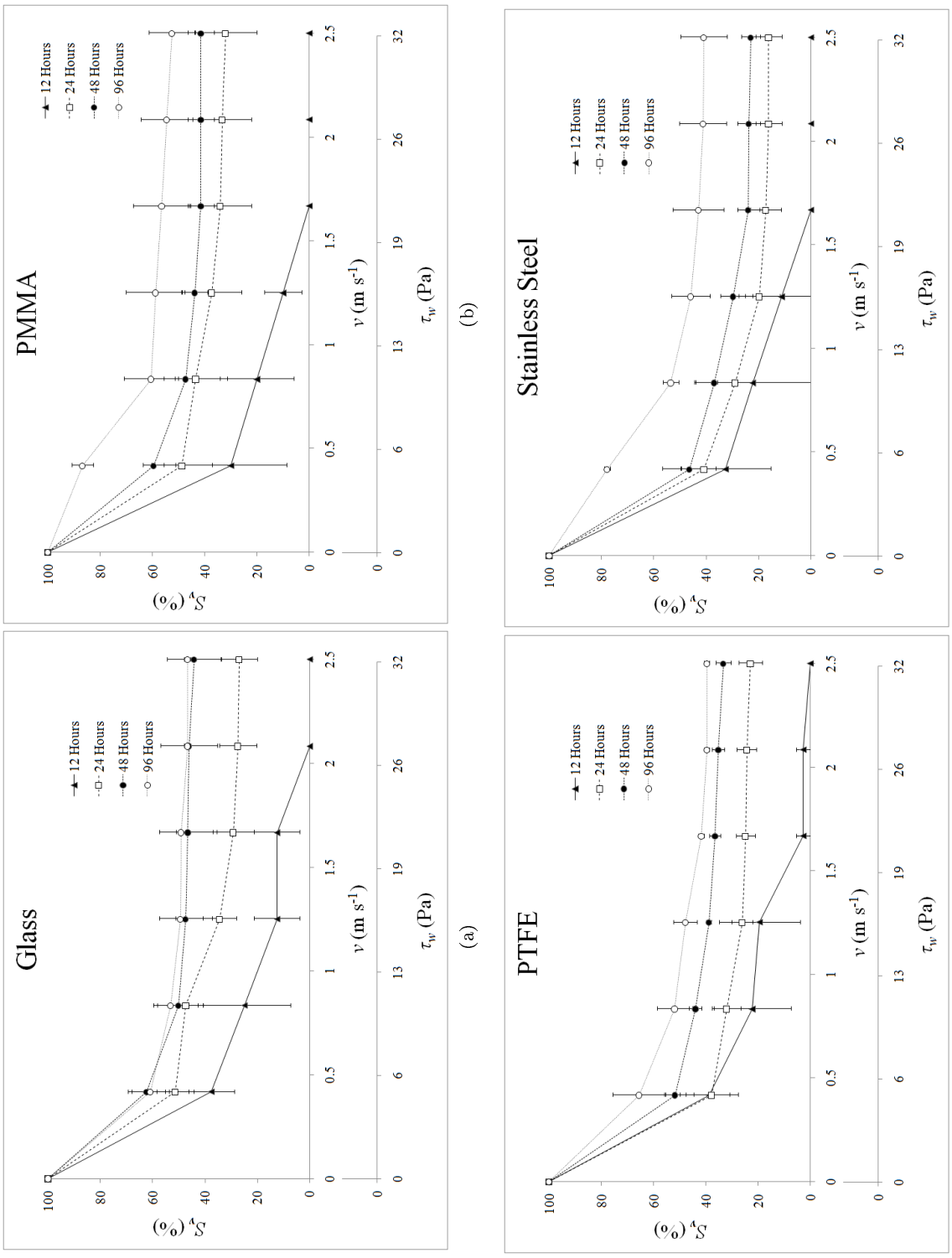

Figure 4.9: *H. banksii* germling survival with increasing fluid velocity/shear pressure for different settlement times on (a) glass, (b) PMMA, (c) PTFE and (d) stainless steel. ($\pm$ S.E., n = 3).

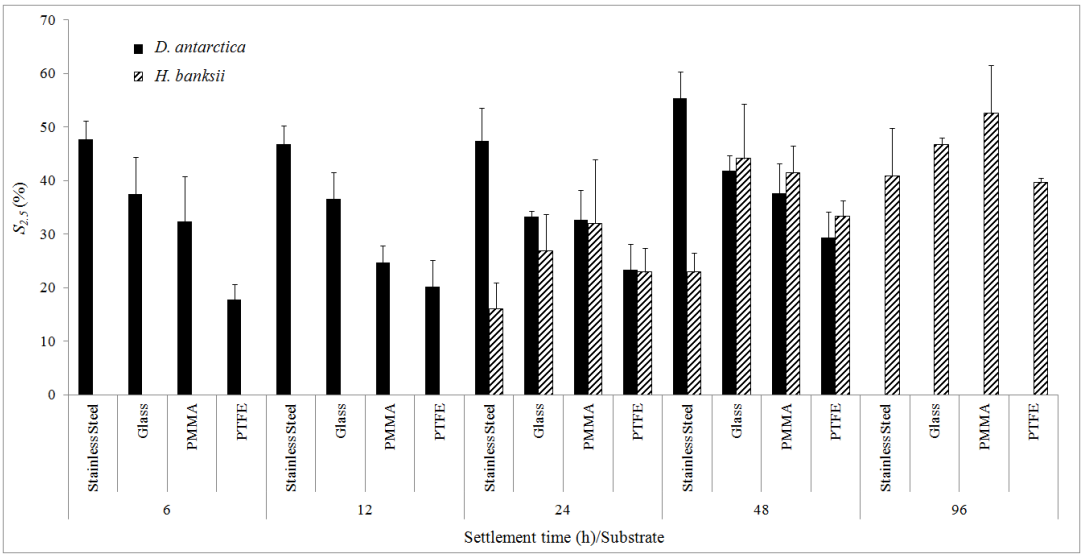

Figure 4.10: Comparing $S_{2.5}$ for both *D. antarctica* and *H. banksii* germlings at all settlement times. Note there is no data for *H. banksii* at 6 hours and no data for *D. antarctica* at 96 hours. At 12 hours *H. banksii* has an $S_{2.5}$ of 0% on all surfaces. $S_{2.5}$ is similar between species for settlement times of 24 and 48 hours with the exception of on stainless steel, where *D. antarctica* appears to adhere much more strongly than *H. banksii*. ($\pm$ S.E., n = 4 (*D. antarctica*), n = 3 (*H. banksii*))

highest survival rates with *D. antarctica*, but had the lowest survival rates for *H. banksii* samples. The mechanism of adhesion responsible for *D. antarctica*'s rapid adhesion to the substrate may involve some interaction with metal ions or oxides that the *H. banksii* adhesive is not only not capable of also exploiting, but might be involved to some extent in attenuating *H. banksii*'s adhesive strength.

The three remaining substrates, glass, PMMA and PTFE, all exhibit similar values for $S_{2.5}$, so with the exception of with stainless steel, *D. antarctica* does not necessarily exhibit stronger adhesion, but it does exhibit more rapid adhesion. It should be noted that the drag force acting on a settled germling is, in part, a function of germling size. *H. banksii* germlings should experience a higher drag force than *D. antarctica* germlings, but without knowing the area of adhesive contact of each species it is difficult to quantify a value for adhesive strength independent of the specific organism. In the future, electron microscopy imaging and measurement of the size of the adhesive pads produced by *D. antarctica* and *H. banksii* germlings, combined with computational fluid dynamic modelling of drag forces, could yield an absolute measurement for adhesive strength that can be compared to other adhesives of biological and synthetic origin.

The survival data seen here for *H. banksii* is much lower than seen on the substrates in Chapter 3. Given the variability of natural systems, some variation is to be expected, and it is difficult to directly compare the data from two separate reproductive events from *H. banksii* samples from different locations. That said, however, the discrepancy is quite large, particularly $S_{2.5}$ values for 24 and 96 hours settlement time where, in Chapter 3, survival was up near 100%.

It is interesting to note that *D. antarctica* never exhibited as much adhesive success as germlings of *H. banksii* at 24 and 96 hours settlement in Chapter 3. This is unexpected for two reasons: (i) the exposed habitats that *D. antarctica* normally occupies puts pressure on zygotes to achieve rapid, lasting adhesion to the substrate. In the wave exposure experiments by Taylor and Schiel (2003), zygotes of *D. antarctica* did adhere more rapidly and reliably than zygotes of *H. banksii*; (ii) since hydrodynamic drag force exerted on a germling has a positive correlation with germling size, I would expect that the *H. banksii* germlings would be subject to higher drag forces than *D. antarctica* and would display correspondingly lower survival. It is possible that the expression of strong adhesion by *D. antarctica* is a phenotypically plastic response and is dependent on environmental cues such as water motion. The culturing setup for these experiments uses trays containing still water which may not elicit the same adhesive response as a natural environment. A possible future experiment could be to assess the effect of water motion during culturing on adhesive success of germlings of *D. antarctica* (and *H. banksii*).

Looking at the change in survival percentage with increasing flow rate, almost invariably the most rapid decrease in survival (indicated by steepest section of line) occurs during exposure to the lowest shear stress (0.42 m/s, 5.4 Pa). This indicates that for every batch of settled germlings there is a range of adhesion strengths exhibited, and a significant proportion of the germlings exhibit low adhesion strength that is overcome by the lowest experimental flow velocity/shear pressure. Further experiments observing flow velocities lower than 0.42 m/s could yield more accurate data regarding this early removal. Conversely, the fact that germling survival remains above 0% for most treatments indicates the flow channel cannot generate sufficient shear stress to cause total germling detachment. I would have liked to have been able to generate the shear stress that corresponds to total detachment for each treatment, but technical constraints on the flow channel and pumping system meant this could not be done. An alternative to increasing shear stress is to increase the length of exposure to be longer than 15 seconds; the concern with this is that it could make the duration of experiments prohibitively long.

4.4 Conclusions

In this chapter I used the flow channel to look at the adhesion strength of two species of algae, *Durvillaea antarctica* and *Hormosira banksii*, to a range of substrates. The substrates were selected based on relevance and commonality in fields such as medicine, food preparation and engineering. They included glass, PMMA, PTFE and stainless steel. *D. antarctica* exhibited more rapid formation of a base level of adhesion with the substrate than *H. banksii*, with particularly strong adhesion to stainless steel. In contrast, the adhesion strength of *H. banksii* germlings to stainless steel was arguably the weakest among the four materials tested. After considering survival rates in light of substrate roughness and wettability, it appears that substrate surface chemistry has more influence on adhesion strength in these experiments. While the substrate topography and surface roughness presented in this chapter were not a controlled variable, it would be interesting to look at the effect of controlled substrate topography on germling adhesion. In the next chapter I look

at the impact of defined micro-topographies on germling survival while substrate chemistry is kept constant.

Bibliography

Barthlott, W. and C. Neinhuis (1997, April). Purity of the sacred lotus, or escape from contamination in biological surfaces. *Planta 202*(1), 1–8.

Bitton, R., M. Berglin, H. Elwing, C. Colin, L. Delage, P. Potin, and H. Bianco-Peled (2007, December). The Influence of Halide-Mediated Oxidation on Algae-Born Adhesives. *Macromolecular Bioscience 7*(12), 1280–1289.

Callow, M. E., A. R. Jennings, A. B. Brennan, C. E. Seegert, A. Gibson, L. Wilson, A. Feinberg, R. Baney, and J. A. Callow (2002). Microtopographic Cues for Settlement of Zoospores of the Green Fouling Alga Enteromorpha. *Biofouling 18*(3), 229–236.

Finlay, J. A., S. M. Bennett, L. H. Brewer, A. Sokolova, G. Clay, N. Gunari, A. E. Meyer, G. C. Walker, D. E. Wendt, M. E. Callow, J. A. Callow, and M. R. Detty (2010). Barnacle settlement and the adhesion of protein and diatom microfouling to xerogel films with varying surface energy and water wettability. *Biofouling 26*(6), 657–666.

Finlay, J. A., M. E. Callow, L. K. Ista, G. P. Lopez, and J. A. Callow (2002, December). The Influence of Surface Wettability on the Adhesion Strength of Settled Spores of the Green Alga Enteromorpha and the Diatom Amphora. *Integrative and Comparative Biology 42*(6), 1116–1122.

Frazer, R. Q., R. T. Byron, P. B. Osborne, and K. P. West (2005). PMMA: An Essential Material in Medicine and Dentistry. *Journal of Long-Term Effects of Medical Implants 15*(6), 629–639.

Hider, R. C., Z. D. Liu, and H. H. Khodr (2001). Metal chelation of polyphenols. In L. Packer (Ed.), *Methods in Enzymology*, Volume 335 of *Flavonoids and Other Polyphenols*, pp. 190–203. Academic Press.

Hong, T.-F., W.-J. Ju, M.-C. Wu, C.-H. Tai, C.-H. Tsai, and L.-M. Fu (2010, May). Rapid prototyping of PMMA microfluidic chips utilizing a CO2 laser. *Microfluidics and Nanofluidics 9*(6), 1125–1133.

Leigh, J. A. (1975, July). Use of PMMA in expansion dental implants. *Journal of Biomedical Materials Research 9*(4), 233–242.

Mathur, A., S. S. Roy, M. Tweedie, S. Mukhopadhyay, S. K. Mitra, and J. A. McLaughlin (2009, November). Characterisation of PMMA microfluidic channels and devices fabricated by hot embossing and sealed by direct bonding. *Current Applied Physics 9*(6), 1199–1202.

Onda, T., S. Shibuichi, N. Satoh, and K. Tsujii (1996, January). Super-Water-Repellent Fractal Surfaces. *Langmuir 12*(9), 2125–2127.

Petrone, L., R. Easingwood, M. F. Barker, and A. J. McQuillan (2011, March). In situ ATR-IR spectroscopic and electron microscopic analyses of settlement secretions of Undaria pinnatifida kelp spores. *Journal of the Royal Society, Interface / the Royal Society 8*(56), 410–422.

Ragan, M. A. and K.-W. Glombitza (1986). Phlorotannins, brown algal polyphenols. *Progress in Phycological Research 4*, 129–241.

Schultz, M. P., J. A. Finlay, M. E. Callow, and J. A. Callow (2000, September). A turbulent channel flow apparatus for the determination of the adhesion strength of microfouling organisms. *Biofouling 15*(4), 243–251.

Stewart, R. J., T. C. Ransom, and V. Hlady (2011, June). Natural underwater adhesives. *Journal of Polymer Science Part B: Polymer Physics 49*(11), 757–771.

Sun, M., C. Luo, L. Xu, H. Ji, Q. Ouyang, D. Yu, and Y. Chen (2005, September). Artificial Lotus Leaf by Nanocasting. *Langmuir 21*(19), 8978–8981.

Sun, T., L. Feng, X. Gao, and L. Jiang (2005, August). Bioinspired Surfaces with Special Wettability. *Accounts of Chemical Research 38*(8), 644–652.

Tarakhovskaya, E. R. (2014, January). Mechanisms of bioadhesion of macrophytic algae. *Russian Journal of Plant Physiology 61*(1), 19–25.

Taylor, D., S. Delaux, C. Stevens, R. Nokes, and D. Schiel (2010). Settlement rates of macroalgal propagules: Cross-species comparisons in a turbulent environment. *Limnology and Oceanography 55*(1), 66.

Taylor, D. I. and D. R. Schiel (2003, June). Wave-related mortality in zygotes of habitat-forming algae from different exposures in southern New Zealand: the importance of 'stickability'. *Journal of Experimental Marine Biology and Ecology 290*(2), 229–245.

Taylor, S. W., D. B. Chase, M. H. Emptage, M. J. Nelson, and J. H. Waite (1996, January). Ferric Ion Complexes of a DOPA-Containing Adhesive Protein from Mytilus edulis. *Inorganic Chemistry 35*(26), 7572–7577.

Taylor, S. W., G. W. Luther, and J. H. Waite (1994, December). Polarographic and Spectrophotometric Investigation of Iron(III) Complexation to 3,4-Dihydroxyphenylalanine-Containing Peptides and Proteins from Mytilus edulis. *Inorganic Chemistry 33*(25), 5819–5824.

Weaver, K. D., J. O. Stoffer, and D. E. Day (1993). Preparation and properties of optically transparent, pressure-cured poly(methacrylate) composites. *Polymer Composites 14*.

Chapter 5

Adhesion to Topographical Substrates

5.1 Introduction

Surface chemistry is clearly an important factor when considering its interaction with adhesive organisms, but surface topography is increasingly being investigated as a crucial element in the design and performance of environmentally friendly anti-fouling surfaces. Topographical features of different scales have varying impacts on the adhesion success of biofoulers; generally, features larger than 1 mm (macro-topography), facilitate adhesion success through protecting the fouling organism from environmental or hydrodynamic challenge (Myan et al., 2013). Micro- (1 µm - 1000 µm) or nano- ($<$ 1 µm) topographies influence adhesion success in other ways; features of a similar size to a fouling organism can impact adhesion success by manipulating the points available for an organism to form adhesive contact with the substrate (Callow et al., 2002; Scardino et al., 2006). Structures in the nano-scale and low in the micro-scale can also impact the wettability of a substrate, which can in turn impact the ability of an adhesive to spread on a surface. Surface wettability has been implicated in substrate selection and adhesion strength of algal zoospores and diatoms (Callow et al., 2000; Finlay et al., 2002), human endothelial cells (van Wachem et al., 1985) and bacteria (Fletcher and Pringle, 1985).

The observance of several naturally fouling-resistant materials in nature has generated interest in a bio-mimetic approach to fouling prevention. Of the numerous strategies employed by organisms to prevent fouling (Wahl et al., 1998) the use of topography to deter fouling is attractive as a non-toxic, passive, potentially low maintenance fouling prevention mechanism. In the past few decades, naturally occurring, fouling-resistant surfaces have seen increasing popularity as the subject of research (Wahl et al., 1998; Bers and Wahl, 2004; Barthlott and Neinhuis, 1997; Sullivan and Regan, 2011; Bixler et al., 2014). Findings around these surfaces have stressed the importance of topography in fouling resistance. Terrestrially, the leaf of the sacred lotus (*Nelumbo nucifera*) is a model structure in fouling-resistance. Small, hill-like structures on the surface of the leaf,

approximately 6 µm in diameter, result in a super hydrophobic surface which causes water to bead up and roll off the leaf, taking dust and other contaminants with it (Barthlott and Neinhuis, 1997). Transfer of the topography using soft-lithography techniques (casting) in polydimethylsiloxane (PDMS) by Sun et al. (2005) resulted in a surface displaying similar behaviour to the natural lotus leaf, confirming the influence of geometry on the wettability, and consequently the anti-fouling properties of the lotus leaf.

While the lotus leaf is an impressive example of a self-cleaning, fouling-resistant surface, other interesting fouling-resistant surfaces can be found in species that spend significantly more time underwater yet resist succumbing to the biofouling that affects nearly every inorganic surface around them. These wet-environment, fouling-resistant surfaces include, among others, shark skin, the carapace of the edible crab (*Cancer pagurus*), the shell of the blue mussel (*Mytilus edulis*), the egg case of the lesser spotted dogfish (*Sycliorhinus canicula*), and the skin of the brittle star (*Ophiura texturata*). Studies on topographies derived from these surfaces have shown some promise as fouling-resistant surfaces. A surface inspired by the topography of shark skin, albeit on a different scale, Sharklet AF^{TM}, has been successful in disrupting settlement of zoospores of the green alga *Ulva linza* and cyprids of the barnacle *Balanus amphitrite* (Carman et al., 2006; Schumacher et al., 2007), but performance against a larger range of taxa is unknown. Studies by Bers and Wahl (2004) on topographies derived from *C. pagurus*, *M. edulis*, *S. canicula* and *O. texturata* exhibited a degree of fouling deterrence; however the anti-fouling properties decreased with increasing time spent in the fouling environment. These surfaces were placed in seawater in a natural environment, so were exposed to a range of fouling taxa, and it is likely that this resulted in a build up of low-level fouling such as bacterial biofilms. The incidence of the low level fouling subsequently lead to a masking of topography, and combined with other chemotactic effects stimulated the settlement of higher foulers (Bers and Wahl, 2004).

It has been suggested that specific feature shape is secondary in importance to feature size when impeding fouling (Myan et al., 2013), and the anti-fouling effect relies on interactions between specific feature size and the size of the fouling organism. This is exemplified in the response of *U. linza* zoospores ($5 - 7$ µm diameter) to two different topographical designs where a feature size of 2 µm was most effective in disrupting settlement (Cao et al., 2010; Carman et al., 2006). Attachment point theory posists that the adhesion strength of an organism corresponds to the number of points of adhesive contact between the organism and a surface: more attachment points leads to greater adhesive success (Scardino et al., 2006). The size-specific nature of fouler-substrate interactions mean that topography-based anti-fouling strategies that effectively deter fouling from a range of taxa will need to present a range of topographical feature sizes simultaneously, such as on hierarchical or fractal structures (Myan et al., 2013). An example of this was shown by Schumacher et al. (2007), where a Sharklet AF^{TM} model was created with two hierarchical topography sizes and successfully deterred settlement of *U. linza* and *B. amphitrite* at the same time.

In this chapter the flow channel is used to test the effect of simple topography on the adhesion success of zygotes of the brown alga *Hormosira banksii*. While fouling by *H. banksii* does not pose any particular threat to shipping or aquaculture, *H. banksii* propagules represent a useful model for investigating the effect of topography on brown algal settlement. Zygotes of *H. banksii* measure

64-74 µm in diameter (Osborn, 1948), an order of magnitude larger than the zoospores of *U. linza* which have been the focus of many adhesion studies. Topographical surfaces were created using PDMS, which is commonly used in nanofabrication and microfluidic applications. Topographical feature size was selected based on the size of *H. banksii* zygotes. It was hypothesised that a feature size slightly smaller than the diameter of the *H. banksii* zygotes would demonstrate the lowest settlement numbers and survival in the flow channel through limiting the number of adhesion points, while a feature size slightly larger than the zygote diameter would facilitate increased adhesion through higher numbers of adhesion points.

5.2 Materials and methods

5.2.1 Topography design and justification

Topographical features were selected based on two primary considerations; (i) simplicity of design and ease of manufacture, and (ii) features being of relevant size given the zygote size of *H. banksii*. Repeating, square bottomed grooves, orthogonal to the flow direction, were chosen as the basis for the topographical substrate design. Groove depth was kept constant while the groove width was varied. Groove widths were designed as a function of *H. banksii* zygote diameter (d_{Horm} = 64-74 µm). Zygote diameter was overestimated to 80 µm to account for cell growth and manufacturing inaccuracies with the PDMS surfaces. As a result, grooves were designed in three widths; 40 µm (approximately = 0.5 × d_{Horm}), 80 µm (approximately = d_{Horm}) and 160 µm (approximately = 2 × d_{Horm}). All grooves were separated by ridges measuring 40 µm wide. The grooves were designed to be 27 µm deep, or 1/3rd of the approximated cell diameter. The grooved topography was designed to fit in the centreline of a narrow slide made of PDMS; the topographical area was 40 mm long and 3.5 mm wide, allowing it to fit within the lower surface of the flow channel defined in Chapter 2. Flat surfaces of cast PDMS were also prepared to be used as control surfaces for adhesion testing. 3D representations of the grooved topographies can be seen in Figure 5.1 (a, c, e).

5.2.2 Topographical substrate preparation

Slides with topographical features were prepared using photo-lithography and PDMS casting techniques. The slides were prepared by an undergraduate engineering student at the University of Canterbury and the full procedure is contained in his research report (Nowell-Usticke, 2014). A brief summary of the process is outlined below.

5.2.2.1 Creating the mould

Negatives of the three topographies (40, 80 and 160 µm grooves) were created using SU-8 2025, a negative photo-resist, set on a silicon wafer. Masks were designed in Tanner's EDA-L Edit software and printed using a Heidelberg Instruments µPG101 mask writer. SU-8 photo-resist was applied

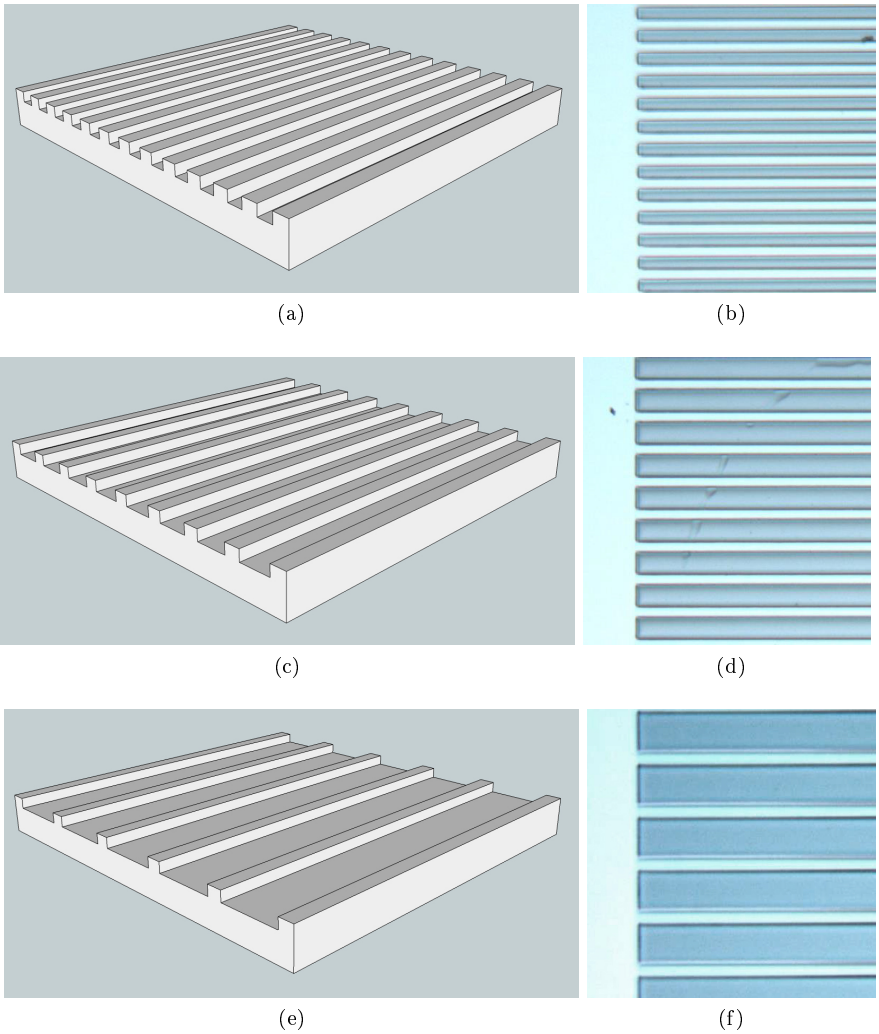

Figure 5.1: 3D representations of topographical sections (a, c, e) and photographs of SU-8 negatives used for PDMS casting (b, d, f). (a, b) 40 µm grooved topography, (c, d) 80 µm grooved topography, (e, f) 160 µm grooved topography. Groove depth is 27 µm and grooves are separated by 40 µm wide ridges.

to a silicon wafer with a thickness of 27 µm by spin coating. The photo-mask was then layered on top of the SU-8 photo-resist and the photo-resist was exposed to curing UV light. The cured photo-resist was then treated with developer (AZ 326 MIF) to remove non-cured SU-8, leaving a series of raised rectangular blocks which formed the negative for creating the grooves in the silicone slides (Figure 5.1: b, d and f). Each silicon wafer could accommodate three topography negatives side by side.

5.2.2.2 Casting the PDMS

The mould was treated with trimethylchlorosilane prior to addition of PDMS mixture. Sylgard 184 silicone (Dow Corning, MI, USA), a two silicone part elastomer, was prepared at a ratio of 10:1 w/w PDMS base with curing agent. The PDMS mixture was degassed under vacuum in a desiccator for at least two hours before being poured into the mould to a depth of approximately 3 mm. The PDMS and mould were placed under vacuum in a desiccator to further degas the PDMS. The PDMS was baked for 2 hours at 80°C before being removed from the mould and baked a second time for 2 hours at 80°C. The cured PDMS castings each contained three topographical strips, so were cut into three approximately microscope slide-sized pieces (20 mm x 75 mm) to fit in the flow channel.

5.2.3 Topographical substrate characterisation

5.2.3.1 Contact angle measurement

PDMS is natively hydrophobic due to the abundance of methyl groups attached to the siloxane backbone. For the prevention of air bubble formation and optimal performance in the flow channel the substrate should be hydrophilic. The presence of air bubbles on topographical substrates such as these could potentially lead to protected pockets in which settled zygotes do not get challenged by any hydrodynamic force. It was unknown if simply soaking PDMS in seawater would be sufficient to make it hydrophilic or if it would need to be treated with oxygen plasma before being immersed in seawater. Samples of cured PDMS were used to test the effect of oxygen plasma and seawater soaking on hydrophobicity. Samples were either treated with oxygen plasma for 12 seconds at 100 W (Emitech K1050X, Quorum Technologies Ltd., East Sussex, UK) or left untreated. All samples were then soaked in 0.22 µm filtered seawater (collected from Sumner, Christchurch, New Zealand) for 2, 15, 24 or 48 hours and contact angles were measured using a goniometer (CAM200; KSV Instruments Ltd, Helsinki, Finland). An additional control sample of PDMS was prepared which had neither oxygen plasma treatment nor soaking in seawater. Advancing contact angles (θ_{AW}) were measured following deposition of a 10 µl droplet of deionized water on each surface. 10 images of the water droplet, spaced 3 s apart, were taken following a 30 s delay after initial deposition of the water droplet. The ten images were analysed using the associated goniometer software (KSV CAM Software v 4.01), which fit the droplet shape to the Young-Laplace equation. The average contact angle was then calculated across the ten images and this average represented the contact

Table 5.1: Recorded advancing contact angles (θ_{AW}) for PDMS surfaces (± S.E., n = 3, *n = 12)

	Contact angle (θ_{AW})	
Soak Time	**Non-Plasma-treated**	**Plasma-treated**
2 Hours	99.3° ± 4.3°	63.0° ± 5.5°
15 Hours	100.0° ± 1.5°	75.0° ± 4.0°
24 Hours	106.7° ± 3.8°	71.7° ± 6.0°
48 Hours	100.3° ± 2.8°	58.0° ± 11.0°
Average	101.6° ± 1.7°*	66.9° ± 3.7°*

angle measurement for a single replicate. Contact angle measurements were performed three times on each substrate and averaged further.

5.2.4 Seaweed collection, settlement and culturing

Seaweed collection, gamete release, settlement and culturing was identical to that performed in Sections 3.2.3 and 3.2.4 in Chapter 3, except that seaweed for this experiment was collected from Pile Bay (43°37'13.6"S, 172°45'38.7"E) in November of 2014. Three replicates of each surface were prepared for adhesion assessment with the flow channel.

5.2.5 Adhesion assessment in flow channel

Germling adhesion strength to three replicates of the four topographies (40, 80, 160 and control) was assessed after settlement times of 12, 24 and 48 hours. The flow channel was operated according to the protocol outlined in Appendix B. Briefly, fluid velocity in the channel increased from 0.42 m/s (5.4 Pa) at the lowest flow rate to 2.50 m/s (32.4 Pa) at the highest, increasing in six even steps 15 seconds in duration. Videos of germlings in the flow channel were processed in VLC to extract single frames from the beginning of the experiment and at the end of each flow step. Germling numbers were counted in each frame to establish the germling survival rate for each flow velocity and shear pressure.

5.3 Results and discussion

5.3.1 Contact angle measurement

Contact angle was recorded for PDMS that had been both treated with oxygen plasma and soaked in seawater (Plasma-treated), soaked in seawater only (Non Plasma-treated), or neither treated with plasma nor soaked in seawater (Control). Representative photographs of contact angles are shown in Figure 5.2, and contact angle values are reported in Table 5.1. Two-way analysis of variance (ANOVA) showed that oxygen plasma treatment had a significant effect on surface hydrophobicity ($p < 0.01$) but there was no change in hydrophobicity attributable to variations in soaking time ($p = 0.25$). Soaking the PDMS in seawater alone is not sufficient to change the surface

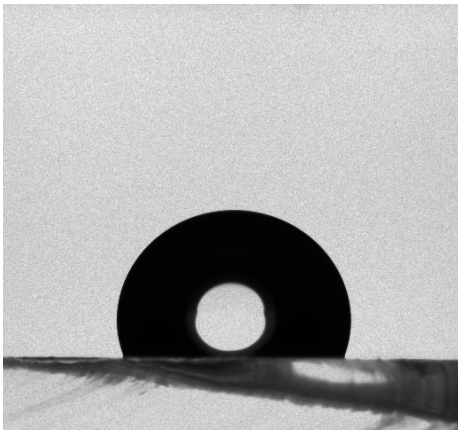

(a) Control

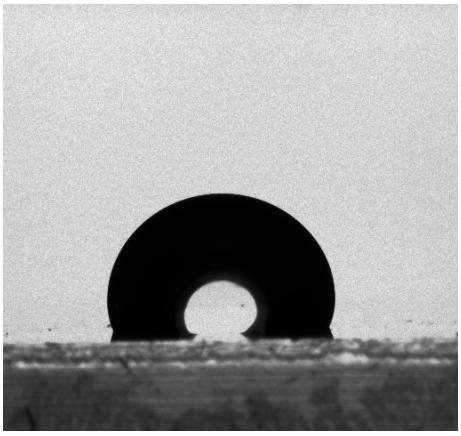

(b) Non-plasma treated, 48 hour

(c) Plasma treated, 48 hour

Figure 5.2: Example images of water droplets on PDMS surfaces. (a) Control - no plasma treatment, no seawater soaking, (b) No plasma treatment, 48 hour seawater soaking, (c) Plasma treatment and 48 hours seawater soaking.

to hydrophilic; Non Plasma-treated PDMS samples, with soaking, maintained a hydrophobic character, with an average contact angle (across all soaking times) of 101.6° ± 1.66°. Control samples of PDMS had an average contact angle of 104° ± 1.5°. Contact angles for both the control sample and the non-plasma sample were similar to the 105° reported by Khorasani and Mirzadeh (2004) for virgin PDMS. Treating the PDMS with plasma and storing in seawater yielded an average contact angle average of 66.9° ± 3.6°. The higher error seen in measurements taken from the treated PDMS is due to PDMS's natural tendency to recover hydrophobic character when exposed to air relatively quickly after plasma treatment. While the soaking in seawater prevents this recovery, exposure to air when assessing the surfaces with the goniometer leads to a change back toward a hydrophobic character. Differences in the time between removing the PDMS sample from seawater and assessment with the goniometer therefore causes considerable variation in the observed contact angles between replicates. However, even considering the variation between replicate contact angle measurements, it is clear that treatment with oxygen plasma followed by immediate storage in seawater is sufficient to establish a hydrophilic surface. All PDMS slides used for flow channel experiments were therefore treated with oxygen plasma and immediately stored in filtered seawater for later inoculation.

5.3.2 Starting densities and recruitment

Germling settlement patterning was clearly influenced by topography. Figure 5.3 shows the difference in germling adhesion positions on the different surfaces after a settlement time of 24 hours (before flow channel exposure). Germlings exhibit a random settlement pattern on the control surface, while germling settlement on 40 µm occurs in pseudo-lines that correspond to the positions of the grooves. Clear settlement within grooves on the 80 µm surfaces is visible in Figure 5.3c, while the germlings settled on the 160 µm grooved surface occupy the bottom of the wider grooves, often in pairs of lines where two germlings are able to fit side by side within the groove. There is evidence of germlings settling on the ridges between grooves, particularly on the 40 and 80 µm surfaces (circled in Figure 5.3), and from here on these will be referred to as ridge-settled germlings. Ridge-settled germlings often exist as part of a germling cluster, with germlings on either side of them occupying grooves. Because the groove depth is only one third of the height of the germlings, at least two thirds of the germling diameter will protrude from the surface when a germling occupies a groove. The settlement of germlings along the grooves would then lead to the presence of additional topographical features where groove-settled germlings form new ridges with the space between the germlings forming a groove. Germlings settling on a ridge in close proximity to several groove-settled germlings could benefit from cooperative mucilage/adheisve production and coverage as well as some hydrodynamic protection from germlings settled upstream.

Figure 5.4 shows average starting densities (D_0) for each substrate at each settlement time. Average starting density was the lowest after 12 hours settlement time and there was a clear increase after 24 hours settlement time for all surfaces. All substrates were inoculated using the same volume and same concentration of zygote suspension so the number of zygotes inoculating the slides was consistent. The lower D_0 values seen with lower settlement times is therefore likely the result

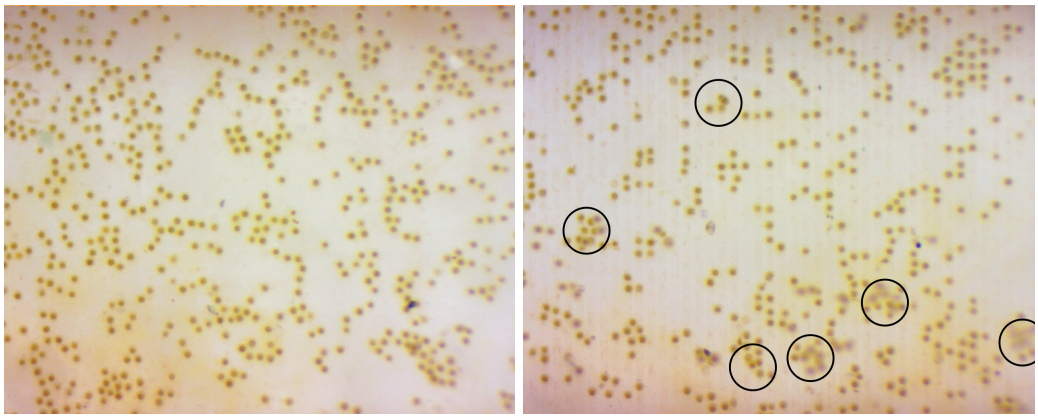

(a) (b)

(c) (d)

Figure 5.3: Settlement patterning of *H. banksii* germlings 24 hours post-settlement as seen under a dissecting microscope at 3× zoom. (a) Control (flat) surface, (b) 40 µm grooved surface, (c) 80 µm grooved surface, (d) 160 µm grooved surface. Circles indicate examples where clustering of germlings has resulted in individual germlings settling on the ridge between two grooves.

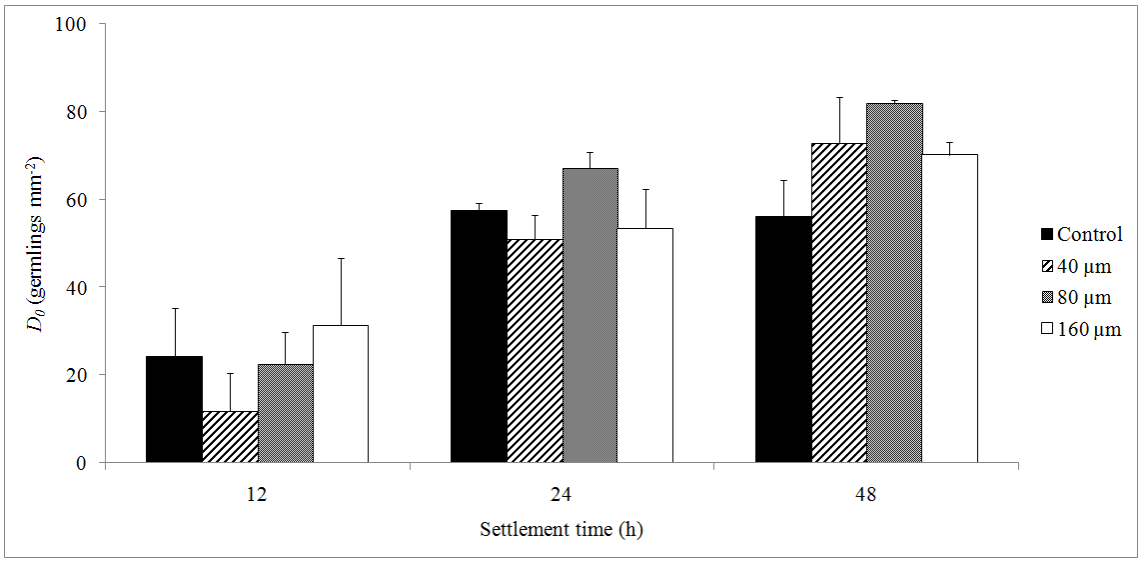

Figure 5.4: Settlement density (D_0) with increasing settlement time (± S.E., n = 3).

of germlings being dislodged when the substrate is transferred from the settlement tray to the flow channel, which also occured in Chapters 3 and 4. A higher degree of dislodgement at low settlement times indicates the germling's adhesion is less able to withstand the stress of the slide being moved. Increases in D_0 between 24 and 48 hours settlement time is substrate-dependent. Two-way ANOVA of D_0 for all substrates and settlement times confirmed a significant difference in starting density as a result of settlement time ($p < 0.05$), but no significant variation as a result of substrate type ($p = 0.18$). Comparison of D_0 within each substrate type indicated that D_0 stabilised after 24 hours with no significant difference between 24 and 48 hour values on the Control and 160 µm substrate ($p = 0.89$, $p = 0.15$, respectively). In contrast, D_0 on 40 and 80 µm surfaces continued to increase between 24 and 48 hours ($p = 0.03$, $p = 0.02$, respectively). Although not significant, there is a suggested lower starting density on the 40 µm topography after 12 hours, but this is not carried through to the other settlement times, and as noted, D_0 continues to increase on the 40 µm topography. It is likely that the elevated surface area presented by the 40 and 80 µm topographies assist with the formation of a stronger adhesive connection as settlement time and adhesive deposition both increase. However, the same mechanism appears not to be exploited on the flat control surface or in the wide spacing of the 160 µm surface.

As the substrates were all seeded with a finite number of zygotes, there will be a theoretical upper limit to the value of D_0. D_0 may have continued to rise after 48 hours settlement on the 40 and 80 µm topographies, but no data were collected beyond this settlement time. Overall average D_0 achieved after 24 and 48 hours were 57 ± 3 and 70 ± 4 germlings per mm^2, respectively, which is much higher than D_0 achieved in either of the other two experiments with *H. banksii* (Chapters 3 and 4), where D_0 was between 16 and 20 germlings per mm^2. It is highly likely that the higher average D_0 seen in this chapter is the result of a more concentrated zygote suspension used when inoculating the surfaces .

5.3.3 Flow channel adhesion experiments

Shear pressure is not included in the analysis or figures of these data as the topographical substrates cannot be considered a flat wall, so shear pressure estimations such as those calculated in Chapter 2 do not apply to this experiment. Germling survival at each flow velocity was calculated as in Chapters 3 and 4 using the following:

$$S_v = \frac{D_v}{D_0} \times 100$$

where S_v is percentage survival at a given flow velocity and D_v is germling density at that velocity. Where appropriate, comparisons between treatments are made using the single point metric of survival percentage at the conclusion of the flow channel exposure ($S_{2.5}$). Significant variation in the starting densities (Figure 5.4) meant that statistical analyses between survival data across the different settlement times was not reliable. An increase in average survival percentage (S_v) with increasing settlement time does seem obvious (figures 5.5a, 5.5b and 5.5c), and it is likely that an increase in adhesion strength over time is responsible for the change seen in both D_0 and S_v.

The survival graphs show that, at any settlement time, the surface with the 80 µm grooves exhibited the highest survival rate under the entire range of flow velocities investigated. Higher survival on the 80 µm topography was expected; the 80 µm groove width easily accommodates the width of a zygote, and zygotes were seen to be settled within the grooves in large numbers (Figure 5.3c). For germlings within 80 µm wide grooves, the close proximity of the side walls, in addition to the groove floor, provides three theoretical points of adhesive contact. Higher numbers of attachment points are associated with increased settlement of organisms, as outlined in attachment point theory (Scardino et al., 2006, 2008). The use of deeper grooves, such as a groove depth that is equivalent to the germling diameter, might lead to a further increases in survival, but manufacturing of topographies deeper than 27 µm was difficult to achieve consistently so they could not be tested in this thesis.

Of the remaining topographies, there is no clear poorest performer in terms of germling survival. The 40 µm topography exhibits poor survival at the highest velocity flow (2.5 m/s) after 12 and 24 hours ($S_{2.5}$ = 0.2% and 3.7%, respectively) but performs similarly to the control and 160 µm surfaces after 48 hours ($S_{2.5}$ = 89.9%). The 40 µm was expected to generate the lowest survival rate as a result of limited number of adhesion points (two), for germlings centred over a groove. The relative increase in survival success on the 40 µm surface after 48 hours may be due to the continued deposition of adhesive into the groove which would compensate for the lack of adhesion points, especially considering the shallow groove depth used in this experiment. Deeper topographical features may have impaired adhesion for longer as it would take more adhesive to fill the groove and make contact with the bottom surface of the groove. Additionally, even though all seawater was sterilised by filtering through a 0.22 µm filter, specimens of *H. banksii* could not be sterilised and bacteria present on the surface of the plants would have been transferred to seawater when creating the gamete suspensions. Bacterial contamination of the culturing seawater may then have lead to the rapid bacterial colonisation of substrates and the development of bacterial biofilms

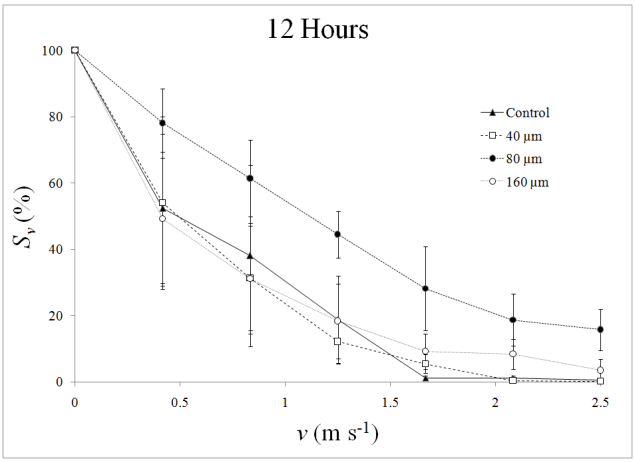

(a)

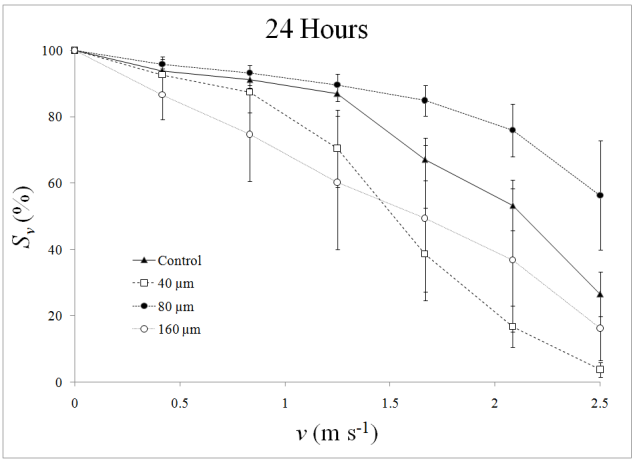

(b)

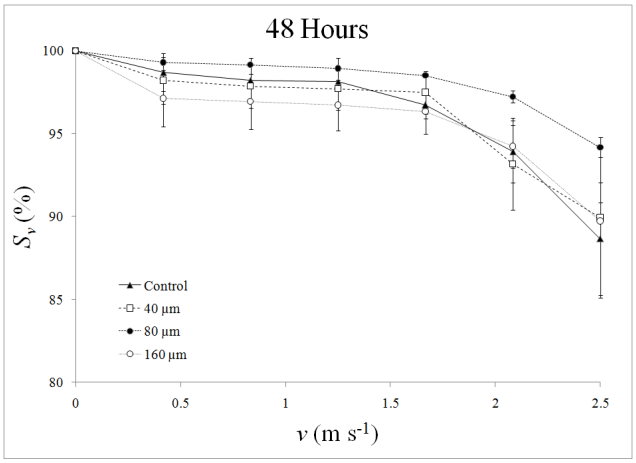

(c)

Figure 5.5: Survival rate vs fluid velocity after (a) 12 hours settlement time; (b) 24 hours settlement time; (c) 48 hours settlement time. ($\pm$ S.E., n = 3).

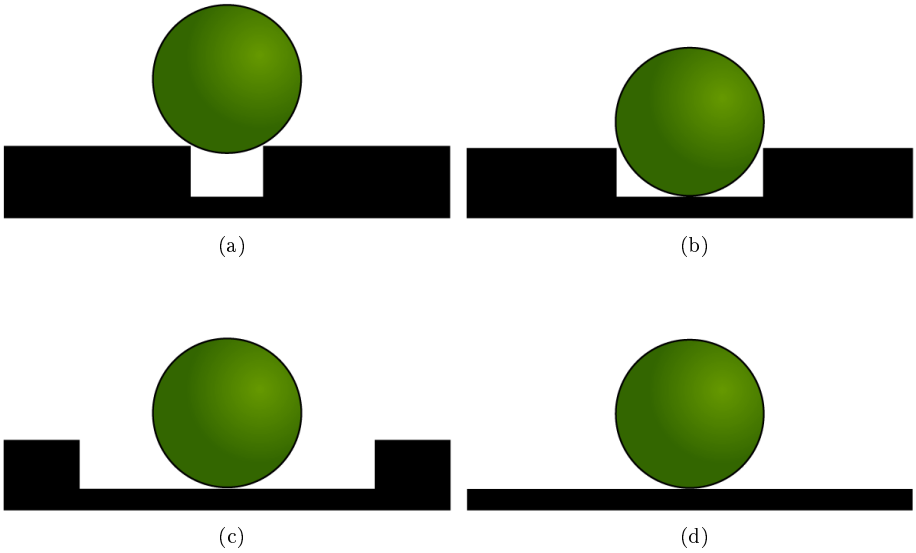

Figure 5.6: Representations of spherical germlings 80 µm in diameter on (a) 40 µm groove, (b) 80 µm groove, (c) 160 µm groove and (d) flat surface.

leading to a time-dependent masking of topography with particular effect on the 40 µm substrates. This is supported by observations made by Bers and Wahl (2004) that the anti-fouling effect of topography diminishes with time on topographies immersed in a marine environment.

The Control and 160 µm surfaces performed similarly in terms of survival. Considering attachment point theory with regards to these two substrates, the flat Control surface only offers a single point of attachment for a germling if that germling is not part of a cluster. The 160 µm grooves offer a maximum of two attachment points for a germling that is on one side of the groove, but a single attachment point for germlings settled in the centre of the groove. Again, the cooperative effect of germling clustering would change the number of attachment points available to the germlings on the 160 µm surface.

Similar survival rates on the 40 µm, 160 µm and Control surfaces could also be the result of similar fluid flow field properties, especially considering the relatively shallow depth of the grooves. Figure 5.6 depicts 2D representations of spherical cells sitting on the various topographies. Flow around a cell on the 40 µm, 160 µm and Control surfaces (Figure 5.6, a, c and d) would be relatively similar, with a degree of lift generated by fluid moving past and interacting with the lower half of the cell. In contrast, cells in the 80 µm groove (Figure 5.6, b) would be somewhat protected as the lower third of the cell is mostly shielded against the flow. Deeper grooves would possibly have a greater protective effect on the 80 and 160 µm topographies, resulting in higher survival rates.

5.3.3.1 Germling settlement position and survival

Numbers of ridge-settled germlings were counted before and after exposure to the lowest flow rate to determine what proportion of germlings settled on the substrate occupied a ridge and how ridge-

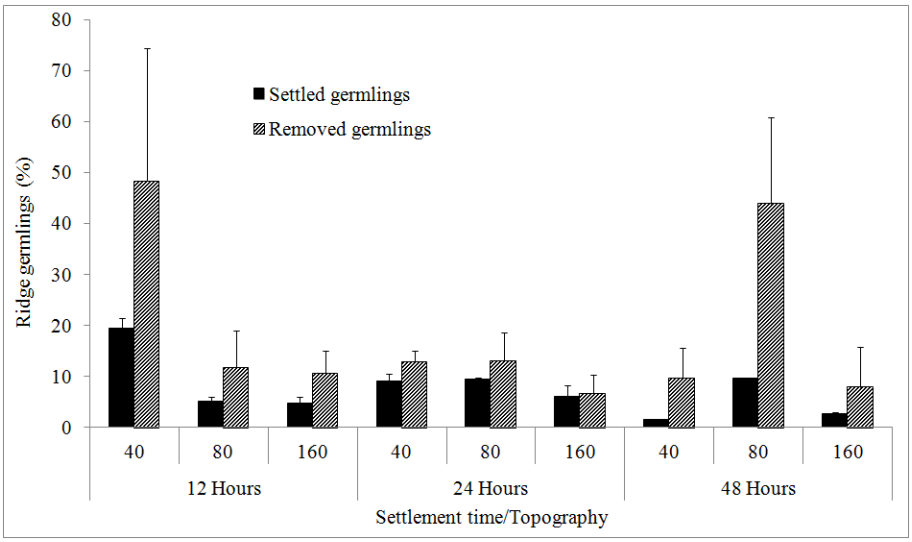

Figure 5.7: Chart showing percent of total germlings ridge-settled vs percent of removed germlings ridge-settled. Note the consistent overrepresentation of ridge-settled germlings in removal data (± S.E., n = 3).

settlement affected survival. Analysis of germling removal after exposure to the lowest flow rate (0.42 m/s) indicates that ridge-settled germlings are detached more readily than groove settled germlings on all topographies at all settlement times. On the 40, 80 and 160 µm topographies, ridge-settled germlings accounted for approximately 10% ± 3%, 8% ± 1% and 4% ± 1% of settled germlings, respectively. However, in terms of germling detachment, ridge-settled germlings accounted for 24% ± 10%, 23% ± 8% and 8% ± 3% of detached germlings on 40, 80 and 160 µm topographies, respectively. Ridge-settled germlings were up to six times more likely to be removed at low flow rates than would be expected if they were removed in proportion to their occurrence in settlement. Figure 5.7 illustrates the over-representation of ridge-settled germlings in germling removal statistics. It appears, for ridge-settled germlings, that the protective benefits of clustered settlement are outweighed by the increased hydrodynamic stress resulting from an elevated position in the channel flow.

5.3.4 Implications for aquaculture

While the primary goal of research focused on topographical effects on fouling seems to be aimed at preventing unwanted fouling, a side-effect could be the design of surfaces that preferentially encourage settlement of a specific, desired species, which has potential benefits in the field of aquaculture. Unwanted biological fouling on aquaculture equipment can result in decreased yields and increased processing time (Fitridge et al., 2012), but it may be possible to use topography to create aquaculture equipment that passively inspires the formation of productive mono-cultures. The increased survival rate of *H. banksii* germlings on surfaces with 80 µm wide grooves suggests that surface topography can be tuned to facilitate rather than undermine adhesion strength. Future

research in this area should bear this in mind, as failed designs in anti-fouling might represent ideal designs for positive aquaculture equipment design.

5.4 Conclusions

In this chapter the flow channel was used to assess the impact of topographical feature size on the settlement and adhesion strength of *H. banksii* propagules. Surfaces containing topography made of repeating square bottomed grooves were prepared in PDMS, inoculated with zygotes of *H. banksii* and challenged with increasing flow velocities. Increased survival was witnessed on topographies with a feature size slightly greater than the size of *H. banksii* zygotes, but there was no topography that resulted in a clear, long lasting disruption of settlement. The increased survival on the 80 µm topographical surfaces is consistent with predictions that cell adhesion would be most favoured on surfaces offering the most surface area/highest number of attachment points (three theoretical sites of adhesion) while initial lower survival responses on the 40 µm surface fit expectations of lower adhesion strength when faced with lower adhesion sites (two theoretical adhesion sites). The decreased impact of topography on settlement/survival after increased time spent in the fouling environment indicates that topography alone is not enough to permanently disrupt fouling by *H. banksii*, and the same is possibly true for biofouling in general. However, a multifaceted approach using a combination of strategies like defined topography, surface chemistry and the use of immobilised enzymes may be the answer to providing long-term, low maintenance fouling protection for surfaces in marine environments.

Bibliography

Barthlott, W. and C. Neinhuis (1997, April). Purity of the sacred lotus, or escape from contamination in biological surfaces. *Planta 202*(1), 1–8.

Bers, A. V. and M. Wahl (2004, February). The Influence of Natural Surface Microtopographies on Fouling. *Biofouling 20*(1), 43–51.

Bixler, G. D., A. Theiss, B. Bhushan, and S. C. Lee (2014, April). Anti-fouling properties of microstructured surfaces bio-inspired by rice leaves and butterfly wings. *Journal of Colloid and Interface Science 419*, 114–133.

Callow, M. E., J. A. Callow, L. K. Ista, S. E. Coleman, A. C. Nolasco, and G. P. López (2000, August). Use of Self-Assembled Monolayers of Different Wettabilities To Study Surface Selection and Primary Adhesion Processes of Green Algal (Enteromorpha) Zoospores. *Applied and Environmental Microbiology 66*(8), 3249–3254.

Callow, M. E., A. R. Jennings, A. B. Brennan, C. E. Seegert, A. Gibson, L. Wilson, A. Feinberg, R. Baney, and J. A. Callow (2002). Microtopographic Cues for Settlement of Zoospores of the Green Fouling Alga Enteromorpha. *Biofouling 18*(3), 229–236.

Cao, X., M. E. Pettitt, F. Wode, M. P. Arpa Sancet, J. Fu, J. Ji, M. E. Callow, J. A. Callow, A. Rosenhahn, and M. Grunze (2010, June). Interaction of Zoospores of the Green Alga Ulva with Bioinspired Micro- and Nanostructured Surfaces Prepared by Polyelectrolyte Layer-by-Layer Self-Assembly. *Advanced Functional Materials 20*(12), 1984–1993.

Carman, M. L., T. G. Estes, A. W. Feinberg, J. F. Schumacher, W. Wilkerson, L. H. Wilson, M. E. Callow, J. A. Callow, and A. B. Brennan (2006, January). Engineered antifouling microtopographies: correlating wettability with cell attachment. *Biofouling 22*(1), 11–21.

Finlay, J. A., M. E. Callow, L. K. Ista, G. P. Lopez, and J. A. Callow (2002, December). The Influence of Surface Wettability on the Adhesion Strength of Settled Spores of the Green Alga Enteromorpha and the Diatom Amphora. *Integrative and Comparative Biology 42*(6), 1116–1122.

Fitridge, I., T. Dempster, J. Guenther, and R. de Nys (2012, August). The impact and control of biofouling in marine aquaculture: a review. *Biofouling 28*(7), 649–669.

Fletcher, M. and J. H. Pringle (1985, March). The effect of surface free energy and medium surface tension on bacterial attachment to solid surfaces. *Journal of Colloid and Interface Science 104*(1), 5–14.

Holland, R., T. M. Dugdale, R. Wetherbee, A. B. Brennan, J. A. Finlay, J. A. Callow, and M. E. Callow (2004). Adhesion and motility of fouling diatoms on a silicone elastomer. *Biofouling 20*(6), 323–329.

Khorasani, M. T. and H. Mirzadeh (2004, February). In vitro blood compatibility of modified PDMS surfaces as superhydrophobic and superhydrophilic materials. *Journal of Applied Polymer Science 91*(3), 2042–2047.

Myan, F. W. Y., J. Walker, and O. Paramor (2013, December). The interaction of marine fouling organisms with topography of varied scale and geometry: a review. *Biointerphases 8*(1), 30.

Nowell-Usticke, J. (2014, November). A Study of the Effect of Micro-patterned Topographies on the Zygote Adhesion of Hormosira banksii.

Osborn, J. E. (1948). The structure and life history of Hormosira banksii (Turner) Decaisne. In *Transactions of the Royal Society of New Zealand*, Volume 77, pp. 47–71. J. Hughes, Printer.

Petrone, L., R. Easingwood, M. F. Barker, and A. J. McQuillan (2011, March). In situ ATR-IR spectroscopic and electron microscopic analyses of settlement secretions of Undaria pinnatifida kelp spores. *Journal of the Royal Society, Interface / the Royal Society 8*(56), 410–422.

Scardino, A. J., J. Guenther, and R. d. Nys (2008, January). Attachment point theory revisited: the fouling response to a microtextured matrix. *Biofouling 24*(1), 45–53.

Scardino, A. J., E. Harvey, and R. D. Nys (2006, January). Testing attachment point theory: diatom attachment on microtextured polyimide biomimics. *Biofouling 22*(1), 55–60.

Schumacher, J. F., N. Aldred, M. E. Callow, J. A. Finlay, J. A. Callow, A. S. Clare, and A. B. Brennan (2007). Species-specific engineered antifouling topographies: correlations between the settlement of algal zoospores and barnacle cyprids. *Biofouling 23*(5-6), 307–317.

Sullivan, T. and F. Regan (2011, December). The characterization, replication and testing of dermal denticles of Scyliorhinus canicula for physical mechanisms of biofouling prevention. *Bioinspiration & Biomimetics 6*(4), 046001.

Sun, M., C. Luo, L. Xu, H. Ji, Q. Ouyang, D. Yu, and Y. Chen (2005, September). Artificial Lotus Leaf by Nanocasting. *Langmuir 21*(19), 8978–8981.

van Wachem, P. B., T. Beugeling, J. Feijen, A. Bantjes, J. P. Detmers, and W. G. van Aken (1985, November). Interaction of cultured human endothelial cells with polymeric surfaces of different wettabilities. *Biomaterials 6*(6), 403–408.

Wahl, M., K. Kröger, and M. Lenz (1998, January). Non-toxic protection against epibiosis. *Biofouling 12*(1-3), 205–226.

Chapter 6

Conclusions and Future Directions

In this thesis I introduced a novel, low cost flow channel for the adhesion testing of small, sessile marine organisms. I used the flow channel to test the adhesion strength of two common species of New Zealand macroalgae: *Hormosira banksii* and *Durvillaea antarctica*. The adhesion testing was performed with two main goals: (i) to test the operation of the flow channel and confirm its suitability for use in adhesion studies and, (ii) to collect adhesion data to add to the body of knowledge in the field of marine bioadhesives. Greater understanding of the adhesion properties of marine organisms can then inform the development of bio-inspired wet-resistant adhesives and antifouling strategies.

6.1 The flow channel

The flow channel was required to accommodate microscope slide-sized substrates of varying thickness, connect simply to existing pumping equipment, and allow the viewing of settled germlings while the flow channel was in operation. My final design satisfied these requirements and resulted in a small, microfluidic, low cost flow channel that connected easily with the feed pump system of an ÄKTAcrossflow (crossflow) for accurate computer-controlled pumping. The clear Perspex top of the flow channel allowed for the visualisation of inoculated surfaces using a readily available dissecting microscope with a digital camera eyepiece. While the crossflow is not a low-cost or readily available piece of equipment, the flow channel can be connected to any other pumping system that can provide a smooth, controllable flow rate. For an extremely low cost solution this could be simple bilge pump paired with a valve and rotameter for flow control. Setups such as this would have the added benefit of increased portability.

6.2 Adhesion experiments

6.2.1 Skin model experiment

In Chapter 3, I tested the adhesion strength of germlings of *H. banksii* to surfaces relevant to the biomedical industry, including poly(methyl methacrylate) (PMMA) and three hydrogel surfaces. Two of the hydrogels were proteinaceous (gelatin), and designed to approximate human skin; the other was a carbohydrate-based hydrogel. The purpose of the experiment was to see if the adhesive produced by *H. banksii* zygotes/germlings was effective on the biomedical surfaces, and consequently, if *H. banksii*'s adhesive warranted further investigation as inspiration for biomimetic adhesives with biomedical applications. *H. banksii* exhibited a clear increase in adhesion strength with increasing settlement time, with germling survival remaining at or above 80% throughout adhesion testing when given at least 24 hours to settle. There was no difference in adhesion strength across the different surfaces, indicating that the adhesive produced by *H. banksii* has the ability to interact with a range of surface types equally well. In the marine environment this translates to an ability to exploit a range of available surfaces, including those with contamination from biofilms and other adsorbed compounds. In terms of medicine, these findings indicate that the adhesive produced by *H. banksii* deserves further investigation as inspiration for a versatile medical adhesive, particularly if the curing time can be reduced.

6.2.2 Common materials experiment

In Chapter 4, I compared the adhesion strength of germlings of both *H. banksii* and *D. antarctica*, two closely related fucoid seaweed species common in New Zealand. *H. banksii* typically occupies the intertidal zone in sheltered locations, while *D. antarctica* persists in exposed locations. I wanted to compare the settlement strength of the two species to see how their different habitats might influence their adhesion abilities to a range of materials commonly used in engineering. There was a settlement time-dependent increase in adhesion strength for *H. banksii* with very weak adhesion at less than 24 hours, while *D. antarctica* achieved and maintained maximum adhesion strength after only 6 hours. *D. antarctica* exhibited some variation in adhesion strength with the different substrates, performing consistently well on stainless steel. *D. antarctica* zygotes adhere more rapidly to the substrate than *H. banksii*, and the process appears to use some mechanism that benefits from contact with or proximity to stainless steel, a mechanism that is not shared by *H. banksii*.

6.2.3 Topographical substrate experiment

In Chapter 5, I looked at the influence of simple topography (square-bottomed grooves) on the adhesion behaviour of *H. banksii*. Topographical feature sizes were selected based on the size of *H. banksii* zygotes. Generally, a topographical feature size slightly larger than the size of *H. banksii* zygotes facilitated germling adhesion, while features smaller than the zygote disrupted adhesion somewhat. The effect of the adhesion disruption by the smaller topography diminished

with increasing settlement time. Besides a time dependent increase in adhesive strength, this could also be due to a time-dependent masking of topographical features by adhesive deposition or bacterial biofilm formation. Settlement position, either in a groove or on the ridge between grooves, influenced germling attachment in that germlings settled on ridges were up to six times more likely to be removed than their groove-settled counterparts. Technical limitations in manufacturing meant that only relatively shallow grooves, approximately one third the diameter of *H. banksii* zygotes, could be tested. While the findings from Chapter 5 didn't suggest anything new for fouling control, the increased adhesion of *H. banksii* on one of the topographies lead me to suspect that designed topographical surfaces could have a function in aquaculture, where an appropriately engineered topography could facilitate the adhesion of economically important marine species in favour of other foulers.

6.2.4 Challenges encountered in experiments

Working at the interface of engineering and biology comes with its own challenges. Engineering often requires a high level of accuracy and reliability, while biological systems can be fickle and full of natural variation.

Particularly challenging were the attempts to get my seaweed specimens to reproduce reliably. Even during peak reproductive season and using techniques that had previously been successful I still had numerous unsuccessful gamete releases. Often my seaweed specimens would either fail to produce gametes in sufficient numbers or the gametes (particularly sperm) would be in poor health, resulting in failed fertilisation. The only solution was to collect fresh seaweed, sometimes from a different location, and try again. *H. banksii* never again achieved the same rapidity of attachment seen in Chapter 3 on the PMMA and hydrogels, and while some variation in adhesion is to be expected as a result of natural variation, the consistency with which *H. banksii* failed to achieve previous levels of adhesion is puzzling.

A significant, recurring source of variation in my experiments resulted from the transfer of testing slides from their culturing trays to the flow channel. Shear stresses generated as the slide was lifted out of the culturing tray would remove weakly attached germlings, particularly at low settlement times, resulting in varied settlement densities that impacted my ability to perform statistical analyses on the results. Settlement density tends to stabilise with higher settlement times, so restricting adhesion testing to higher settlement times is one option for circumventing this problem. However, collecting adhesion strength and germling removal behaviour at lower settlement times is critical if we are to understand the mechanisms of early adhesion. It would be possible to take an initial recording of germling starting density before the slide is transferred to the flow channel by observing the slide within the culturing tray under the dissecting microscope, although this still doesn't eliminate the exposure to an unmeasured and variable shear stress as the slides are moved to the flow channel. For these experiments, the shear stress generated in this transfer was much less than that generated at the lowest flow rate in the flow channel. If future experiments are to look at lower flow rates for lower settlement times, then the transfer shear stress is going to become much more significant in relation to the experimental shear stresses generated, so this will

need to be looked at.

6.3 Recommendations for future work

There is plenty to study in the fields of marine bioadhesives and marine fouling, and I hope that continued use of this flow channel can help expand the body of knowledge in these fields. The following are some recommendations for future work in this field using this or similar equipment.

An obvious extension of this work is to investigate a wider range of adhesive-producing organisms. By studying the adhesion processes of a larger number of organisms we can look for similarities in adhesion processes between organisms to identify some fundamental, cross-species adhesion mechanisms.

Including a larger and more diverse range of surfaces would further help us understand the mechanisms operating at the adhesive-substrate boundary. Surfaces tested in the future could include substrates with defined chemistries and wettabilities and a broader range of topographical substrates. Additionally, substrates could be functionalised with immobilised digestive enzymes that target specific molecule classes; impacts on adhesion strength due to certain enzymes could then indicate the presence and importance of certain molecules and/or functional groups.

Analyses of substrates post-germling-removal could also help us identify the adhesive compounds involved. If germling removal is a result of cohesive failure, that is failure of the internal bonds between adhesive constituents, as opposed to adhesive-substrate bonds, then germling removal might result in a "footprint" of adhesive residue left behind. The structure and chemical nature of this adhesive footprint could be analysed by electron microscopy and immunolabelling or staining techniques.

The maximum flow rate that the crossflow could provide while maintaining smooth flow was 350 ml/min. It would be possible to generate higher shear stresses in the flow channel using higher flow rates. Higher shear stresses should result in higher removal rates in germlings at higher settlement times. However, given the dimensions of the flow channel, flow much above 300 ml/min would generate Reynolds numbers greater than 2300 which would indicate the flow had changed from a laminar to a transitional or turbulent regime.

At the other end of the scale, for low settlement times, the lowest flow rate of 50 ml/min (0.42 m/s) was often sufficient to remove a substantial proportion of *H. banksii* germlings. Observing the adhesion behaviour of germlings at flow rates lower than 50 ml/min would therefore generate a better picture of germling removal for weakly attached germlings.

6.4 Closing remarks

The work presented in this thesis, including the flow channel, are small contributions to the ever-expanding field of marine bioadhesive research. Possible outcomes of an increased understanding of marine bioadhesives span from biomimetic design of effective underwater adhesives to thwarting

the same bioadhesives with new fouling control strategies. Advances in these areas have potential to benefit health, environmental and economic interests, and the study of seaweed-based adhesives will play a crucial role in realising these benefits.

Appendix A

Re-plumbing the Crossflow

The ÄKTAcrossflow had to be re-plumbed to function as a pumping system for the flow channel. A list of plumbing changes is given below (Table A.1) along with plumbing diagrams of original and modified flow schemes.

Table A.1: Plumbing changes made to ÄKTAcrossflow. Reference letters indicate position of change in the flow scheme in Figure A.1a.

Reference	Connection	Original Line	Replacement Line
A	Reservoir out	F5L	AS600
B	Feed pump in	Reservoir out	Feed Line
C	Retentate valve block out 1	RVB1L	F2L ►Channel in
D	Reservoir in	R5S	Plugged
E	RPCV & Transfer purge ► Reservoir in	-	Plugged

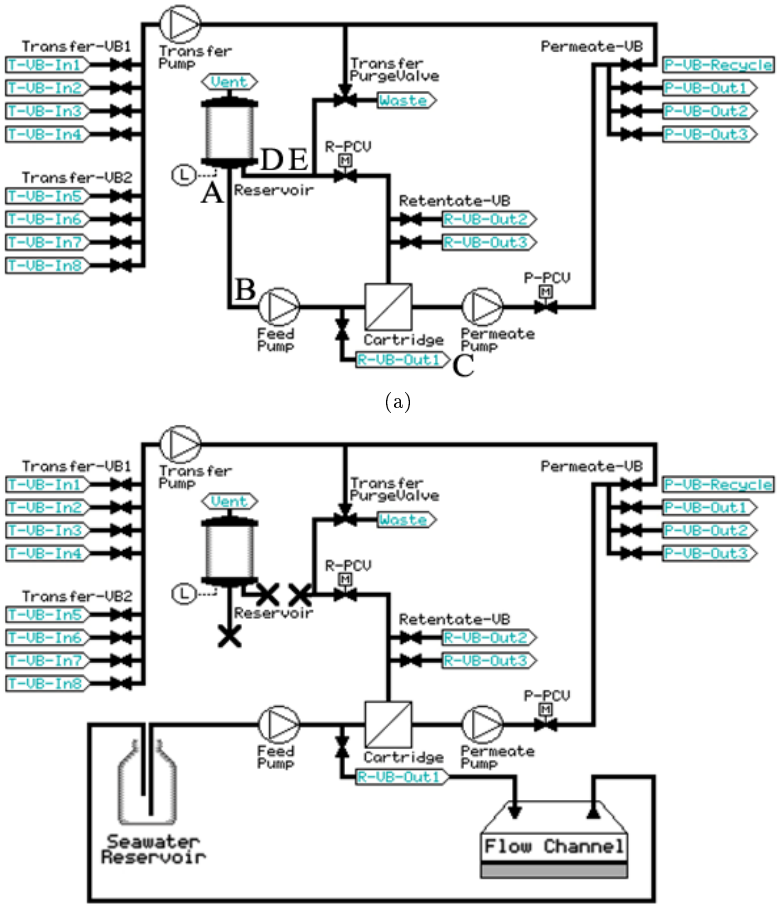

Figure A.1: Flow diagram of ÄKTAcrossflow (a) before re-plumbing, and (b) after re-plumbing.

Appendix B

Operating the flow channel

Instructions in this appendix are given for operating the flow channel using Unicorn software for the crossflow and ToupView to control microscopy capture and video recording.

B.1 Preparing crossflow and flow channel for experiment

The crossflow is stored with a 20% ethanol solution to prevent the growth of bacteria. Before using the crossflow, the ethanol solution must be flushed from the system with fresh water. The system must then be primed with seawater.

1. Place inlet hose in bottle containing at least 500 ml of 0.22 µm filtered, sonicated, purified water (Milli-Q, Millipore).
2. Place outlet hose in an empty beaker (do not recycle rinsing solution through system). This will be waste.
3. Run rinsing program:
   (a) Open RVB-Out-1
   (b) Run Feed Pump at 100 ml/min for five minutes
   (c) Stop Feed Pump
   (d) End Program
4. Transfer inlet hose to bottle containing at least 500 ml of 0.22 µm filtered, sonicated seawater.
5. Run rinsing program:
   (a) Open RVB-Out-1
   (b) Run Feed Pump at 100 ml/min for five minutes
   (c) Stop Feed Pump

(d) End Program

6. Discard waste from beaker. The crossflow and flow channel are now primed with seawater.

B.2 Running experiments

The following describes the procedure for operating the flow channel for a single replicate slide:

B.2.1 Loading slide into flow channel

1. Apply hose clamps to the inlet and outlet tubing immediately next to the flow channel; this prevents siphoning of water through the tubing when the flow channel is disassembled and water-tightness is lost.
2. Undo the four corner bolts using a socket wrench.
3. Lift off Perspex top including gasket.
4. Place slide on centre of flow channel base.
5. Carefully re-position Perspex top and gasket. Ensure complete contact between gasket and upper surface of testing slide so a water-tight seal can form.
6. Re-apply corner bolts and tighten bolts evenly until lower surface of Perspex top is in contact with upper surface of testing slide to ensure correct channel height. Observe flow channel from side to confirm contact.

B.2.2 Priming flow channel

1. Remove hose clamps from inlet and outlet tubing, this will allow some seawater to siphon back into the channel.
2. If the flow channel is dry or contains air bubbles it needs to be primed:
   (a) Manually open RVB-Out-1
   (b) Run Feed Pump at 0.5 ml/min until flow channel is fully primed and air bubbles have been removed. The shear stress generated by priming flow is equal to 1% of the lowest experimental shear stress value so is deemed negligible.
   (c) Stop Feed Pump
   (d) End Program

Table B.1: Flow steps in pumping regime with start time.

Time (s)	Flow (ml/min)	Function
0	0	Pre-experimental step
30	50	Flow rate 1
45	100	Flow rate 2
60	150	Flow rate 3
75	200	Flow rate 4
90	250	Flow rate 5
105	300	Flow rate 6
120	0	End of experiment

B.2.3 Adhesion testing

1. Place primed flow channel under dissecting microscope.
2. Bring surface of testing slide into focus at 3× zoom using ToupView microscopy software. Ensure field of view lies in the 'Testing section' (Section 2.4.4).
3. Initiate test pumping regime 'Anton 2' (program outlined in Table B.1). Using ToupView, initiate a 2 minute long video to record the surface as the pumping regime is executed. Define an appropriate name for the video footage.
4. Once flow regime has finished, remove flow channel from beneath dissecting microscope.
5. Apply hose clamps and disassemble flow channel as above. Discard slide.

B.3 Storing crossflow and flow channel when finished

The crossflow and flow channel must be stored with a 20% ethanol solution to prevent the growth of bacteria.

1. Place inlet hose in bottle containing at least 500 ml of 0.22 µm filtered, sonicated, purified water (Milli-Q, Millipore).
2. Place outlet hose in an empty beaker (do not recycle rinsing solution through system). This will be waste.
3. Run rinsing program:
   (a) Open RVB-Out-1
   (b) Run Feed Pump at 100 ml/min for five minutes
   (c) Stop Feed Pump
   (d) End Program

4. Transfer inlet hose to bottle containing at least 500 ml of 0.22 µm filtered, sonicated 20% ethanol solution in purified water.

5. Run rinsing program:

   (a) Open RVB-Out-1

   (b) Run Feed Pump at 100 ml/min for five minutes

   (c) Stop Feed Pump

   (d) End Program

6. Discard waste from beaker. The crossflow and flow channel are now ready for storage.